Master Thesis

Interplay of crystal symmetries and non-Hermiticity in quantum lattice models

Mathematisch-naturwissenschaftliche Fakultät der

by

Anar Bold

Supervising Professor:

Prof. Dr. Titus Mangham-Neupert

A thesis submitted in partial fulfillment for the
Master of Science (M.Sc.)

in the

Condensed matter theory group

Physics Institute

February 2022

“Gott erschuf den Festkörper - der Teufel die Oberfläche”

Wolfgang Pauli

Abstract

Real systems exchange energy with their environment at least to some extent. One alternative to describe dissipative systems is to build a non-Hermitian (nH) Hamiltonian to provide a simple description of open systems (that is, having gains and losses), which was already demonstrated in a wide spectrum of applications, ranging from mapping into classical systems, containing optical systems, electrical circuits, and mechanical systems, up to quantum materials [1, 2]. NH Hamiltonians are strikingly sensitive to the boundary conditions resulting in the breakdown of the bulk-boundary correspondence (BBC, being a signature of topological materials) and the existence of the skin effect. The notion of skin effect is mostly understood in one-dimensional systems, where the anomalous localization of all eigenstates results from non-reciprocal, direction-dependent hoppings. One dimensional nH models have been studied widely. NH higher dimensional models are our current interest and our objective is to reconstruct the bulk boundary correspondence in models in 2D and 3D within tight-binding formalism. The Wess-Zumino term which was introduced by Kawabata et al.[3] as a topological invariant for two-dimensional models was also studied for these models analytically and numerically.

Contents

Dedicated to my mom and grandma

Chapter 1

Introduction

I Motivation

One way of describing a system with dissipation is using a non-Hermitian Hamiltonian formulation. Dissipation occurs in photonic systems in the form of radiational loss, in periodically driven systems, in electronic systems having finite quasiparticle life time, and in electronic circuits as a passive RLC circuit form [4–6]. In some topological non-Hermitian systems, one observes a so-called skin effect at the boundaries. The skin effect is a phenomenon in which an extensive number of eigen modes are localized at the boundary, scaling with the system size.

Due to the skin effect, the shape of the bulk spectrum is completely different from the spectrum with open boundaries. Consequently, the conventional bulk boundary correspondence (cBBC) breaks down, because one can not predict any more from the bulk Hamiltonian the existence of the boundary states (or modes). The establishment of the bulk boundary correspondence for the non-Hermitian (nH) systems is one of the current interests in condensed matter research. Due to the huge number of localized states the Bloch theorem also fails in nH systems [7].

There were different approaches to reestablishing the bulk boundary correspondence (BBC) for non-Hermitian systems. Depending on the dimension of the system and its symmetries, one should find different topological invariants. The spectrum of nH systems can be displayed on the complex plane and thus it is necessary to redefine the notion of an energy gap [7]. Two different types of energy gaps can be defined on the complex plane, line gap and point gap. The definitions of them are given in the theoretical part in chapter 3. In case of line gap, the Hamiltonian can be continuously and adiabatically deformed to a Hermitian Hamiltonian while at the same time keeping the symmetry of

the system. Thus the physics in that case is not intrinsically nH. In contrary, the point gap topological phase can not be contracted to a Hermitian Hamiltonian but unitary Hamiltonian, so the resulting physics is intrinsically non-Hermitian [2].

In 1D systems the non-trivial topology comes from the point gap topology of periodic boundary (PBCondition) Hamiltonian. There the 1D spectral winding number is non-zero. Therefore due to the point gap topology of PB Hamiltonian the skin effect appear. In Hermitian counterpart non-trivial topology is not possible without symmetry protection. There were experiments in one dimensional systems where skin effect was detected, which inspires further studies on their generalisation higher dimensional systems [8].

To understand the topology of nH systems it is necessary to understand the basic principles of Hermitian topology. For this reason chapter 2 introduces the historical background of topological materials and basic Hermitian topology. First of all, in Hermitian systems nodal systems (semimetals) and fully gapped systems (insulators) can be of topological interest. Nodal systems have can be divided into Dirac nodal system and Weyl nodal systems in Hermitian case. Weyl nodes itself have chirality and they appear in the system always in pairs so that the net chirality is zero. When two Weyl nodes with opposite chirality come together they annihilate to a Dirac node. System with Weyl nodes are topological non-trivial. On the contrary Dirac nodes necessitate time reversal symmetry that makes the topology of the system non-trivial, and without time reversal symmetry the phase is topologically trivial. [9]

Nodal systems can have the so-called exceptional topology in non-Hermitian systems. This is when the topological nature comes from the degenerate point in the system. The degenerate point in non-Hermitian system is called exceptional point, because the degenerate eigenvectors coalesce and that makes the Hamiltonian defective. Exceptional topology seem to have always skin effect which is shown as point gapped energy spectrum of the Hamiltonian in periodic boundary condition (spectrum of Hamiltonian with periodic boundaries is said to be the bulk spectrum). This fact is studied and confirmed in the recent research and mentioned in the next section [8]. Some line gapped systems in the periodic boundary spectrum can have higher order skin effect (this is when the codimension of the skin modes are higher than one [10]) in presence of certain spatial symmetries. In this case, the spectrum of Hamiltonian in open boundary condition has point gap. [3]

While, due to the non-Hermiticity the degeneracy is stable in 2D systems on contrary to the Hermitian case where the stable degenerate nodal phase appears in 3D and in 2D, nodal phase should be protected by symmetries. [1]

The purpose of the thesis was to find a way to reconstruct bulk boundary correspondence.

II Current research progress

1D nH systems have been studied widely in recent years. For more detailed studies refer to the following review paper Ref.[1].

As mentioned above the reconstruction of the bulk boundary correspondence is needed especially in two or higher dimensions. We know that depending on whether the system has internal or spatial symmetry the topological invariant can be determined. Kawabata et al. suggested the geometrical term Wess-Zumino integral for the two-dimensional systems and the term can be quantized under certain spatial symmetries. This term is consistent with the topological phase of the system and therefore the corner skin effect can be predicted for its particular system. [3]

This section is based on the research of Ref.[8] and [11].

Kai Zhang et al. [8] found interesting observations and proposed a theorem of universal non-Hermitian skin effect for the models two and higher dimensions. The theorem says

> The energy spectrum of the Hamiltonian in periodic boundary condition is the mapping of d-dimensional torus to the energy eigenvalues on the complex plane, $\mathbb{C}$. The energy spectrum can be formed either one or more loops without inner area or it can cover one or more finite area. In case of finite area there are always skin effect by opening the boundary conditions, on the contrary in case of loop spectrum there appear no skin effect regardless of the geometry of the system. [8]

Therefore, they also observed that the type of the skin effect is divided into two different cases, the corner skin effect (CSE) and geometry dependent skin effect (GDSE). CSE depends on the type of the point groups. In the case of GDSE, the skin effect can appear in systems such as random polygons. However, this case can be also violated when we have some spatial symmetries such as mirror symmetry given in the example of the paper. One important corollary of the theorem they suggested is that the systems with exceptional points always carry skin effects. Additionally, the appearance of the skin effect can be reflected in the dynamical property of the wave packets in different geometries of the non-Hermitian systems. [8]

We know that in presence of internal symmetries the non-Hermitian matrix can be topologically classified, but in the presence of spatial symmetries it has two benefits. Firstly, when we have a some topological phase by adding additional spatial symmetry it can alter the topological property. Secondly, in presence of certain spatial symmetry the invariant can be computed in an easier way. In the recent work of Ryo Okugawa et

al.[11] the inversion symmetry was generalized for non-Hermitian Hamiltonian so that also the extended Hermitian Hamiltonian (for definition please refer to the chapter 3) version can have the inversion symmetry. Although, the generalized inversion symmetry is not unique [12, 13] and defined as follows for a nH Hamiltonian $H(\boldsymbol{k})$ [11]

$$U_I H(\boldsymbol{k}) U_I^{-1} = H^\dagger(-\boldsymbol{k}), \tag{1.1}$$

where U_I is a unitary matrix and $U_I^2 = 1$. The inversion symmetry becomes proper inversion symmetry when the Hamiltonian is Hermitian. The extended Hermitian Hamiltonian gets inversion symmetry in presence of generalized inversion symmetry in the following way:

$$\tilde{I}\tilde{H}(\boldsymbol{k})\tilde{I}^{-1} = \tilde{H}(-\boldsymbol{k}), \qquad \tilde{I} = \begin{pmatrix} 0 & U_I \\ U_I & 0 \end{pmatrix} \tag{1.2}$$

All the extended Hermitian Hamiltonians have chiral symmetry. The chiral symmetry operator Γ anticommutes with the inversion operator $\tilde{I}$, i.e., $\tilde{I}\Gamma = -\Gamma\tilde{I}$.

In presence of conventional inversion symmetry $PH(\boldsymbol{k})P^{-1} = H(-\boldsymbol{k})$ for a non-Hermitian Hamiltonian any extended Hermitian Hamiltonian has inversion symmetry and therefore the inversion operator takes the form $\tilde{P} = \mathrm{diag}(P, P)$. In that case the chiral operator and the inversion operator commutes, i.e., $\tilde{P}\Gamma = \Gamma\tilde{P}$. [11]

The topology can be predicted by looking at the inversion and chiral operators whether they commute or anticommute for the extended Hermitian case. Due to the conventional inversion symmetry there are no skin effect in the 1D system [3], whereas the generalized inversion symmetry the system carries skin effect. [11]

Furthermore they derived simple formula to calculate the 1D winding number (for the definition please refer to its Ref.[11] in Eq.(3)) if the system has generalized inversion symmetry using the topological correspondence between extended Hermitian Hamiltonian and its non-Hermitian Hamiltonian [1]. This formula predicts the skin effect and also can be used to calculate the weak topological invariant for the higher dimensional systems. [11]

In presence of chiral symmetry and inversion symmetry 1D winding number calculated for ribbon geometric Hamiltonian in 2D predicts the zero energy modes in Hermitian systems, which are localized at the corners in the full open boundary condition. This statement is only valid when the ribbon geometric Hermitian Hamiltonian is gapped at zero energy. In its non-Hermitian case it predicts corner skin modes. In presence

of generalized inversion symmetry for the non-Hermitian Hamiltonian and its extended Hermitian Hamiltonian the same calculation can be done. [11, 14]

Moreover, using the generalized inversion symmetry the zero energy exceptional point in 2D or line in 3D can be detected. [11]

III My research content and the thesis organisation

I studied 4 different models in tight-binding formalism in 2D and 3D. As I mentioned above the reconstruction of bulk boundary correspondence is needed for higher dimensional models. The first model is a 2D nodal system with exceptional degeneracy (semimetal) called π-flux model, which has reciprocal property, i.e. the outcomes by switching the input and output it has the same result. The most of the 1D models are not reciprocal which makes this model interesting to study. The singular value decomposition spectrum is a possible way to reconstruct the bulk boundary correspondence [1] and this method could be used for the reconstruction.

The second model is a 2D model which exhibits corner skin modes and in its Ref.[3] it suggested a topological invariant called Wess-Zumino (WZ) term, the quantization of which is consistent with its corner skin phase and the phase without corner skin states. The quantiization of this WZ term is studied in presence of different spatial symmetries. Furthermore, its quantization is investigated in 3D case and its possible outcomes were studied in relation with the spatial symmetries with respect to the 3rd spatial dimension.

The WZ integral was computed for the 3D model which exhibits corner skin modes by keeping 3rd dimensional k-point constant and by building real space Hamiltonian with respect to the third direction.

The 4th model is a model with single exceptional degeneracy on the surface which also exhibits corner skin states on its surface. The WZ term was computed for that model systematically. [15]

My thesis is organized in the following way. In chapter 2, I introduced the historical background of the topological insulator studies and some introduction to Hermitian topology, because by understanding the topology in Hermitian insulators the unique features of non-Hermitian topology become clearer. In chapter 3, I wrote theoretical background of the non-Hermitian systems and their topology which are relevant to understand my thesis project. In the following chapter 4, all the methods to investigate the properties of the models are described in detail. In each of chapter 5 to chapter 8 the results of the models are demonstrated and all together 4 models were investigated. In

each model I show the spectra with different boundary conditions and their topological invariant WZ term for 2D and 3D models were calculated. Finally, in the last chapter 9 the final conclusion is made.

Chapter 2

Historical background of topological insulators and topology in Hermitian models

One of the main topics in condensed matter physics is the study of phase transitions. Landau developed a theory that describes phase transitions occur due to the symmetry changes of a system [16]. Here, a local order parameter can be defined for an ordered phase, which changes as the symmetry of the system changes. Although, Landau's symmetry breaking theory successfully describes many condensed matter phases, it can not explain topological quantum states [17] (later also discovered topological classical states, for example electrical circuit model [4]). This theory rather describes classical orders which classifies classical statistical states on finite-temperature expressed by positive probability distribution functions. But we need a concept to classify quantum ground states, so called quantum orders in which the states are expressed by complex ground state wave functions. Topological state does not always have a nonvanishing local order parameter, because topological equivalent states could occur between two different symmetric phases. Or, topological phase can occur without breaking any symmetries. [17, 18] Although, symmetries play also a very important role in classification of topological phases as we will see later. There are several works in which it was revealed that a long-range entanglement in the quantum ground state itself gives us the topological order [19–21]. The reason why the quantum states are not easy to determine is that the possibilities of long-range entanglement are very large, so that there are plenty of new states beyond the symmetry breaking criterion. [22]

The concept of 'topology' is a field in mathematics. How this concept was developed to classify physical systems is now our interest. We know from introductory solid state

physics that due to the periodicity of lattice structure, for simplicity let us take 1-dimensional system, we can build Fourier transform if we have an infinite long system. We can realize an infinite long system by connecting the two ends. The Fourier-transformed space is called the reciprocal space or crystal momentum space, into which the periodic properties such as topological features of 'real' space can be mapped [23]. Such Hamiltonian in reciprocal space is the Bloch Hamiltonian and the energy eigenstates can be plotted as a function of crystal momenta which is called dispersion relation. We have an electronic insulator when we have an energy gap around the so-called Fermi level, which separates valence and conduction bands. Topologically, insulators can be generally classified trivial and non-trivial. Topological trivial insulators are the conventional insulators, i.e. atomic insulators. Additionally, vacuum is topologically classified as a trivial insulator. Non-trivial topological electronic states can be found in e.g. topological insulators, topological semimetals and topological superconductors. [24] As from now we can term non-trivial topological insulators as topological insulators.

To characterize the topological state of a system a topological invariant can be defined [24–26]. A topological insulator connected to a trivial insulator has gapless boundary states. i.e., at the interface between two systems, a band gradually interpolates to the conduction band in order to change the topological invariant. [23, 24] In a topological class two different states are regarded as equivalent if the systems can be transformed continuously between each other without closing the energy gap and keeping the symmetry. Due to this topological equivalence the system is persistent in presence of small perturbations, a property which makes topological materials promising for future applications. [18, 24]

To get some intuition, we give an overview of the historical development of topology in condensed matter studies. Klaus von Klitzing discovered in 1980 that the Hall conductance is quantized [27] as integer multiples of fundamental natural constants of e^2/h, which occurs when electrons confined to two dimensions (xy-plane) are placed in a strong magnetic field (in z-direction). The effect is known as integer quantum Hall effect (IQHE). Under strong magnetic field the electrons move in orbits with the cyclotron frequency ω_c this leads to quantized Landau levels with energy $\epsilon_m = \hbar\omega_c(m+1/2)$, here m is an integer. From these Landau levels first N states are filled and the rest is empty. When electric field is applied for example in x-direction the electrons start to drift and this results in Hall conductance:

$$\sigma_{xy} = Ne^2/h, \tag{2.1}$$

[28] here N is an integer, which is calculated by Thouless, Kohmoto, Nightingale and den Nijs (TKNN) [25] in 1982 using the Kubo formula. The invariant N was later

identified as a term already known from topology, because the integer invariant N has the form of the topological invariant n, and was first called the Chern number [24]. The Chern number comes from the mathematical theory of fiber bundles [29]. Physically, it can be explained based on the Berry phase [30] which is a phase factor coming from the adiabatic evolution of the Bloch wave functions $|u_m(\boldsymbol{k})\rangle$. In 2 dimensions, a band structure is a mapping from the crystal momentum $\boldsymbol{k}$, that is defined on a torus, to the eigenenergies of the Bloch Hamiltonian $\mathcal{H}(\boldsymbol{k})$. When a Bloch wavefunction is transported on a closed loop in $\boldsymbol{k}$-torus the Bloch wave function takes a well defined Berry phase calculated by the line integral $\mathcal{A}_m = i\langle u_m|\nabla_k|u_m\rangle$ [24]. The Chern invariant n is the total Berry flux, $\mathcal{F}_m = \nabla \times \mathcal{A}_m$, in the Brillouin zone and is given by:

$$n_m = \frac{1}{2\pi}\int d^2\boldsymbol{k}\mathcal{F}_m, \tag{2.2}$$

$$n = \sum_{m=1}^{N} n_m \quad n \in \mathbb{Z}, \tag{2.3}$$

summed over all occupied bands m and well defined as long as the energy gap remains finite between occupied and empty bands. [25]

The discovery of IQHE was the birth of the field of topological phase studies in condensed matter. The model which was proposed by Haldane in 1988 [31] was a spinless 2D model and can exhibit similar IQHE without external magnetic field and emerging Landau levels. Such materials, which can have topologically non-trivial states without external magnetic field, were later referred to as Chern insulators, because its topological non-trivial phase can be calculated by Chern number. However, experimental realisation of these materials came only mid 2000's.

Until 2000's there were not much connection between the research of IQHE and anomalous Hall effect (AHE). Only after the use of Berry phase formalism to describe the intrinsic behavior of AHE [32–35] that there exists quantum version of AHE [33, 34, 36], the quantum anomalous Hall effect (QAHE). Therefore, it is connected to the topological electronic states. As a result, in terms of Berry phase, Berry connection and Berry curvature the IQHE and QAHE are closely related [18, 30, 37]. Consequently, it turned out to be the model of Haldane was exact the QAHE with the right magnetic components exhibiting strong spin orbit coupling (SOC) and thus, the Chern number is non-zero. [18] Both QIHE and QAHE do not have time reversal symmetry (TRS). [23]

Since the generalized reformulation of Berry phase in 1984 [38] until mid 2000's the studies of electric polarization [39], methods for constructing Wannier functions [40], orbital magnetization [41, 42], understandings of the spatial decay of Wannier functions [43], and other procedures to determine the localization of electronic states [44–46] were

well explored. However, these theories implicitly assumed TRS and thus they describe in general normal insulating case, because in presence of TRS the Chern number is zero and therefore the phase is non-topological. [47]

As mentioned before, at the interface of two different topological phases in insulators exist gapless conducting states. Thus the boundary state is a bulk property, when the system is placed in vacuum. This phenomenon is called the bulk boundary correspondence (BBC). From this follows insulators which have non-zero Chern numbers exhibit gapless boundary states and are called Chern insulators. Chern insulating phase exists when there is no time reversal symmetry (TRS). Both QIHE and QAHE do not have TRS. However, there are states which are topologically non-trivial in presence of TRS. Then, there must be defined another topological invariant to fulfill the BBC and this is the topological invariant ν which is $\mathbb{Z}_2$ number [48], i.e., the value ν takes 0 or 1, trivial or non-trivial, either of two different phases in the system.

We take a look at the TRS and the definition of the $\mathbb{Z}_2$ number a little more in detail. A Bloch Hamiltonian which is invariant under TRS (given by an antiunitary operator Θ) satisfies:

$$\Theta\mathcal{H}(\boldsymbol{k})\Theta^{-1} = \mathcal{H}(-\boldsymbol{k}) \tag{2.4}$$

There are equivalence classes of Hamiltonians which fullfills above condition and which can be smoothly deformed into each other by keeping the energy gap open. $\Theta^2 = -1$ is satisfied for spin-1/2 particles. This condition leads us to the Kramer's theorem [49] which demonstrates the fact that a TRS invariant Hamiltonian has at least two-fold degenerate eigenstates. The proof for this is given as follows: if there is non-degenerate state $|\psi\rangle$ with $\Theta|\psi\rangle = \alpha|\psi\rangle$ for some constant eigenvalue α thus when we apply two times the TRS operator then $\Theta^2|\psi\rangle = |\alpha|^2|\psi\rangle$, and this is not permitted because $|\alpha|^2 \neq -1$. In the electronic system, up and down spins become degenerate when the system has no spin-orbit coupling. However, when the system has spin-orbit coupling, this symmetry has non-trivial outcomes. [24, 50]

There are numerous ways to formulate mathematically the $\mathbb{Z}_2$ invariant ν [50, 51] (for other references refer to [24]). One method (done by Fu and Kane 2006 [50]) is to build a unitary matrix $w_{mn}(\boldsymbol{k}) = \langle u_m(\boldsymbol{k})|\Theta|u_n(-\boldsymbol{k})\rangle$ (called sewing matrix) based on the occupied Bloch eigenstates $|u_n(-\boldsymbol{k})\rangle$. Due to the antiunitarity of Θ ($\Theta^2 = -1$), the unitary matrix has $w^T(\boldsymbol{k}) = -w(-\boldsymbol{k})$. In the Brillouin zone there are 4 points at which $\boldsymbol{k}$ and $-\boldsymbol{k}$ coincide, the so called time reversal symmetry invariant points Λ_a (TRIM - Time Reversal symmetry Invariant Momenta). Then $w(\Lambda_a)$ is antisymmetric. An antisymmetric matrix has the property that the squareroot of determinant of the matrix is its Pfaffian, so we can define $\delta_a = \mathrm{Pf}[w(\Lambda_a)]/\sqrt{\mathrm{Det}[w(\Lambda_a)]} = \pm 1$. Then the

$\mathbb{Z}_2$ invariant is defined by:

$$(-1)^{\nu} = \prod_{a=1}^{4} \delta_a \tag{2.5}$$

The above one is an example of topological classification based on the presence of a symmetry in the system. Analogously, basing on the internal symmetries such as time reversal symmetry (TRS) $\mathcal{T}$, particle hole symmetry (PHS) $\mathcal{C}$, chiral symmetry (CS) Γ and the combinations thereof one can construct a periodic table which specifies where we can find a non-trivial topological phases. This symmetry classification of topological phases was first constructed by Altland and Zirnbauer as a classification of random matrices (AZ symmetry classification) [52]. In the periodic table the relations between the internal symmetries, dimension of the system, unitarity or antiunitarity of the symmetry operator (operator$^2 = \pm 1$) and their topological classification by $\mathbb{Z}$, $\mathbb{Z}_2$ or trivial phase represented as 0 are connected to each other. [53]

Table 2.1: *AZ symmetry classification [24]*

Symmetry				d							
AZ	$\mathcal{T}$	$\mathcal{C}$	Γ	1	2	3	4	5	6	7	8
A	0	0	0	0	$\mathbb{Z}$	0	$\mathbb{Z}$	0	$\mathbb{Z}$	0	$\mathbb{Z}$
AIII	0	0	1	$\mathbb{Z}$	0	$\mathbb{Z}$	0	$\mathbb{Z}$	0	$\mathbb{Z}$	0
AI	1	0	0	0	0	0	$\mathbb{Z}$	0	$\mathbb{Z}_2$	$\mathbb{Z}_2$	$\mathbb{Z}$
BDI	1	1	1	$\mathbb{Z}$	0	0	0	$\mathbb{Z}$	0	$\mathbb{Z}_2$	$\mathbb{Z}_2$
D	0	1	0	$\mathbb{Z}_2$	$\mathbb{Z}$	0	0	0	$\mathbb{Z}$	0	$\mathbb{Z}_2$
DIII	-1	1	1	$\mathbb{Z}_2$	$\mathbb{Z}_2$	$\mathbb{Z}$	0	0	0	$\mathbb{Z}$	0
AII	-1	0	0	0	$\mathbb{Z}_2$	$\mathbb{Z}_2$	$\mathbb{Z}$	0	0	0	$\mathbb{Z}$
CII	-1	-1	1	$\mathbb{Z}$	0	$\mathbb{Z}_2$	$\mathbb{Z}_2$	$\mathbb{Z}$	0	0	0
C	0	-1	0	0	$\mathbb{Z}$	0	$\mathbb{Z}_2$	$\mathbb{Z}_2$	$\mathbb{Z}$	0	0
CI	1	-1	1	0	0	$\mathbb{Z}$	0	$\mathbb{Z}_2$	$\mathbb{Z}_2$	$\mathbb{Z}$	0

It is worth to look at Haldane's model a little more in detail. Haldane took a simple model of graphene which exhibits quantum Hall effect without external magnetic field. Also, in other literatures one usually takes the example of graphene because it introduces the concept of 2D quantum spin Hall insulator (as we will look at it as next) and also because the existing Dirac electrons in graphene has a necessary analogue at the surface of a 3D topological insulator. The Dirac points which are present in graphene of Haldane model (firstly, he did not consider the spin d.o.f.) are protected by inversion $\mathcal{P}$ and TRS, meaning that when we break the symmetries the degeneracy at the Dirac point will be lifted. Haldane imagined that by breaking the TRS one could get a non-zero

integer Hall conductivity at each Dirac point [24]. The non-zero Hall conductivity can be explained by the term in eq.(2.2). The system has 2 Dirac points because of the TRS which is explained by *fermion doubling theorem* [54] and this is the reason why we get integer value of the Hall conductivity [24]. When the inversion symmetry is broken the system becomes a normal insulator. [47]

Non-trivial topological phases appear in gapless nodal systems and fully gapped systems. In future I use the term "non-trivial topological system" just as "topological system".

In condensed matter in the vicinity of the nodal degeneracy the dispersion is linear. This kind of dispersion can be described by the relativistic Dirac and Weyl equations. Even though the electrons in the system are not relativistic, the presence of periodic potential of the crystal allows such description. There are subtle differences between Dirac semimetals and Weyl semimetals and the details are reviewed in the work of N.P.Armitage et al. [9].

The particles resulting from the Weyl equations are called Weyl fermions and the Weyl fermions have a chirality or handedness. If two Weyl fermions with opposite chirality move freely in Brillouin zone (BZ), then they coalesce and results in Dirac fermion. The simplest realization to have stable Weyl nodes is to keep the inversion symmetry in the system. Due to the Weyl fermionic property the system would suffer non-conservation of the electric charge. To avoid this non-physical consequence the system should always have pairs of Weyl fermions with opposite chirality, so that the net chirality is equal zero. This is one example of the fermion doubling theorem [54]. In the case of Dirac dispersion in graphene, the degeneracy is protected by inversion and TRS. In the presence of TRS the Dirac points must come in pairs, which is another example of the fermion doubling theorem. [9]

As mentioned above, in presence of TRS there is also a non-trivial topological phase. The next question was how to realize this kind of system. A 2-dimensional topological insulator was later called quantum spin Hall insulator. In 2005 this system was theoretically formulated and also predicted to exist in graphene and in 2D semiconductor system with uniform strain gradient [48, 55–57]. Then, this was proven experimentally in the following year on HgCdTe quantum well structures [58]. In graphene the spin-orbit coupling term commutes with the spin operator so that the Hamiltonian decouples from the up and down spin terms. The spin 1/2 of the electron was ignored in the model of Haldane. The theory of the quantum spin Hall insulator is simply two duplicates of Haldane model with plus and minus sign for conductivity. In addition this does not violate TRS, because TRS flips both spins and the sign of the conductivity σ_{xy}. Furthermore, due to the TRS the states at $k = 0$ are protected by Kramer's degeneracy

even if the spin conservation is violated. This confirmed that the spin Hall insulator is a stable topological phase.

There are the so-called "chiral" and "helical" states in the context of topological insulators. The "chiral" states are chiral in the sense that the states move only in one direction along the edges of the 2D system. The "helical" states are two states propagating in opposite directions, for example spin up and down spin currents in spin Hall insulator. Because the helicity of a particle is the correlation between spin and momentum, the term helical is used in analogy with helicity.

In the year 2006, theoretical groups independently formulated the 3D generalization of the topological quantum spin Hall insulators and used the term "*topological insulator*" for these electronic phases [51, 59–61]. Fu, Kane and Mele (2007) [62] showed the link between bulk and the gapless surface states, which is then called bulk boundary correspondence. The 3D topological insulator was experimentally realized in the year 2008 by the group led by Hasan at the Princeton University [63].

Besides the topological classification it is interesting to see that how Wannier function (Fourier transformation of the Bloch wave functions) behaves in normal insulating phase and Chern insulating phase. The Wannier functions (WF) are exponentially localized in the case of normal insulator (i.e., Chern number is zero) and the localization diverges when it is in Chern insulator phase (i.e., when Chern number is non-zero) due to the singularities of wave functions in reciprocal space. However, in the case of TRS the states are also exponentially localized, which means the divergence of the WF is only in the case Chern insulator non-trivial phase and it does not necessarily hint to the other non-trivial states. [64]

Some topological non-trivial insulator can be smoothly transformed into a topologically trivial state without closing the bulk gap of the system in absence of symmetry. [24] For this reason, there is a notion of a symmetry protected topological phase, in which the symmetry has to be broken in order to change the phase into a trivial state.

Symmetry protected topological phases exist not only due to the internal symmetries, but also it exists in the presence of spatial symmetries, i.e., which are non-locally acting in position space, such as rotation, mirror reflection, or other spatial group symmetries. They are called topological crystalline insulators (TCI). [24] The gapless boundary states exist only when the surface of the TCI support the same symmetry of the bulk. [65]

Furthermore, there are higher order topological phases in which the boundary states are localized at the hinges and corners. These boundary states have codimension higher than one (which means for example there are states at the corners localized in 2D system.

The corner states have dimension 0 and codimension 2) and come from the interplay of crystalline symmetries and topology of the system. [10, 66, 67]

In the standard quantum mechanics we have Hermitian operators to describe observable quantities in closed systems. All topics above are for Hermitian systems. In recent years there is intense interest in non-Hermitian (nH) systems. Real physical systems are connected to the environment and have gain and loss of energy and particles. This presence of interactions with the environment makes their description more composite. Although non-Hermiticity was ubiquitous in physics for many decades [7], there are even more motivations to study such systems recently. Especially, since we have already investigated widely topological properties within the framework of Hermitian systems, it is compelling to further study nH topological systems.

Besides other approaches to describe open systems [7, 68, 69], the effective nH formalism is conceptually clearer and relatively intuitive for mesoscopic systems (mesoscopic systems refer to the size of the system which ranges from several nanometers to several micrometers). The basic theory of the non-Hermitian Hamiltonian is introduced in chapter 4. Some experimental realisations are already found in a wide spectrum ranging from classical systems consisting of optical settings, electric circuits, and mechanical systems to the quantum systems. [70–72]

In nH systems the conventional bulk-boundary correspondence is broken due to the phase transition of the system between open boundary and periodic boundary cases. There are interesting nH properties which can not be found in the Hermitian models such as nH skin-effect, exceptional degeneracies in the nodal phases which accompany the open Fermi-Seifert surfaces ([1], which appear due to the branch cuts of the eigenvalues) and the topological classification of the nH random matrices based on the nH generalized symmetries for both gapped and gapless phases will be discussed in the next chapter 4. More in detail refer to the review letter of E.J.Bergholtz et al. [1].

Chapter 3

Theoretical Background of non-Hermitian Hamiltonians

I General properties of non-Hermitian Hamiltonians and its topology

This section is taken from Ref.[1].

Non-Hermitian (nH) Hamiltonians have their unique features that can not be found in Hermitian systems. We define that the left eigenvector is $\psi_L H = E\psi_L$ and right eigenvector is $H\psi_R = E\psi_R$. By diagonalizing the nH Hamiltonian one can see that the left and right eigenvectors in general not equal. We also notice when the Hamiltonian is not Hermition the time evolution operator is no longer unitary. [1] When a simple nH Hamiltonian is given as $\begin{pmatrix} 0 & \alpha \\ 1 & 0 \end{pmatrix}$, $\alpha \in \mathbb{C}$, then the eigenvalues are $E_\pm = \pm\sqrt{\alpha}$. Additionally, the eigenvalues can be not analytic under system parameters depending on the systems. Here the derivative of the energy w.r.t. α diverges, i.e., $|\partial_\alpha E(\alpha)| \to \infty$ as $\alpha \to 0$. It is interesting that such properties can be used in sensing devices which has been proposed recently [73]. The corresponding left and right eigenvectors are [1]:

$$\psi_{R,\pm} = \begin{pmatrix} \pm\sqrt{\alpha} \\ 1 \end{pmatrix}, \quad \psi_{L,\pm} = \begin{pmatrix} 1 & \pm\sqrt{\alpha} \end{pmatrix}, \tag{3.1}$$

for the two level system there are two left and two right of them. In general each set of left and right eigenvectors do not form orthonormal set. Therefore at the degenerate point the eigenvoctors can coalesce and results in only one left vector and one right vector so that the matrix becomes defective. The degeneracy happens at $\alpha = 0$ and

then the energy eigenvalue becomes $E_\pm = 0$. The degenerate point in nH Hamiltonian is called exceptional point [74] and the topology containing degenerate points is called exceptional topology. In general depending on the system N eigenstates can become linear dependent. We can then say N-order exceptional point. [1]

Another important feature is of nH band structure is the appearance of Fermi arcs. This is caused by the possibility of branch cut in the energy function. The branch cut is at $\arg(\alpha) = \pi$. Consequently, the eigenvectors swap $\psi_{R/L,\pm} \to \psi_{R/L,\mp}$, $E_\pm \to E_\mp$ by encircling the exceptional point as $\arg(\alpha) \to \arg(\alpha) + 2\pi$ due to the energy function crossing over the branch cut. [1]

I.1 Non-trivial topology in one-band non-Hermitian model

In contrast to the Hermitian topology in nH systems one-banded system can be topologically non-trivial. In nH systems the winding number is defined along the path on complex energy plane, whereas in Hermitian case the winding number is eigenstates winding based on the Berry phase. The homotopical winding number is then defined as [75, 76]:

$$w = \frac{1}{2\pi i}\int_{-\pi}^{\pi} dk \partial_k \ln E_k. \tag{3.2}$$

E_k are the energy eigenvalues and k are the indices of crystal momentum. When we have multiband model the E_k will be replaced by $\det H(k)$ in eq.(3.2) and the $H(k)$ is the bulk nH system Hamiltonian. The winding number in eq.(3.2) takes integer ($\mathbb{Z}$) values. [1]

The simplest one dimensional model which shows non-trivial topology on its energy spectrum is the Hatano-Nelson model [77] given by:

$$H = \sum_n (J_L c_n^\dagger c_{n+1} + J_R c_{n+1}^\dagger c_n), \qquad J_L, J_R \in \mathbb{R}, \tag{3.3}$$

$c_n^\dagger(c_n)$ is the creation (annihilation) operator on site n and $|J_R| \neq |J_L|$ in general. The complex energy spectrum is then $E_k = (J_L + J_R)\cos(k) + (J_L - J_R)\sin(k)$. The energy spectra winds around the origin clockwise and counterclockwise direction for $|J_L| - |J_R| < 0$ and $|J_L| - |J_R| > 0$, respectively. The winding number of the Hatano-Nelson model is $w = -1$ and $w = 1$ so that the model has two different topological phase. We know topological phase transition occurs when the energy gap closes. As expected in the above model between the two different topological phases, the phase transition requires $E_k = 0$ for some k when $|J_L| = |J_R|$. The energy spectra of the Hatano-Nelson model represents the minimal example for the point gap [2], which will be defined later.

I.2 Non-Hermitian skin effect

The nH Hamiltonians exhibit an another exotic feature called nH skin effect [78–81]. Skin effect is phenomenon which occurs in the system in open boundary condition where macroscopic number of eigenstates pile up at the boundaries. Skin effect can be interpreted from the existence of the exceptional points. In the proximity or presence of EPs the wave functions need to go through the EPs by opening the boundary from PB to OB. The number of the skin states scale with the system size, because also the number of the EPs scale with the system size.

The skin states can be also forbidden due to the symmetries, for example, in presence of PT-symmetries [82].

In one dimension the boundary would be the two ends. In Hatano-Nelson model the skin effect occurs due to the asymmetric hopping strength $|J_R| \neq |J_L|$, where the end with the skin modes depend on which hopping strength is dominant. The simplest case where we can see the skin effect is when the hopping strength in one direction is turned off, i.e., $J_L = 0$ in the eq.(3.3). The whole Hamiltonian in the open boundary condition can be written in single Jordan block form, so that the eigenenergies become an exceptional point of order N, when N is the total number of sites. [1]

I.3 Two-band non-Hermitian model and its topology

Two-band models in reciprocal space can be written in general form as

$$H(k) = \boldsymbol{d}(k) \cdot \boldsymbol{\sigma} + d_0(k)\sigma_0 \tag{3.4}$$

here $\boldsymbol{d} = \boldsymbol{d}_R + i\boldsymbol{d}_I$ with $\boldsymbol{d}_R, \boldsymbol{d}_I \in \mathbb{R}^3$ which all depend on k, $d_0 \in \mathbb{C}$, $\boldsymbol{\sigma} = (\sigma_x, \sigma_y, \sigma_z)^T$ are the Pauli matrices, and σ_0 is the 2×2 identity matrix. [1]

The energy spectrum is then

$$E_\pm = d_0 \pm \sqrt{d_R^2 - d_I^2 + 2i\boldsymbol{d}_R \cdot \boldsymbol{d}_I} \tag{3.5}$$

here all terms depend on the lattice momentum k, that is left out for simplicity.

The general Hamiltonian becomes Hermitian if the term $\boldsymbol{d}_I$ equals zero. A degenerate points will occur when $\boldsymbol{d}_R$ term is tuned to zero. This results in occurence of stable topological phase only in 3 spatial dimensions, i.e., Weyl semimetal. While in non-Hermitian case for $\boldsymbol{d}_I \neq 0$, generic and stable degeneracy [83] can occur in two-spatial

dimensions due to the two real conditions need to be satisfied [1]

$$d_R^2 - d_I^2 = 0, \qquad \boldsymbol{d}_R \cdot \boldsymbol{d}_I = 0. \tag{3.6}$$

we can see also any non-trivial solution to this eq.(3.6) gives us exceptional degeneracy, where the nH Hamiltonian becomes defective. These phases define the nH Weyl phases according to E.J.Bergholtz et al [1], which are topological stable 2D nodal phases.

Connecting the EPs there are purely imaginary and purely real energy spectrum called nH Fermi-arcs or $i-$Fermi-arcs and these lines are results of the branch cut of the energy eigenfunction [84–87]. These nH Fermi-arcs are comparable to the Fermi-arcs of the 3D Weyl semimetals. However, the difference is that the Fermi-arcs are bulk property and not surface property like in the Hermitian Weyl phase. [1]

II Topological classification of non-Hermitian random matrices

We know that two different Hamiltonian belongs to one topological class as long as these two Hamiltonians can be smoothly transformed to each other keeping the symmetries without closing the energy gap. In addition to the Bloch bands, which is based on the translational symmetry of the lattice structure, AZ symmetry classification of the Hermitian systems for topological insulators and superconductors is widely studied today. We compare the non-Hermitian amendment of the topological classification for gapped phases with Hermitian realm.

II.1 Internal symmetry classification

The classification of topology in condensed matter systems is based on the symmetries of the Hamiltonian. The most fundamental symmetries are the internal symmetries, which is distinct from the space group symmetry. Space group symmetries depend on its specific spacial structure of the system. The internal symmetries are time-reversal symmetry (TRS), particle-hole symmetry (PHS), and chiral symmetry (CS), where TRS and PHS are antiunitary, whereas CS is unitary. [2]

Time reversal symmetry:

$$\mathcal{T}\mathcal{H}^*(\boldsymbol{k})\mathcal{T}^{-1} = \mathcal{H}(-\boldsymbol{k}), \quad \text{where} \quad \mathcal{T}_\pm\mathcal{T}_\pm^* = \pm 1 \tag{3.7}$$

Particle hole symmetry:

$$\mathcal{C}\mathcal{H}^*(\boldsymbol{k})\mathcal{C}^{-1} = -\mathcal{H}(-\boldsymbol{k}), \quad \text{where} \quad \mathcal{C}\mathcal{C}^\dagger = \pm 1 \tag{3.8}$$

Chiral symmetry:

$$\Gamma\mathcal{H}(\boldsymbol{k})\Gamma^{-1} = -\mathcal{H}(\boldsymbol{k}), \quad \text{where} \quad \Gamma\Gamma^\dagger = \Gamma^\dagger\Gamma = \Gamma^2 = 1 \tag{3.9}$$

An internal symmetry is a transformation acting only on the fields. Thus, internal symmetries do not transform space time points, and leaving the Lagrangian or the physical results invariant. [2] Using internal symmetries one can classify the Hermitian random matrices in 10-fold classes. This 10-fold symmetry classification is the famous Altland-Zirnbauer (AZ)[52] classification as mentioned in the previous chapter.

In the Hermitian system by definition $\mathcal{H}^* = \mathcal{H}^T$ the complex conjugation and the transposition are equal. Thus, PHS in eq.(3.8) is equal to $\mathcal{C}\mathcal{H}^T(\boldsymbol{k})\mathcal{C}^{-1} = -\mathcal{H}(-\boldsymbol{k})$. In non-Hermitian systems this equality does not hold. Consequently, the PHS is ramified in the presence of non-Hermiticity and PHS is generalized. Such symmetry generalization occurs for all other symmetries in nH systems. Therefore, 10 symmetry classes in Hermitian systems ramify into 43 symmetry classes [88] in non-Hermitian systems, which was first classified by Bernard and LeClair. In this classification they have overcounted some symmetries and also overlooked some of them. Besides symmetry ramification there are also symmetry unification. Time reversal symmetry and particle hole symmetry can be unified in the non-Hermitian systems. The operation of time reversal symmetry on H is the same as the particle hole symmetry operation on iH. Thus, the total number of generators of the non-Hermitian internal symmetries TRS, PHS, TRS†, PHS† (for the definitions please refer to its paper Ref.[2]) and the combinations of them defines the 38 symmetry classes.TRS and PHS can be combined into the CS, $\hat{\Gamma} := \hat{\mathcal{T}}\hat{\mathcal{C}}$.[2] The detailed discussion of the internal symmetry classification of the nH matrices please refer to the Ref.[2].

II.2 Space group symmetries and their role in topological systems

This section is taken from Ref.[65]

In addition to the AZ symmetry classifications by including the spatial symmetries the topological classification gets enriched. Such additional symmetries have two possible outcomes affecting the formulation of topological systems. Firstly, one can simplify the calculation of topological invariant and secondly, the topological classification can

be changed. Those non-trivial topological systems protected by spatial symmetries are called topological crystalline insulators (TCIs) and superconductors (TCSs). [65]

Space group symmetries act non-locally, in contrast to the internal symmetries which act locally. Space groups describe spatial symmetries of a crystal or a lattice. The operations are composed of lattice translations and point group symmetries which should leave at least one spatial point unchanged. The examples of point groups are inversion, reflection, proper and improper rotations. Followed by the crystallographic restriction theorem in presence of lattice-translation symmetries the rotations with 1-,2-,3-,4-, and 6- fold axes are allowed. A space group operation G maps the point on lth site to the l'th site from the unit cell r to the unit cell at position $u_G\mathrm{r} + R_m$. u_G is a $n \times n$ orthogonal matrix and the site is translated by lattice vector R_i. A unitary operator $\hat{\mathcal{G}}$ acts on the electron field operator, i.e., the fermion annihilation operator $\hat{\psi}(\mathrm{r})$ as follows:

$$\hat{\mathcal{G}}\hat{\psi}_i(\mathrm{r})\hat{\mathcal{G}}^{-1} = (U_G)_i^j\hat{\psi}_j(u_G\mathrm{r} + R_i), \tag{3.10}$$

here U_G is a unitary matrix and the sites in a unit cell and the internal degree of freedom are labeled with i and j. The indices are summed over j. [65]

The fact that the translation operator can be chosen to be diagonal representation in an irreducible representation allows the Bloch basis functions can be used in generating irreducible representation in a space group.

In momentum space the fermionic annihilation operators transform as:

$$\hat{\mathcal{G}}\hat{\psi}_i(\mathrm{k})\hat{\mathcal{G}}^{-1} = (U_G(u_G\mathrm{k}))_i^j\hat{\psi}_j(u_G\mathrm{k}) \tag{3.11}$$

here $(U_G(u_G\mathrm{k}))_i^j = (U_G)_i^j e^{-iu_G\mathrm{k}\cdot R_i}$ (not summing over i). [65]

Example: The Su-Schrieffer-Heeger (SSH) chain is one dimensional and has A and B sublattices (labeling two different atoms). When a reflection $\hat{\mathcal{R}}$ operates the atom A in the $j = 0$th unit cell then the index of the fermionic operator $\hat{a}_j$ flips its sign to $\hat{a}_{-j}$ and the operator for the atom B $\hat{b}_j \to \hat{b}_{-j-1}$. In reciprocal space with the action $\hat{\mathcal{R}}$: $\hat{a}(\mathrm{k}) \to \hat{a}(-\mathrm{k})$ and $\hat{b}(\mathrm{k}) \to e^{-ik}\hat{b}(-\mathrm{k})$. [65]

Let us take an example of ramification of symmetry classification in presence of inversion symmetry for TCIs and TCSs in Hermition systems. We take a d-dimensional Bloch Hamiltonian $H(\mathrm{k})$, and the r_1 direction is invariant under reflection R_1:

$$R_1^{-1}H(-k_1, \tilde{\mathrm{k}})R_1 = H(k_1, \tilde{\mathrm{k}}), \tag{3.12}$$

here $\tilde{\mathrm{k}} = (k_2, ..., k_d)$ and the operator R_1 is unitary. We drop the index 1 for later.

With respect to the given reflection plane and the right choice of a phase for R, R satisfies the conditions:

$$R^\dagger = R, \qquad R^2 = 1 \tag{3.13}$$

then the eigenvalues of R are $+1$ or -1. The commutation relation with the AZ symmetry operators T, C and Γ are:

$$\Gamma R = \eta_\Gamma R\Gamma, \qquad TR = \eta_T RT, \qquad CR = \eta_C RC, \tag{3.14}$$

here $\eta_{\Gamma,T,C} = \pm 1$ tells that if R commutes or anticommutes with the operators Γ, T and C. Thus in presence of the internal symmetries and the reflection symmetry there are altogether 27 symmetry classes, which is tabulated in the Ref.([65]).

III Energy gap in complex energy spectrum

This section is taken from Ref.[2].

In Hermitian systems two systems are in a topological phase if and only if the two Hamiltonians can be continuously deformed to each other and simultaneously, if the symmetry is conserved. Energy gap is the region where no energy states are present. Therefore, energy gap closes only if the spectrum are contractible to a zero dimensional single point $E = E_F$. Thus, the energy spectrum is uniquely defined in Hermitian systems and the gap is open if and only if the spectrum does not cross the Fermi energy level E_F. [2]

However, in nH systems the concept gap is not trivial due to the complex energy spectrum, which can be displayed on the complex plane, $\mathbb{C}$. In non-Hermitian system, we can define 2 different gaps on the complex plane. One of them is point gap at E_P, where the energy spectrum can be contracted to one point. The other one is line gap, when a line can be drawn between two bunch of energy spectrum. [2]

The topological phases are classified also based on its type of energy gap. For instance, when there are no symmetries in the system the topological phase with point gap is present only in odd spatial dimensions (see class A in section). Whereas, topological phase determined by line gap is only present in even spatial dimensions. [2]

III.1 Point gap

In general the complex energy reference point $E = E_P$ for the point gap is non zero. However, due to the symmetries of the system there are sometimes restrictions on the

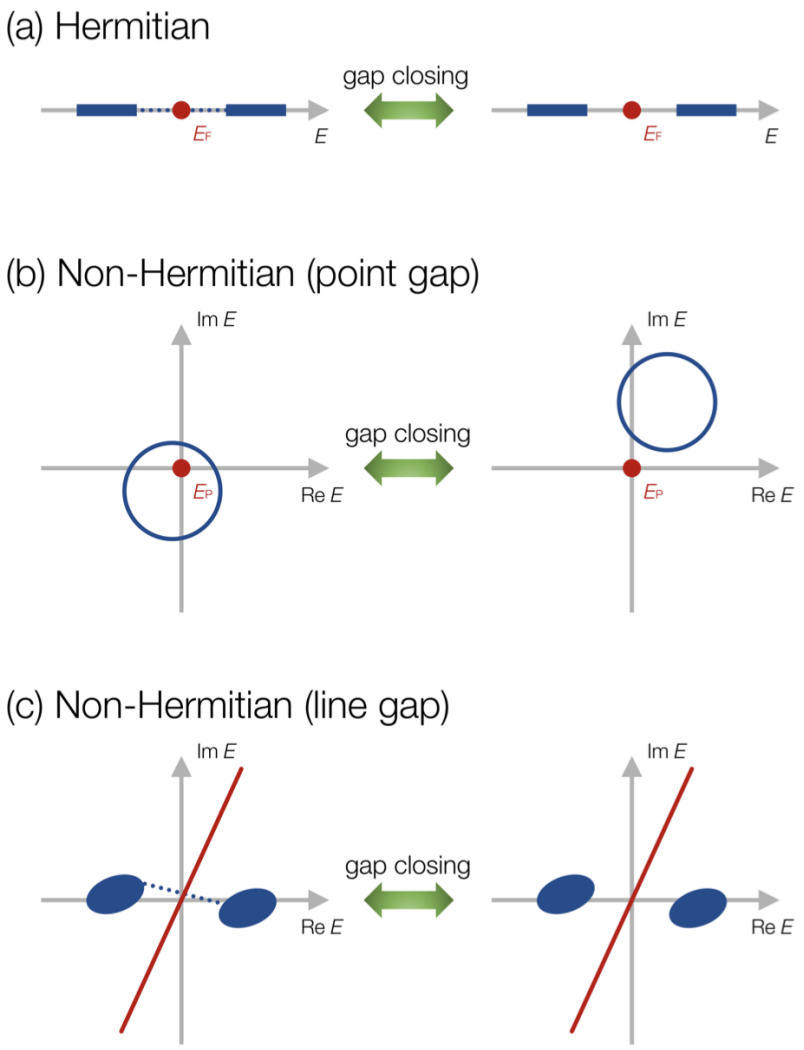

Figure 3.1: *Energy gaps in nH systems. It shows their gap closing. In (a), Hermitian gap closing occurs when the energy spectrum crosses the Fermi level. In (b), point gap closes when the spectrum crosses the reference energy point E_P. In (c), line gap closes when there are energy eigenvalues connect the energy spectrum on the two sides. The figure is taken from Ref.[2].*

E_P. For example, in presence of time reversal symmetry (TRS) $\mathrm{Im}(E_P) = 0$ because the eigenenergies are in (E, E^*) pairs. Also, for having the sub lattice symmetry (SLS) it should be zero $E_P = 0$, because the energy spectrum come in $(E, -E)$ pairs.

> Definition 1: A non-Hermitian Hamiltonian H(k) is defined to have a point gap if and only if it is invertible (i.e. , for all k $\det(H(k)) \neq 0$) and all the eigenenergies are nonzero (i.e. , for all k $E(k) \neq 0$). [2]

III.2 Line gap

A line in the complex energy spectrum, which separates energy spectra to two regions, has also restrictions due to the symmetry. Mostly, we can take as a line gap the real axis $\mathrm{Im}(E) = 0$ or the imaginary axis ($\mathrm{Re}(E) = 0$). For example, in presence of TRS the eigenenergies come in pairs (E, E^*), then the real axis (imaginary gap) would be the line separating the energy spectrum. Whereas, in presence of chiral symmetry CS the energies come in $(E, -E^*)$ pairs, then the imaginary axis (real gap) would be the line.

> Definition 2: A non-Hermitian Hamiltonian $H(\boldsymbol{k})$ is defined to have a line gap in the real (imaginary) part of its complex spectrum [real (imaginary) gap] if and only if it is invertible (i.e., $\forall \boldsymbol{k}\ \det H(\boldsymbol{k}) \neq 0$) and the real (imaginary) part of all the eigenenergies is nonzero [i.e., $\forall \boldsymbol{k}\ \mathrm{Re}(E(\boldsymbol{k})) \neq 0$ ($\mathrm{Im}(E(\boldsymbol{k})) \neq 0$)].[2]

The existence of the imaginary gap means the system has significant nonequilibrium wave dynamics, which has no counterpart in the band theory with Hermiticity. [2]

IV Unitary and Hermitian flattening of energy spectrum

IV.1 Unitary flattening for systems with point gap

Every nH Hamiltonian $H(\boldsymbol{k})$ with a point gap can be flattened to a unitary matrix $U(\boldsymbol{k})$ respecting its symmetry and without closing the point gap. The proof of that statement is in Ref.[2]. Thus the classification of the nH Hamiltonian becomes the classification of that unitary matrix. The extended Hermitian Hamiltonian of that flattened matrix then given by:

$$\tilde{H}(\boldsymbol{k}) := \begin{pmatrix} 0 & U(\boldsymbol{k}) \\ U^\dagger(\boldsymbol{k}) & 0 \end{pmatrix}, \qquad \tilde{H}^2(\boldsymbol{k}) = 1. \tag{3.15}$$

If the nH Hamiltonian $H(\boldsymbol{k})$ has the above discussed symmetries the corresponding extended Hermitian Hamiltonian $\tilde{H}(\boldsymbol{k})$ have the symmetries which are given in the following:

$$\tilde{\mathcal{T}}_\pm \tilde{H}^*(\boldsymbol{k}) \tilde{\mathcal{T}}_\pm^{-1} = \pm \tilde{H}(-\boldsymbol{k}), \quad \tilde{\mathcal{T}}_\pm := \begin{pmatrix} \mathcal{T}_\pm & 0 \\ 0 & \mathcal{T}_\pm \end{pmatrix}; \tag{3.16}$$

$$\tilde{\mathcal{C}}_\pm \tilde{H}^*(\boldsymbol{k}) \tilde{\mathcal{C}}_\pm^{-1} = \pm \tilde{H}(-\boldsymbol{k}), \quad \tilde{\mathcal{C}}_\pm := \begin{pmatrix} 0 & \mathcal{C}_\pm \\ \mathcal{C}_\pm & 0 \end{pmatrix}; \tag{3.17}$$

$$\tilde{\Gamma}\tilde{H}(\boldsymbol{k})\tilde{\Gamma}^{-1} = -\tilde{H}(\boldsymbol{k}), \quad \tilde{\Gamma} := \begin{pmatrix} 0 & \Gamma_{\pm} \\ \Gamma_{\pm} & 0 \end{pmatrix}; \tag{3.18}$$

$$\tilde{\mathcal{S}}\tilde{H}(\boldsymbol{k})\tilde{\mathcal{S}}^{-1} = -\tilde{H}(\boldsymbol{k}), \quad \tilde{\mathcal{S}} := \begin{pmatrix} \mathcal{S} & 0 \\ 0 & \mathcal{S} \end{pmatrix}; \tag{3.19}$$

$$\tilde{\eta}\tilde{H}(\boldsymbol{k})\tilde{\eta}^{-1} = -\tilde{H}(\boldsymbol{k}), \quad \tilde{\eta} := \begin{pmatrix} 0 & \eta_{\pm} \\ \eta_{\pm} & 0 \end{pmatrix}; \tag{3.20}$$

Additionally, all extended Hermitian Hamiltonian respects the chiral symmetry CS (or SLS) because of its off diagonal structure with the given symmetry operator Σ:

$$\Sigma\tilde{H}(\boldsymbol{k})\Sigma^{-1} = -\tilde{H}(\boldsymbol{k}), \quad \Sigma := \begin{pmatrix} 1 & 0 \\ 0 & -1 \end{pmatrix}; \tag{3.21}$$

Thus the topology of the nH Hamiltonian with point gap can be also given by the corresponding extended Hermitian Hamiltonian which respects the above symmetries and they are already obtained in the previous works [89, 90]

IV.2 Hermitian flattening for systems with line gap

In the presence of a line gap on the other side, we can flatten the non-Hermitian Hamiltonian into Hermitian (anti-Hermitian) Hamiltonian by keeping the real gap (imaginary gap) open and without breaking its symmetry. The proof for this statement can be also found in the Ref.[2]. As a result the topology of the corresponding Hermitian matrix is the same as the corresponding non-Hermitian matrix [89, 90]. Additionally, the topology of an anti-Hermitian matrix $H(\boldsymbol{k})$ with $H^{\dagger}(\boldsymbol{k}) = -H(\boldsymbol{k})$ under an imaginary gap has the same topology as the Hermitian matrix $iH(\boldsymbol{k})$ with a real gap [2, 91]. However, the resulting physics of these two anti-Hermitian $H(\boldsymbol{k})$ and the corresponding Hermitian $iH(\boldsymbol{k})$ matrices are different.[2]

V Topological invariant for non-Hermitian systems

Topological invariant for nH systems depends on the type of their energy gap in addition to the dimensionality and the symmetries of the system. In this section we take a look at the definitions of the winding numbers for some particular cases. The type

of the invariant for particular systems can be determined considering separately the symmetries. [2]

The extended Hermitian Hamiltonian $\tilde{H}(\boldsymbol{k})$ and its nH Hamiltonian $H(\boldsymbol{k})$ carry topological correspondence which was shown by Gong et al. [75]. Because the extended Hermitian Hamiltonian $\tilde{H}(\boldsymbol{k})$ respects CS, the topological invariant that specifies the system is given as

$$W_{2n+1} := \frac{n!}{(2\pi i)^{n+1}(2n+1)!} \int tr(H^{-1}dH)^{2n+1} \tag{3.22}$$

this topological winding number is the same as the spectral winding number for the point gaps in systems without symmetries, which is in total contrary to the Hermitian case where the Chern numbers characterize band structures for even dimensional systems without symmetries. Based on the observation of this correspondence between extended Hermitian Hamiltonian and its nH Hamiltonian the periodic table of nH Hamiltonians was first made recently by Gong et al. [75].

V.1 Wess-Zumino term as topological invariant

The Wess-Zumino (WZ) term was originally used in high energy physics and later as a topological term in disordered 2D superconducting systems as well as for the quantum mechanical path integral formulation of a single spin system as a effective Langrangian term. [92, 93]

The WZ term depends on the spatial property of the system. This geometrical topological invariant can be used thus to determine the topological phases for the systems in 2D with certain spatial symmetries and is given as the following integral

$$WZ[H] = \int_{T^2\times[0,1]} tr\left[H^{-1}dH\right]^3 = \int_0^1 \int_0^{2\pi} \int_0^{2\pi} \frac{d^2kdt}{24\pi^2} \epsilon^{ijk} tr(H^{-1}\partial_i H H^{-1}\partial_j H H^{-1}\partial_k H) \tag{3.23}$$

The matrix H in the integral is not the system Hamiltonian but it is an extension of the Hamiltonian we are interested in. They are given in the following way. In the case when one dimensional winding number is zero, there exists smooth path between an invertible Hamiltonians $H(k_x, k_y, t)$

$$H(k_x, k_y, t = 0) = H(k_x, k_y) \tag{3.24}$$

to a final constant Hamiltonian:

$$H(k_x, k_y, t = 1) = H_{const} \tag{3.25}$$

This integral in Eq.(3.23) is a real number which takes value in the circle $[0, 1]$ and which can be quantized under certain spatial symmetry. Further condition on the H_{const} is given later in chapter 6. There are certain ways of extending the Hamiltonian $H(k_x, k_y) \to H(k_x, k_y, t)$ so that the difference between two different extensions $H(k_x, k_y, t)$ and $H'(k_x, k_y, t)$ is integer valued three dimensional winding number of third homotopy class $\pi_3(GL_N(\mathbb{C})) = \mathbb{Z}$ (Two functions are said to be in a homotopy class, if one function can be continuously deformed to other function), where N is the dimension of the system $H(k_x, k_y)$ [94].

VI Bulk-boundary correspondence

This section is taken from Ref.[1].

We know the bulk boundary correspondence from Hermitian systems. That is the property where we can compute the topological invariant from Bloch Hamiltonian (means for infinite system) and if this is non-trivial then the system is topologically non-trivial. In that case, we already know that there are boundary states for the system in OBC. When BBC is valid then the energy dispersion of the case with OBC and PBC have the similar shape. In many nH Hamiltonian the spectra in PBC and OBC look totally different, which is called spectral instability by opening the boundary condition. This is due to the topological phase transition from PBC to OBC. In that case we also always observe the skin states at the boundary. As mentioned previously, the skin states appear due to the existence of the EPs.

However, due to some symmetries in the system the skin states can also be forbidden. Due to the PT-symmetries the skin states do not pile up at the boundaries [82].

Because the conventional BBC is broken in nH systems, we want to reconstruct the BBC for nH systems. There were several tries to reconstruct the BBC, however, they are not yet complete. Further please refer to the Ref.[1]

One of the approaches to reconstruct the BBC is building singular value decomposition (SVD). With SVD we can reconstruct the cBBC for the models where the cBBC is broken in case of eigenvalue spectrum. The spectrum in PBC has the same shape as the spectrum in OBC and in OBC case we see the boundary modes. [95] However, the exotic features of nH properties can not be covered with SVD approach. In the following we look at the definition of the SVD.

VI.1 Singular value decomposition

This section is mainly based on the Ref.[96]

Singular value decomposition (SVD) is used in many context, such as dimension reduction of data based on their biggest singular values [97], reestablishing of bulk boundary correspondence in non-Hermitian systems [1] and renormalization group procedure [22]. An another use is to inspect if a transformation is unitary by performing the singular value decomposition [98].

The definition for SVD is given as follows: Let $\boldsymbol{M}$ be any complex $m \times n$ matrix. Then $\boldsymbol{M}$ can be written in the factorized form as:

$$\boldsymbol{M} = \boldsymbol{U} \cdot \boldsymbol{\Sigma} \cdot \boldsymbol{V}^{\dagger} \tag{3.26}$$

which is called singular value decomposition (SVD). $\boldsymbol{\Sigma}$ is an $m \times n$ diagonal matrix with r distinct positive real entries $\sigma_i = \boldsymbol{\Sigma}_{ii}$ (where $i = 1, 2, ..., r$ and $r \leq m$) which are known as singular values of the matrix $\boldsymbol{M}$. $\boldsymbol{U}$ is an $m \times m$ and $\boldsymbol{V}$ is an $n \times n$ unitary matrix, correspondingly. The column vectors of $\boldsymbol{U}$ and $\boldsymbol{V}$ are left- and right-singular vectors of matrix $\boldsymbol{M}$ and form a set of orthonormal eigenvectors of $\boldsymbol{M}\boldsymbol{M}^{\dagger}$ and $\boldsymbol{M}^{\dagger}\boldsymbol{M}$, respectively and thus the σ_i are the square roots of non-negative eigenvalues of the corresponding matrices. The matrices $\boldsymbol{U}$ and $\boldsymbol{V}$ are not unique, however they can be always chosen so that the entries σ_i are in descending order. Using SVD, we can also determine the range, null space and rank of the matrix $\boldsymbol{M}$. More specifically, the number of the non-zero singular values is the rank of matrix, $rank(\boldsymbol{M}) = r$ and corresponding singular vectors (of the non-zero singular values) span the range of matrix $\boldsymbol{M}$. Therefore, the number of right-singular vectors with vanishing singular values span the null space of matrix $\boldsymbol{M}$: $\boldsymbol{M}\vec{v}_k = \vec{0}, \quad \text{for} \quad k = m - r, m - r + 1, ..., m.$ [96]

Chapter 4

Methods

To reconstruct the bulk boundary correspondence we should be able to construct the bulk Hamiltonian. The models of this research project are given in tight-binding formalism. When the bulk Hamiltonian is given we want to know if there are boundary states. To know if we have just a few boundary states or if there exist skin states, we need a method to see where the biggest probability of the real space eigenvectors can be found. For that purpose, we calculate the inverse participation ratio (IPR) values to see how many states are how much localized on the lattice. However, we do not know where on the lattice the well-localized states can be found, somewhere on the bulk side or at some boundaries. To know that we can construct the probability density profile and see exactly where the biggest probabilities can be found.

Except for the analytical calculation of the Wess-Zumino term, the diagonalization and calculations were done using the linear algebra libraries in Python.

I Tight binding models

This section is taken from Ref.[99].

The models I used in my thesis are the matrix forms in tight-binding formalism. The formalism focuses on the basis orbitals which are used to describe the outermost valence and the lowest conduction states of the given system. The orbitals are never built explicitly, instead they are appproximated by linear combination of atomic orbitals (LCAO) [100], which are usually taken single electron eigenfunctions (orbitals) $\varphi_j(\boldsymbol{r} - \boldsymbol{R}_n)$ of isolated Hydrogen-type atoms:

$$\psi_m(\boldsymbol{r}) = \sum_{\boldsymbol{R}_n} b_m(\boldsymbol{R}_n)\varphi_m(\boldsymbol{r} - \boldsymbol{R}_n), \tag{4.1}$$

here $\boldsymbol{R}_n$ is atomic position in the crystal and $b_m(\boldsymbol{R}_n)$ are the coefficients or the contribution of that orbital. m refers to the m-th energy level. [99, 101] The wavefunction $\psi_m(\boldsymbol{r})$ is the solution of the following time-independent single electron Hamiltonian:

$$H(\boldsymbol{r}) = H_{at}(\boldsymbol{r}) + \sum_{\boldsymbol{R}_n \neq 0} V(\boldsymbol{r} - \boldsymbol{R}_n) = H_{at}(\boldsymbol{r}) + \Delta U(\boldsymbol{r}), \tag{4.2}$$

H_{at} is single atomic Hamiltonian and $V(\boldsymbol{r}-\boldsymbol{R}_n)$ is the potential contribution of the atom at $\boldsymbol{R}_n$ and this is assumed small. Then, the sum can be written as a small potential contribution $\Delta U(\boldsymbol{r})$. [99, 101]

Bloch theorem tells us that the wave function in a crystal changes only by a phase factor with the periodicity of the lattice. To get the energy for the m-th energy band, we assume only the m-th atomic energy level with the energy ϵ_m contributes:

$$\epsilon_m = \int d^3r \psi_m^*(\boldsymbol{r}) H(\boldsymbol{r}) \psi(\boldsymbol{r}) \tag{4.3}$$

$$= E_m - \frac{\beta_m + \sum_{\boldsymbol{R}_n \neq 0} \sum_l e^{i\boldsymbol{k}\cdot\boldsymbol{R}_n} \gamma_{m,l}(\boldsymbol{R}_n)}{1 + \sum_{\boldsymbol{R}_n \neq 0} \sum_l e^{i\boldsymbol{k}\cdot\boldsymbol{R}_n} \alpha_{m,l}(\boldsymbol{R}_n)}, \tag{4.4}$$

here $\psi(\boldsymbol{r})$ is the linear combination of all wavefunctions of each atom in the crystal. E_m is the energy for atomic level-m. $\alpha_{m,l}$, β_m and $\gamma_{m,l}$ are the so-called tight binding matrix elements. [99, 101]

The element β_m is the atomic energy shift which come from the potentials of the neighboring atoms:

$$\beta_m = -\int \phi_m^*(\boldsymbol{r}) \Delta U(\boldsymbol{r}) \phi_m(\boldsymbol{r}) d^3r, \tag{4.5}$$

The interatomic matrix element between the atomic orbitals m and l coming from the neighboring atoms is the next element $\gamma_{m,l}$:

$$\gamma_{m,l} = -\int \phi_m^*(\boldsymbol{r}) \Delta U(\boldsymbol{r}) \phi_l(\boldsymbol{r} - \boldsymbol{R}_n) d^3r, \tag{4.6}$$

The third one is the overlap integral of the atomic orbitals m and l on neighboring atoms:

$$\alpha_{m,l} = -\int \phi_m^*(\boldsymbol{r}) \phi_l(\boldsymbol{r} - \boldsymbol{R}_n) d^3r, \tag{4.7}$$

For good description of band structure using tight binding formalism, the terms $\alpha_{m,l}$ and β_m are assumed to be small. [99, 101]
In the tight binding formalism the second quantized Hamiltonian using the atomic orbitals as basis states is written as follows:

$$H = -t \sum_{\langle i,j\rangle,\sigma} (c^{\dagger}_{i,\sigma} c_{j,\sigma} + h.c.), \tag{4.8}$$

where t is the hopping integral, $c^{\dagger}_{i,\sigma}(c_{j,\sigma})$ is the creating (and annihilating) operators with the spin polarization σ between the nearest neighbors $\langle i,j\rangle$ and their hermitian conjugates $(h.c.)$. The hopping term t corresponds to the interatomic matrix element γ in above tight binding formalism. When $t = 0$ the case corresponds to isolated atom and it is impossible for the electron to hop. When t is non zero the electrons can reside on both sides so that the kinetic energy can be lowered. [37, 101]

Using tight binding models one can illustrate intuitively the Berry phases, Berry curvature, electric polarisation, magnetoelectric couplings, and topological insulators. [37]

II Wyckoff positions

By calculating the Wyckoff position we can know where the states can be found in a unit cell and understand the probability density profile. On the other side, by looking at the probability density profile we can maybe guess also what symmetry the system could possess. The definition for the Wyckoff positions are given by

> **Definition 2.** The orbit $\boldsymbol{a}_\alpha = g_\alpha \boldsymbol{q} | g_\alpha \notin G_{\boldsymbol{q}}$, $\alpha = 1, ..., n$ of a symmetry site $\boldsymbol{q}$ modulo lattice translations are classified by a **Wyckoff position** of multiplicity n. Note that we define the multiplicity with respect to the primitive, rather than the conventional cell.[102]

$$C_2 \mathcal{T} \psi(k_x, k_y) = C_2 e^{-i\boldsymbol{k}\cdot\boldsymbol{r}} \psi(k_x, k_y) = e^{i\boldsymbol{k}\cdot\boldsymbol{r}} \psi(-k_x, -k_y) \tag{4.9}$$

$e^{-i\boldsymbol{k}\cdot\boldsymbol{r}}$ is the eigenvalue for the translation operator on the Bloch wave function and $\boldsymbol{r} = (a, b)$ is the hopping length in 2D.

Applying the C_2 operator on the eigenvector (eigenstate in the valence band) at the high symmetry points we get the eigenvalues, which are listed in the table below.

By setting $a = 1$ and $b = 1$ we get for the TRIM points in 2 dimensions the following points $\Gamma = (0, 0)$, $M = (\pi, \pi)$, $X = (\pi, 0)$ and $Y = (0, \pi)$

Table 4.1: *C_2 eigenvalues of inversion symmetric 2D systems for s- and p-orbitals and corresponding Wyckoff positions.*

k points / Wyckoff positions	$\Gamma = (0,0)$	$M = (\pi,\pi)$	$X = (\pi,0)$	$Y = (0,\pi)$
$(0,0)$ (s-orbital)	1	1	1	1
$(\frac{1}{2},\frac{1}{2})$ (s-orbital)	1	1	-1	-1
$(0,\frac{1}{2})$ (s-orbital)	1	-1	1	-1
$(\frac{1}{2},0)$ (s-orbital)	1	-1	-1	1
$(0,0)$ (p-orbital)	-1	-1	-1	-1
$(\frac{1}{2},\frac{1}{2})$ (p-orbital)	-1	-1	1	1
$(0,\frac{1}{2})$ (p-orbital)	-1	1	-1	1
$(\frac{1}{2},0)$ (p-orbital)	-1	1	1	-1

For non-Hermitian Hamiltonians we donot have Fermi level, instead there are line gap and point gap on the energy spectrum on complex plane. To find The Wyckoff position in non-Hermitian systems we take the states with negative real energy part, because as mentioned above the nH Hamiltonian can be smoothly transformed to the Hermitian Hamiltonian if there is line gap. Therefore, the energy eigenstates with negativ real part would correspond to the occupied states. However, the Wyckoff positions for nH Hamiltonians are not well defined.

III Inverse participation ratio

The inverse participation ratio (IPR) is the measure of a state $|\psi\rangle$ how this is spread over a basis $|\alpha\rangle_{j=1}^{N}$, here N is the dimension of the basis. Explicitly said, if p_i is the probability of finding the (normalized) state $|\psi\rangle$ in $|\alpha\rangle_i$, then the IPR is defined as follows $I_\psi = \sum_i |\psi|^4 = \sum_i p_i^2$. Thus, if $|\psi\rangle$ is only located in a single state $|\alpha\rangle_0$, then $p_{i_0} = 1$ and $I_\psi = 1$(largest IPR), on the contrary, if $|\psi\rangle$ equally located in every state $|\alpha\rangle_i$ (equally distributed), $p_i = 1/N \quad \forall i$, then $I_\psi = 1/N$ (smallest IPR). Then the IPR is equal zero in thermodynamic limit. Therefore, the IPR is a measure of the localization of $|\psi\rangle$ in the corresponding basis. [103]

In other words, if the state is an eigenfunction $\langle r|\psi\rangle = \psi(r)$ at lattice site r of a tight binding model in its real space (lattice space) with the N number of lattice sites then the IPR with the above definition gives us the inverse number of orbitals which contribute

to this state. On the contrary, if we define the IPR (the actual definition of inverse participation ratio) to be $I'_\psi = 1/(N\sum_i |\psi(r)|^4) = 1/(N\sum_i p_i^2)$, then this quantity gives us the proportion of the total number of atoms in that system contributing to the corresponding eigenstate. [104] We can see this difference in the following example. When we have a wavefunction spreads over l lattice sites supposing with the equal probability amplitude $|\psi_i(r)|^2 = 1/l$ and zero on the remaining lattice sites. Then we have $I'_\psi = l/N$ and $I_\psi = 1/l$. [104]

Now, we define the IPR in non-Hermitian system. Let us use the notation $IPR(|R_n\rangle)$ of a mode $|R_n\rangle$ instead of I_ψ. In Hermitian systems the left eigenvector and right eigenvector are the same for each state, therefore the IPR for Hermitian system is defined as follows using only the "right" eigenvector [105]:

$$IPR(|R_n\rangle) = \frac{\left(\sum_{j,\sigma=A/B} |\langle j,\sigma|R_n\rangle|^2\right)^2}{\sum_{j,\sigma=A/B} |\langle j,\sigma|R_n\rangle|^4}, \tag{4.10}$$

here the 'right' eigenmode is in the real space basis $|j,\sigma\rangle$ of the single particle Hilbert space. The j-index denotes the unit cell and the $\sigma = A/B$ the sublattice. This definition has more complicated form in order to normalize the eigenstate $\langle j,\sigma|R_n\rangle$. [105] If we have a nH Hamiltonian, then using the bi-orthogonal formulation of quantum mechanics [106], the observable can be calculated $\langle\mathcal{O}\rangle_{RL} = \langle\phi^L|\mathcal{O}|\phi^R\rangle$. Then to calculate the (bi)localization using the left and right eigenvectors the IPR can be defined in the following way [105]:

$$IPR^{RL}(|R_n\rangle) = \frac{\left(\sum_{j,\sigma=A/B} |\langle L_n|j,\sigma\rangle\langle j,\sigma|R_n\rangle|\right)^2}{\sum_{j,\sigma=A/B} |\langle L_n|j,\sigma\rangle\langle j,\sigma|R_n\rangle|^2}, \tag{4.11}$$

When studying the singular value decomposition $H = U\Lambda V^\dagger$, we could also write the IPR for the $|U_n\rangle(|V_n\rangle)$ is the n^{th} column of U(V) matrices

$$IPR^{SVD}(|U_n\rangle) = \frac{\left(\sum_{j,\sigma=A/B} |\langle V_n|j,\sigma\rangle\langle j,\sigma|U_n\rangle|\right)^2}{\sum_{j,\sigma=A/B} |\langle V_n|j,\sigma\rangle\langle j,\sigma|U_n\rangle|^2}. \tag{4.12}$$

IV Probability density profile

To build the probability density profile we first have to find the eigenstate from the Hamiltonian built in real space. Then we can calculate the probability at each site of the lattice. The number in $[0,1]$ would be the probability for electron to be found at one lattice site. When the hoppings of the system is given then we can find the real space

tight-binding Hamiltonian by systematically building the matrix for a chosen size N of the system.

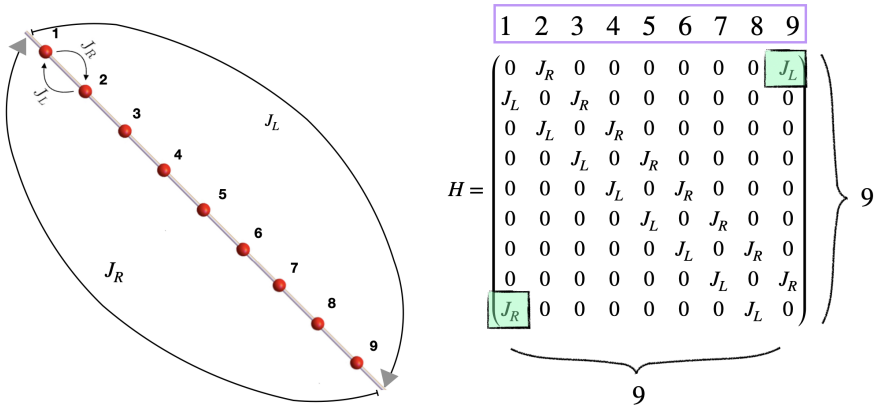

Figure 4.1: *Building the real space matrix from the hopping strengths for 9 unit cells. On the left, we see Hatano-Nelson model with 9 unit cells and the hopping J_L and J_R connecting the sites 1 and 9 are the boundary condition. On the right, the hopping strengths in green boxes are in presence of periodic boundary condition and without them in open boundary condition.*

Whereas when the system is given in Bloch form, then we should make the Fourier transform in each direction depending on the dimension of the system. Then Fourier transformed blocks are used to build the whole hopping real space matrix. These can be all done numerically on python. After building the real space Hamiltonian we can calculate the eigenvectors $\psi(\boldsymbol{x})$ of the Hamiltonian using the linear algebra libraries in python. Depending on the numeration of the lattice site on building the real space Hamiltonian we should reshape the whole length of the probability density amplitudes $|\langle\psi(\boldsymbol{x})|\hat{r}|\psi(\boldsymbol{x})\rangle|^2$ to 2 or 3 dimensions, here $\hat{r}$ is the position operator. Examples of the density profile for 2D are given in Fig.(4.2).

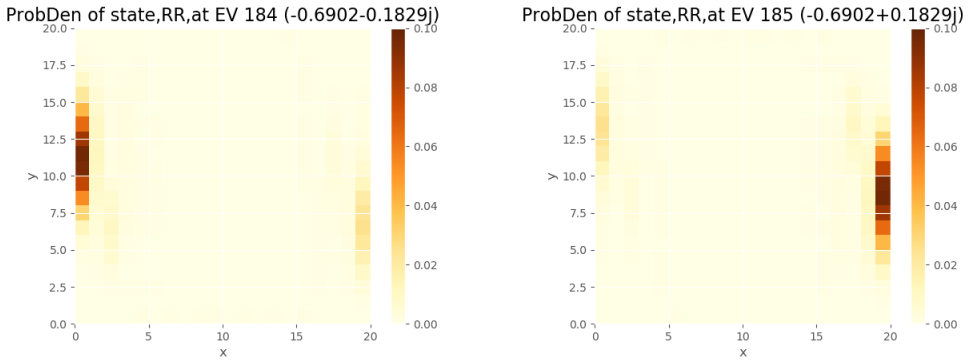

Figure 4.2: *The probability density profile for π-flux (2D model). In brackets we have its energy eigenvalue. The numbers 184 and 185 are the numbers come from their eigenvalues numbering to sort with its real part of the eigenvalues for a system with 20×20 unit cells. 184 and 185 correspond to the states in the middle of the spectrum. They are taken with the biggest IPR values and we see that the eigenstates with biggest IPR values are in the middle of the spectrum, because we would expect that they are in the middle of point energy gap.*

Chapter 5

The 1st model: π-flux model

I Introduction

The Hermitian π-flux Hamiltonian is given by the first term with the hopping strength t in the Hamiltonian in Eq.(5.1). The second term with the hopping strength ir is the non-Hermitian diagonal hopping term. The model and its spectrum is illustrated on Fig.(5.1) [4]

$$H(k_x, k_y) = t \begin{pmatrix} 2\cos k_y & 1 + e^{-ik_x} \\ 1 + e^{ik_x} & -2\cos k_y \end{pmatrix} + ir \begin{pmatrix} 0 & e^{ik_y} \\ e^{-ik_y} & 0 \end{pmatrix} \tag{5.1}$$

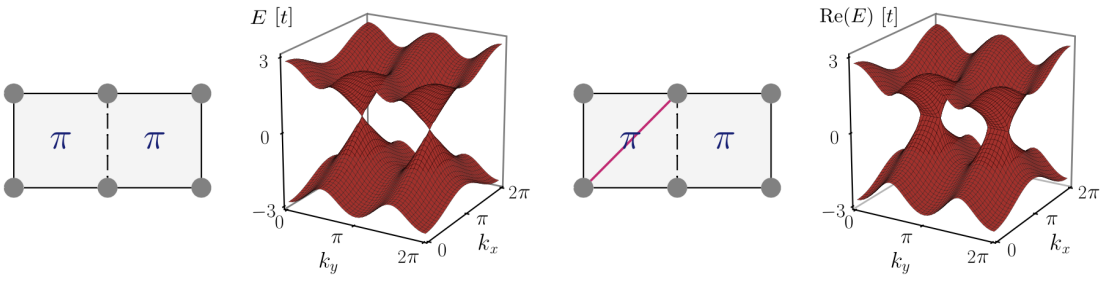

Figure 5.1: *The hopping strengths on the lattice. Solid black line is hopping t and dashed line is for $-t$. On the left the π-flux model which is Hermitian model and its spectrum is shown. On the right the red diagonal hopping is the nH term in the Hamiltonian. On the right, the corresponding spectrum is shown by taking only real part of the energy. [4] The figure is taken from Ref.[4]*

The Hermitian π-flux model has 2 Dirac cones since the Dirac cones must come in pairs [54]. By adding the nH term, each Dirac cone forms two EPs. The whole Hamiltonian might not contain any symmetries. However, the degenerate points are stable because the EPs are stable in already 2D, which is different from Hermitian systems [7]. The real part of the energy degeneracy, we see in Fig.(5.1), is the Fermi-arc mentioned in

the Ref.[7], which connects a pair of EPs. By plotting the imaginary part of the energy spectrum we will see the iFermi-arc (only imaginary energy eigenvalues due to the branch cut).

The π-flux model is reciprocal as it satisfies the condition $H(k_x, k_y) = H^T(-k_x, -k_y)$. By adding nH term the Hamiltonian is still reciprocal and it is interesting to study. As we mentioned in the previous Chapters until now one-dimensional models were investigated mostly and those models had different hopping strength to right and left so that the skin states were piled up at one of two ends. On the contrary π-flux skin states pile up at both of the edges in 2D.

The nH hopping depends on k_y we can build a ribbon geometric Hamiltonian which is in y-direction periodic and x-direction open. Then the whole ribbon geometric Hamiltonian is also $\tilde{H}^T(k_y) = \tilde{H}(-k_y)$ reciprocal, where the $k_y \in [0, 2\pi]$ is the boundary momentum. [7] However, at each k_y the system breaks the reciprocity. The 1D ribbon model exhibits skin effect and we can calculate the winding number if the winding number can predict the skin effects, in which case the 1D winding number is called the *weak* topological invariant. We will see also the skin effect appears in the y-direction and not in the x-direction. For particular k_y skin effect appears and reciprocity relates to the existence of the skin states at $-k_y$ at the other boundary. The strongest localization was found at $\pi/2$ and $3\pi/2$, where the Dirac points were touching in Hermitian π-flux model. Because the Hamiltonian $\tilde{H}(k_y)$ is reciprocal at the (time-reversal invariant momenta = TRIM) points $k_y = 0, \pi$, the states are there delocalized. [4]

II Results

II.1 Exceptional degeneracy and energy spectrum

Firstly, I plotted the energy dispersion of π-flux Hermitian and non-Hermitian cases (see Ref.(5.2)). We see the EPs by taking the absolute values of the energy eigenvalues. When we plot the real part of the energies we can see the nH Fermi-arcs which connect the EPs. We can also observe the number of the exceptional points are even due to the non-Hermitian Fermion doubling theorem for 2D models [107], which appear by adding nH term to the system and the a Dirac cone can double to 2 EPs.

I also plotted the energy spectrum from real space Hamiltonian in fully open boundary condition (OBC) and periodic boundary condition (PBC) (see Fig.(5.3)). Due to the exceptional degeneracy we see the point gap in the PBC spectrum with reference energy $E_p = 0$, which confirms the bulk topology is non-trivial since there is a point gap.

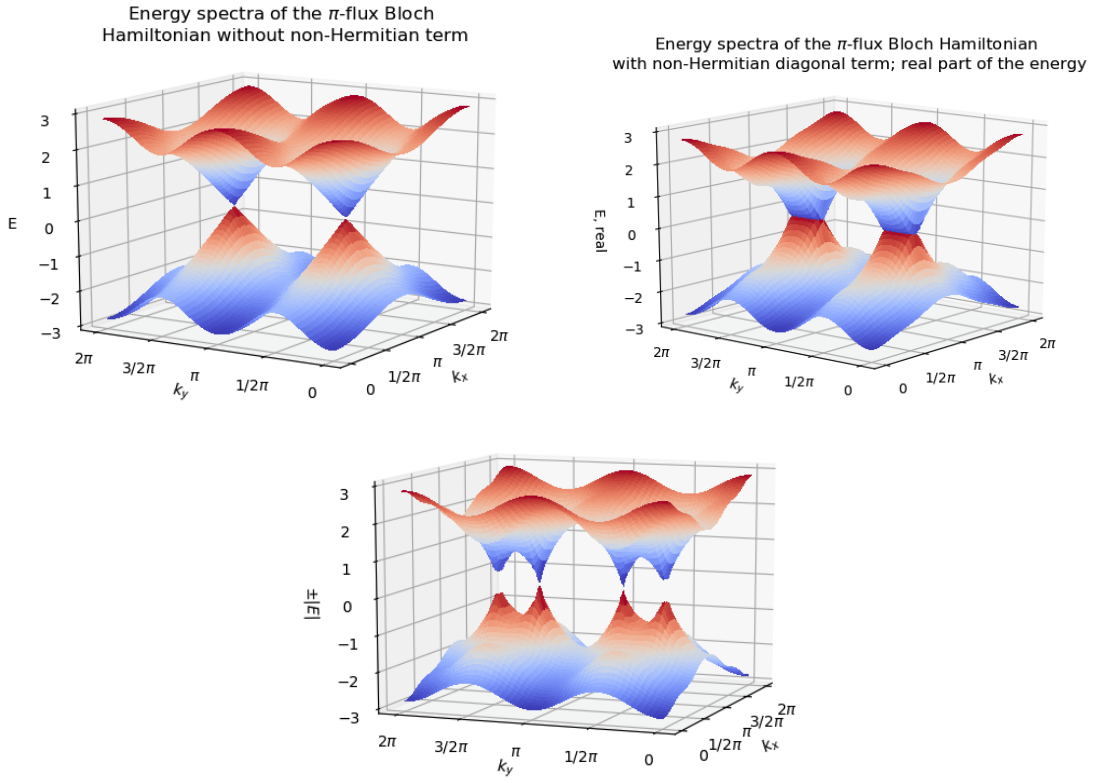

Figure 5.2: *On the top left, is the energy dispersion of the π-flux Bloch Hamiltonian in the Hermitian case. We see here the system has degeneracy at two points, which are called Dirac dispersion. On the top right, we see the real part of the energy dispersion with the nH hopping. We can also see the 4 EPs in the figure below by taking the absolute values of the energies. The gap at the exceptional point is due to the coarser k-grid.*

Each energy point is color-coded according to their IPR values of the corresponding eigenstates. The number of well localized eigenstates can be seen approximately on the IPR histogram (see Fig.(5.3)). There are 4 most localized states and they can be found inside the point gap of the energy spectrum with fully OBC. These most localized states must be the states with $k_y = \pi/2, 3\pi/2$ in $\tilde{H}(k_y)$ Hamiltonian where the initial Dirac point was located in the energy dispersion and we can confirm this later in the results for the ribbon geometric case.

II.2 Probability density profile

We know that the IPR values of the eigenstates tell us only how well a state can be localized, but it does not tell us the position of the localization on the lattice. Thus, to see where the highly localized mode can be found, we can plot the density profile of each eigenvector, which is shown in the Fig.(5.4). It makes sense that the localization of the skin modes are found in y-direction, because the nH term is k_y dependent. Also, x-axis of the Dirac points is at $k_x = \pi$ where the system is reciprocal and this means

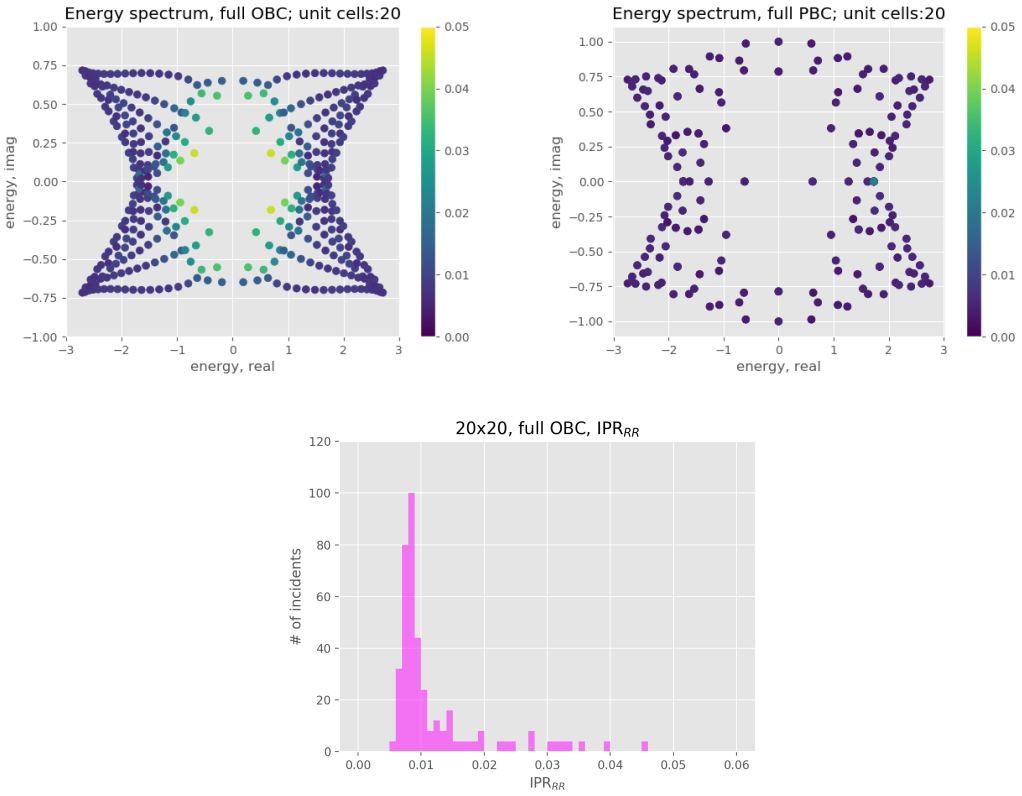

Figure 5.3: *On the top left, energy spectrum of the π-flux model in fully OBC for a system size 20x20 unit cells and the eigenvalues are color-coded according to their IPR values. On the top right, we see the energy spectrum for fully PBC and color-coded with their IPR values. On the bottom, the histogram of the IPR values for all states in the system in fully OBC. If a state ψ_i is fully localized on one edge (although we cannot say with IPR values where the states are localized in the whole lattice), the IPR of the i-th state should be $I_{\psi_i} = \frac{1}{400} \cdot 20 = 0.05$. As we see on the histogram most of the states are not well localized (in this system there are $20 \times 20 = 400$ states).*

that the states are in that direction delocalized. The most localized 4 states are shown on Fig.(5.4). The numbers above the figures are the sorted values w.r.t. the real part of the eigenenergies and with that number the most localized IPR values are found.

I have calculated the IPR values of the states with different boundary conditions with all possible 4 conditions, i.e. xOByPB, xPByOB, fully OB, and fully PB, all in the real space. The states in x-direction PB are not well localized. However, the states are well localized in the y direction PB case, which also explains the probability density profile on Fig. (5.4), where the states are very well localized at the hinges along the y-axis. As in the Ref.[4] stated, the states on one boundary are well localized. It is also true that there are states with the same localization on the opposite boundary due to the reciprocal connection between the states at k_y and $-k_y$.

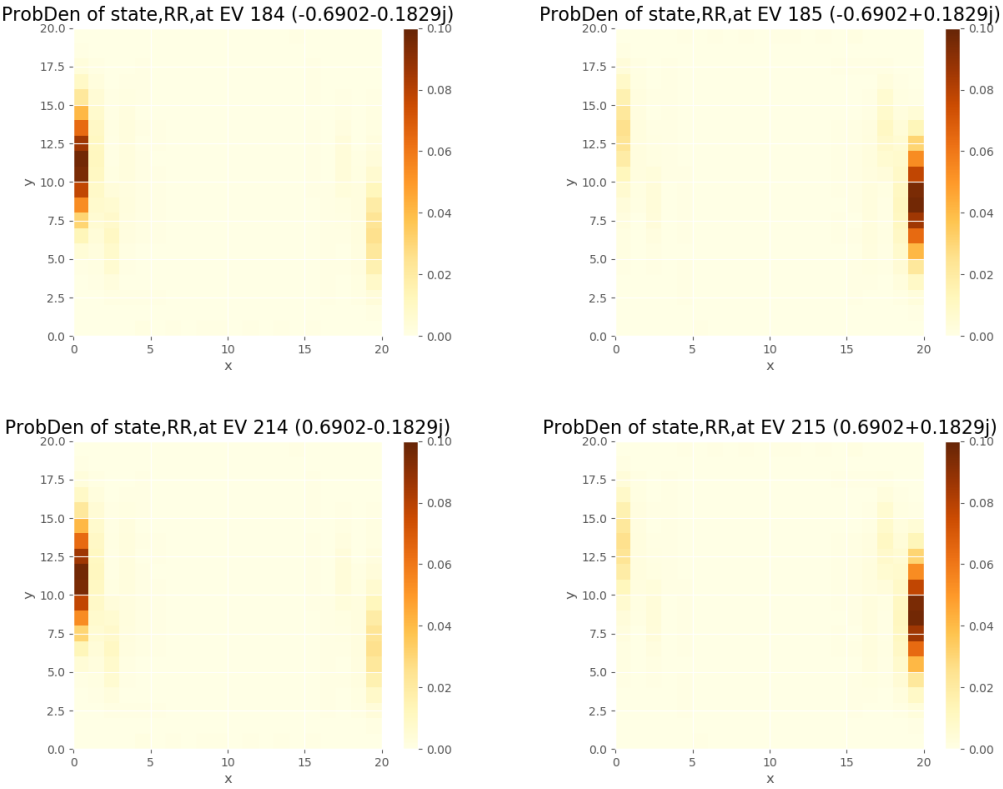

Figure 5.4: *The probability density profile of the most localized 4 states. The localization was determined by the IPR values of the whole eigenstates of the system with 20x20 unit cells in full OBC. The color bar shows the probability strength per unit cell. The probability density is calculated with the right and right eigenvectors (RR). The complex number in the bracket is the energy eigenvalue of that state. The numbers after the EV are the numbers that sorted the energy eigenvalues w.r.t. the real part of the eigenenergy and using them chosen from their IPR values. These numbers are approximately in the middle of the numbers 400 because the edge states can be found inside the point gap as we see in Fig.(5.3) on the top left.*

II.3 Ribbon geometry

To investigate the system further we make the system in x or y direction periodic and this is possible because we know the hoppings in the real space explicitly. I perform the Fourier transform to the Hamiltonian along the periodic side. By taking the open chain (for example) in x-direction, we have a k_y dependence and construct this Hamiltonian which can be called ribbon/slab geometric Hamiltonian. Then, we can look at the energy dispersion for the ribbon geometric Hamiltonians which depends on k_y values (see Fig.(5.6)). Each real and imaginary part of the energy eigenstates for the Hamiltonian $\tilde{H}(k_y)$ with open boundary ribbon and periodic boundary ribbon cases were plotted. Ribbon geometric Hamiltonian with open boundary means the 2 ends of the model in x-direction are not connected. Periodic boundary when they are connected with the x-direction hopping strength. In the Fig.(5.6) we see that the bulk boundary correspondence is violated as the spectral flow from the dispersion of periodic ribbon case to

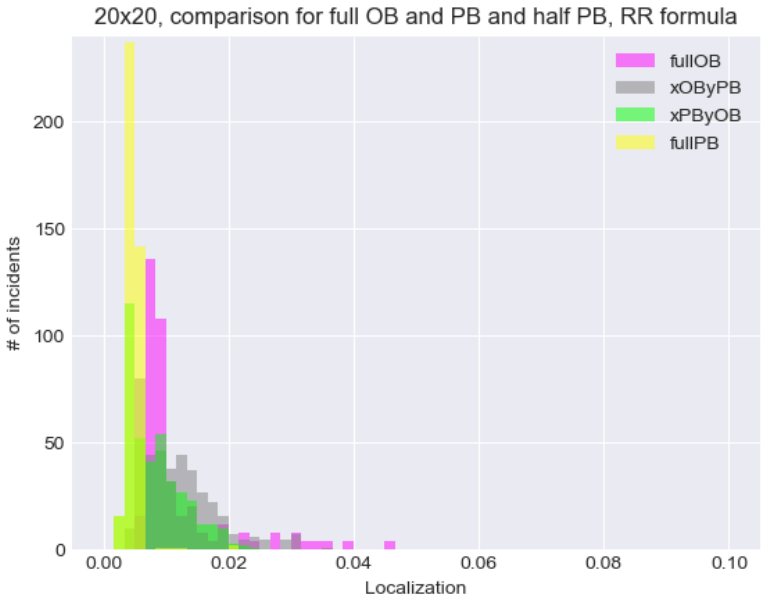

Figure 5.5: *Localization with different boundary conditions for the 4 cases: fully OBC, xOByPB, xPByOB, and fully PBCs. The most localized states are expected for the conditions fully OBC and xOByPB, which are pink and gray coloured histogramms.*

the dispersion with open ribbon cases does not resemble. Spectral flow means how the spectrum changes by opening the boundary conditions. In the real energy dispersion of the OB ribbon, we see the band touching at the initial Dirac momenta for the Hermitian π-flux dispersion.

II.4 1D winding number

At a fixed k_y (or k_x, depending on in which direction PB) the model can be seen as a one-dimensional model and we can calculate the 1D winding number to see if the invariant can predict the skin states.

When we have a first order skin effect the 1D winding number is expected to be non-trivial for the quasi 1 dimensional model, which is realized by ribbon-geometric Hamiltonian.

The boundary hopping of the ribbon ends was changed to see how the spectrum would change according to the hopping strength at the boundary. Even with the small hopping strength the spectrum did not change much compared with the hopping strength as much as the system hopping. When the boundary hopping is zero the spectrum collapses and there are no point gap any more. The spectrum of the all ribbon geometric Hamiltonian with the periodic boundary with any strength would look like the spectrum on Fig.(5.7) on the top.

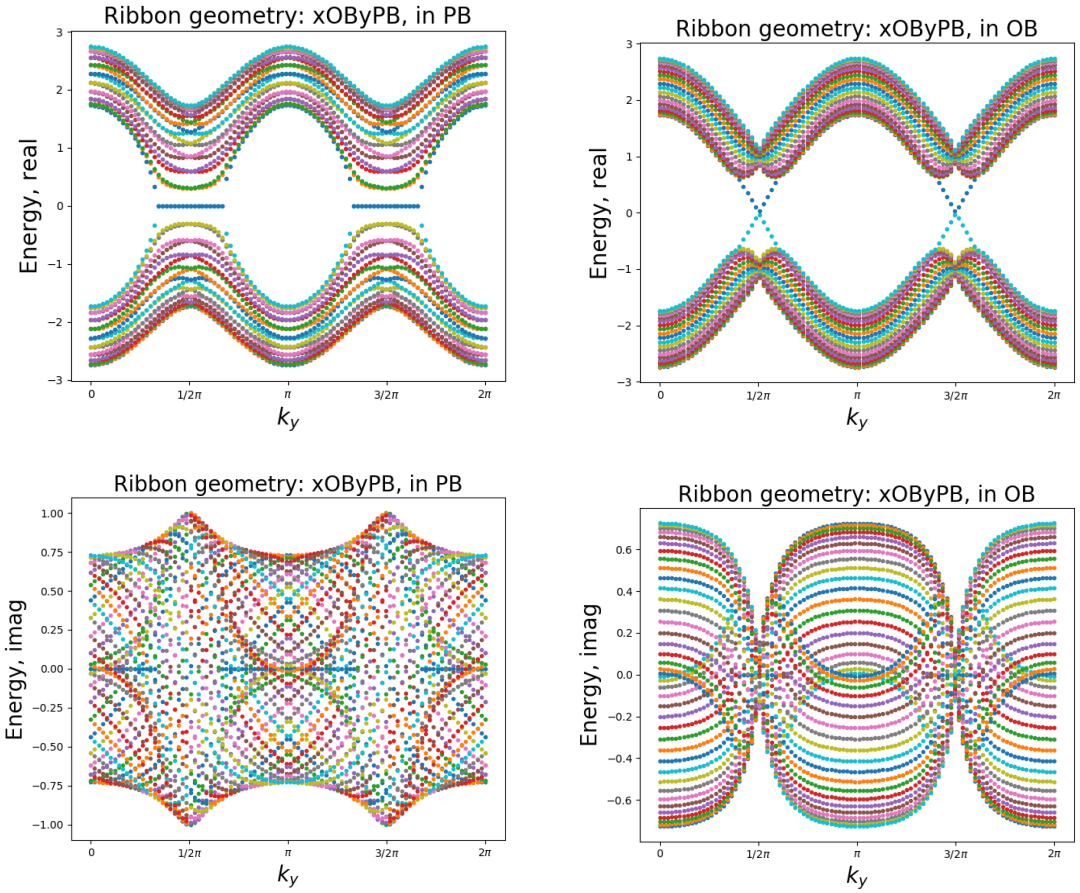

Figure 5.6: *On the left (top and bottom), real and imaginary part of the energy dispersion of the Hamiltonian in x open chain and in k_y dependent ribbon geometric case with the PBC by connecting ends in x. On the right (top and bottom), the real and imaginary part of the energy dispersion with the Hamiltonian with the same boundary conditions as on the left but open ribbon ends in x. We see the spectral flow breaking after opening the boundary of the ribbon Hamiltonian from left to right. In the periodic boundary case, we see the nH Fermi-arc or nH iFermi-arc type zero energy states on the real and imaginary energy dispersions which connect pair of exceptional points.*

When the boundary of the ribbon geometry are connected (now with the proper system strength) (Fig.(5.7) on the top left) we can compute the 1D winding numbers. The spectra for the $k_y = \pi/2, 3\pi/2$ cases are on top of each other so that we can see only one of the colors which is cyan. Here the winding number is -1. Then when we look at the energy spectrum of the 20x20 lattice with xOByPB cases below that figure we see the state in the middle is most localized according to the IPR value.

We see also (Fig.(5.7) on the top left) for the other k_y values when the winding is non-zero the states in the real space are also relatively well localized according to the IPR values. However, for the k_y points except $k_y = \pi/2, 3\pi/2$ values, we have line gap and point gap. If we have only point gap for the case of $k_y = \pi/2, 3\pi/2$, then the energy spectrum has only point gap. When the spectrum is not showing point gap at all in closed ribbon geometry, then the IPR values are also very small.

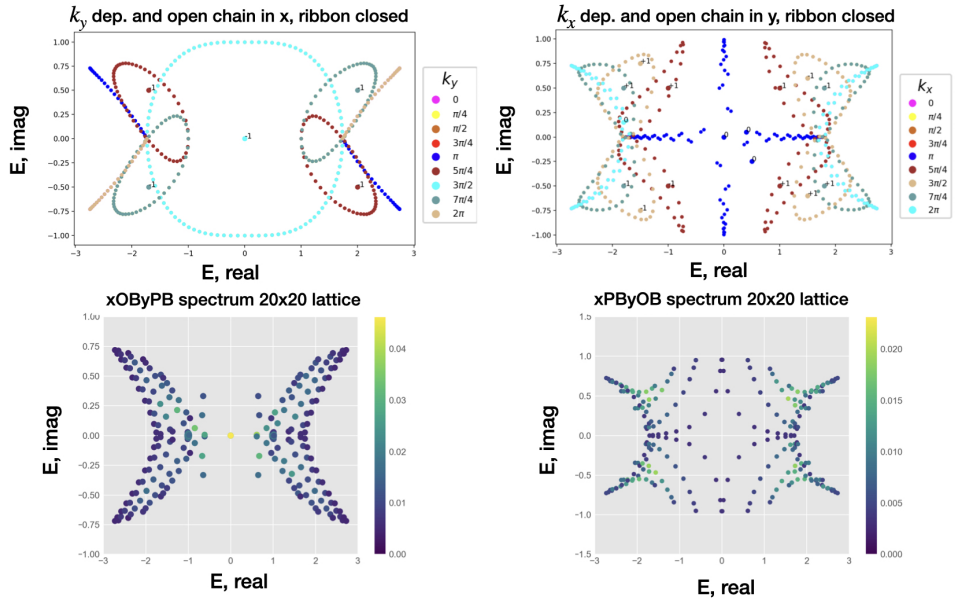

Figure 5.7: *On the top, we see the energy spectra for ribbon geometric Hamiltonian for every fixed k_y and k_x values given by the colors. On the side bar, we see the corresponding color-code with the k-values. On the bottom, we see the energy spectra for the lattices with xOByPB condition (on the left) and xPByOB condition (on the right) with the size 20×20. The energy spectrum is color-coded with its IPR values which are given on the side bar. The IPR values are calculated with the right and right eigenvectors. In the ribbon geometric case, the 1D winding numbers were calculated and noted inside the point gaps and the reference energy for the calculation of the winding numbers are noted beside the values with the corresponding colors.*

In case of k_x ribbon geometric case the energy spectra have 8-formed winding (Fig.(5.7) on the top right) so that we have positive winding number and negative winding number for a fixed k_x value due to their winding direction. Then, we look at their energy spectrum on the real space and indeed the most localized states can be found where the winding number is not zero. As predicted the winding number at $k_x = \pi$ is zero and its real space spectrum also totally delocalized (Fig.(5.7) on the bottom right), because the states are reciprocal due to the reciprocity condition.

II.5 SVD spectrum and recovery of BBC

Due to the fact that the bulk boundary correspondence is broken, we have to search other method to predict the boundary states or skin states. We could look into the singular value decomposition [1]. Additionally, I have plotted the singular value decomposition for the open boundary condition and perdiodic boundary condition for ribbon geometric Hamiltonian. In the case of SVD (in Fig.(5.8)) spectra we see that the bulk boundary correspondence is restored, because the form of the spectra in both cases are similar and in OBC there are zero states (Fig.(5.8) on the right bottom).

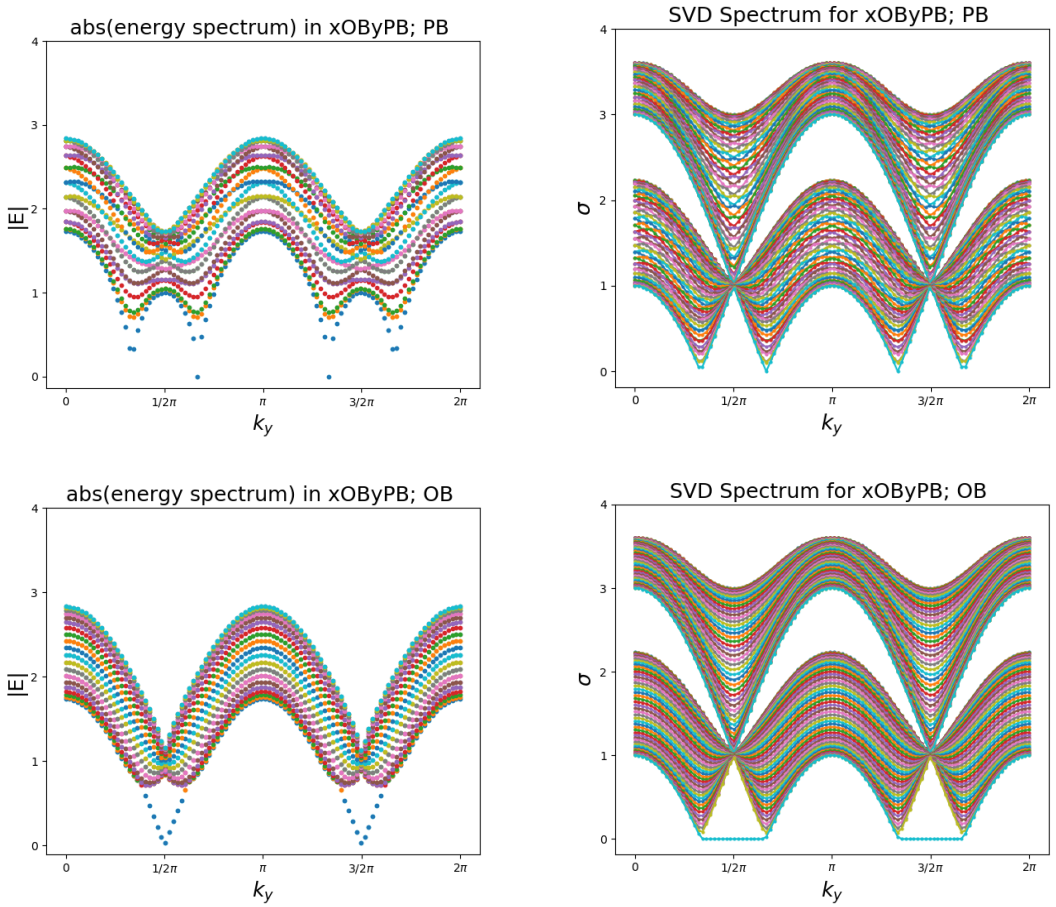

Figure 5.8: *On the top left, we see the energy dispersion in absolute values for the ribbon geometric Hamiltonian in the form of xOByPB case. On the top right, we see the dispersion of the SVD spectrum with the same ribbon geometry. Both cases on the top are with the connected boundary condition of the ribbons. On the bottom, we see the corresponding energy and SVD spectra in the open ribbon boundary cases.*

III Discussion for the π-flux model

The aim of the thesis is to restore the BBC. By plotting the probability density profile we see the system has first order skin effect.

1D winding number can be used as a weak topological invariant, because we have a 2D system. To calculate the 1D winding number we had to build the ribbon geometric Hamiltonian. As we have seen above the 1D winding number in our model indeed predict the well localized states at the boudary. The most localized state is when we do not have any line gap in the ribbon geometric spectrum. Additionally, those most localized states are at the $k_y = \pi/2, 3\pi/2$ values where the initial Dirac points were located. However, along the k_x direction the Dirac point location is at π so that the states from there totally not localized (because of the reciprocity on that point).

Due to the first order skin effect in the ribbon geometric case xOByPB we could calculate the spectral winding number and determine the source $(+1)$ and sink (-1) numbers for each k_y value in the periodic boundary by connecting the x-ends, where the point gaps are circulating around the EPs. Correspondingly, the energy eigenstates are very well localized at the boundary so that it confirms it can predict the boundary skin states.

As in the paper "universal skin effect" [8] stated that there exist skin states in π-flux model due to its exceptional degeneracy.

Finally we looked at the singular value decomposition spectrum (SVD) which is expected to recover the conventional type of bulk boundary correspondence which was mentioned in the Ref.[1]. As we see at the spectrum in OB and PB the shape of the dispersion looks similar and it is indeed recovers the cBBC. However, as in the Ref.[1] mentioned that the SVD looses the information about the nH behavior, we cannot (for example) see the degeneracy of the energy spectrum in OB ribbon geometric case, where only there the states are mostly localized and not all of the zero singular values of SVD spectrum.

Chapter 6

The 2nd model - A model with second order skin effect

I Introduction

Now we are going to introduce a two dimensional non-Hermitian model [3] that exihibits the second-order skin effect. The 2D Bloch Hamiltonian is given as

$$H(\vec{k}) = -i(\gamma + \lambda \cos k_x) + \lambda(\sin k_x)\sigma_z + (\gamma + \lambda \cos k_y)\sigma_y + \lambda(\sin k_y)\sigma_x \tag{6.1}$$

where γ and λ are real parameters, and σ_is are Pauli matrices.

The real space hopping of this Hamiltonian is shown in the figure (6.1). Here, the number of the skin states scale with the system size $\mathcal{O}(L)$, $2L$ is the size of the system.

Its extended Hermitian Hamiltonian $\tilde{H}$ is then

$$\tilde{H}(k_x, k_y) = \begin{pmatrix} 0 & H(\boldsymbol{k}) \\ H(\boldsymbol{k})^\dagger & 0 \end{pmatrix} \tag{6.2}$$

$$= (\gamma + \lambda \cos k_x)\tau_y + \lambda(\sin k_x)\sigma_z\tau_x + (\gamma\lambda \cos k_y)\sigma_y\tau_x + \lambda(\sin k_y)\sigma_x\tau_x, \tag{6.3}$$

where τ_i's $(i = x, y, z)$ are the Pauli matrices that introduce an additional degree of freedom. This extended Hermitian Hamiltonian was first introduced by Benalcazar, Bernevig, and Huges (BBH) [108] and is the prototypical second-order topological insulator. Hermitian Hamiltonians of the off-diagonal form of eq.(6.3) have chiral symmetry and thus it belongs to the chiral symmetry class. There is topological correspondence between the Hamiltonian and the off-diagonal nH Hamiltonians [65].

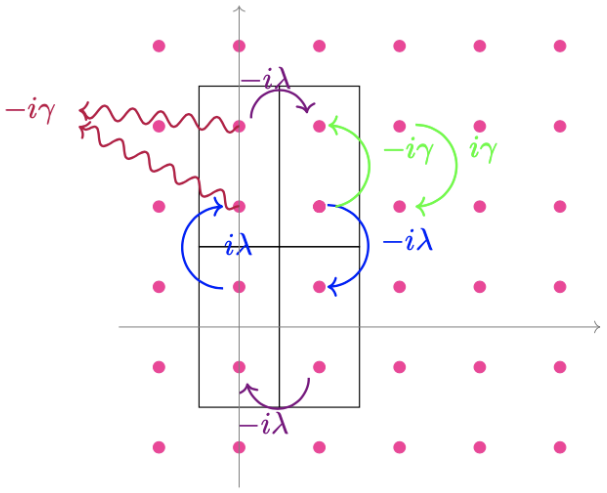

Figure 6.1: *The hopping constants of the second Hamiltonian with the second-order skin effect. The model is two-dimensional and consists of unit cells containing two lattice points. The onsite potentials are shown with the red wiggles. The hopping in the unit cell is given by the green arrows. The hoppings between unit cells in the y-direction are given by blue arrows and in the x-direction in violet.*

The zero-energy second-order corner states appear in $\tilde{H}(\vec{k})$ when $|\gamma/\lambda| < 1$. This is analytically proven in ref.[3]. Then the corresponding nH Hamiltonian has second-order skin states. Higher-order modes appear due to systems' spatial symmetries. The system has no edge modes under open boundary conditions along one direction because the one-dimensional winding number is zero. On the other side, this says that the first-order skin effect does not appear. The model has inversion symmetry and in that case, the 1D winding number is zero. [3]

Both the extended Hermitian and the nH Hamiltonians have proper inversion symmetry

$$\sigma_y \tilde{H}_{BBH}(\vec{k})\sigma_y^{-1} = \tilde{H}_{BBH}(-\vec{k}) \tag{6.4}$$

$$\sigma_y H(\vec{k})\sigma_y^{-1} = H(-\vec{k}) \tag{6.5}$$

Additionally, $\tilde{H}_{BBH}(\vec{k})$ respects mirror symmetry

$$(\sigma_z\tau_y)\tilde{H}_{BBH}(k_x,k_y)(\sigma_z\tau_y)^{-1} = \tilde{H}_{BBH}(-k_x,k_y) \tag{6.6}$$

$$(\sigma_x\tau_y)\tilde{H}_{BBH}(k_x,k_y)(\sigma_x\tau_y)^{-1} = \tilde{H}_{BBH}(k_x,-k_y) \tag{6.7}$$

Respectively, $H(\vec{k})$ respects

$$\sigma_z H^\dagger(k_x, k_y)\sigma_z^{-1} = -H(-k_x, k_y) \tag{6.8}$$
$$\sigma_x H^\dagger(k_x, k_y)\sigma_x^{-1} = -H(k_x, -k_y) \tag{6.9}$$

They both also respect the transposition-accompanying mirror symmetry

$$\sigma_x \tilde{H}_{BBH}^T(k_x, k_y)\sigma_y^{-1} = \tilde{H}_{BBH}(-k_x, k_y) \tag{6.10}$$
$$\sigma_z \tilde{H}_{BBH}^T(k_x, k_y)\sigma_z^{-1} = \tilde{H}_{BBH}(k_x, -k_y) \quad \text{and} \tag{6.11}$$
$$\sigma_x H^T(k_x, k_y)\sigma_x^{-1} = H(-k_x, k_y) \tag{6.12}$$
$$\sigma_z H^T(k_x, k_y)\sigma_z^{-1} = H(k_x, -k_y) \tag{6.13}$$

As shown in Ref.([3]) , the inversion symmetries (6.12) and (6.13) vanish the skin effect of $H(\vec{k})$ along the x and y direction, respectively. Besides, $\tilde{H}_{BBH}(\vec{k})$ respects four-fold-rotation symmetry

$$\mathcal{R}_4 \tilde{H}_{BBH}(k_x, k_y)\mathcal{R}_4^{-1} = \tilde{H}_{BBH}(-k_y, k_x) \tag{6.14}$$

where $\mathcal{R}_4$ is a unitary matrix given as

$$\mathcal{R}_4 = \begin{pmatrix} 0 & -i\sigma_y \\ 1 & 0 \end{pmatrix} \tag{6.15}$$

Accordingly, $H(\vec{k})$ respects four-fold-rotation *type* symmetry

$$-i\sigma_y H^\dagger(k_x, k_y) = H(-k_y, k_x) \tag{6.16}$$

In Ref.[3] it was found that in x periodic boundary and y open boundary there are $O(L)$ number of eigenstates are localized at both edges of ribbon geometric system. The energy spectrum of these boundary modes is separated from the bulk spectrum contrary to the chiral states of the Chern insulator. Under x open boundary and y periodic boundary conditions at $|\gamma/\lambda| = 1$ there appear boundary modes with the same $k_y = \pi$ wavenumber, which build $2L$ exceptional points and have 2 linear independent eigenstates. One of them localizes at one edge while the other one localizes to the other edge. There are no relations known between the corner states at the fully open boundary and these edge states at the ribbon geometric cases yet.

Kawabata et al. [3] proposed a topological invariant called Wess-Zumino term which was previously used more in high energy physics. In condensed matter context it can

be used as a topological invariant in a system with a point defect in the Hermitian case. Then the extended Hermitian system has zero modes and these zero modes localize at the point defect forming chiral states around the point defect like the dynamics in the Hatano-Nelson model. Similarly, they proposed, when we have corner zero modes in extended Hermitian Hamiltonian WZ term is non-zero. Then the nH part of the Hamiltonian has corner skin modes. And this is possible only when we do not have first-order skin modes which were removed by inversion symmetry. In that case we consider the adiabatic changes of the Hamiltonian near the edges $H(k_x, k_y, t = 0) := H(k_x, k_y)$ into the vacuum Hamiltonian $H(k_x, k_y, t = 1) := H_{const}$. More on the WZ term see Ref.[3].

The WZ is quantized in $\{0, 1/2\}$ in presence of rotation type symmetry or reflection type symmetries. We will reproduce the quantization below in the results.

II Results

II.1 The energy spectrum under various boundaries and the density profile

Now we want to reproduce the energy spectra under various boundaries as in its paper was done. In the figure (6.2) the energy spectra in the different boundary conditions, i.e. fully OBC, xOByPB, xPByOB, fully PBC, are plotted with the IPR color code. Additionally, the energy spectra in different boundary conditions are shown in three different phases, one above a critical value which is $|\gamma/\lambda| = 1.5$ where the system is in trivial phase, one at the critical value $|\gamma/\lambda| = 1$, and the other one under the critical value $|\gamma/\lambda| = 0.5$ where the system is in topological phase. As we see in the fully OBC we have a clear point gap. Thus we want to look its localization of the most localized states and see they are at the opposite boundaries localized.

As mentioned above in the introduction for the model we see also corner localized states building a circle in the spectrum for the boundary condition xPByOB. Moreover, the linear dependent degenerated eigenstates (as mentioned above) looks less degenerate for the boundary condition xOByPB and $\gamma/\lambda = 1$ case. This could come from the instability of the critical point in calculating linear algebra library in python.

Figure 6.2: *Energy spectra under various boundary conditions from left to the right. From top to bottom topological non-trivial phase, critical phase, and normal insulating phase with its corresponding parameters values γ and λ.*

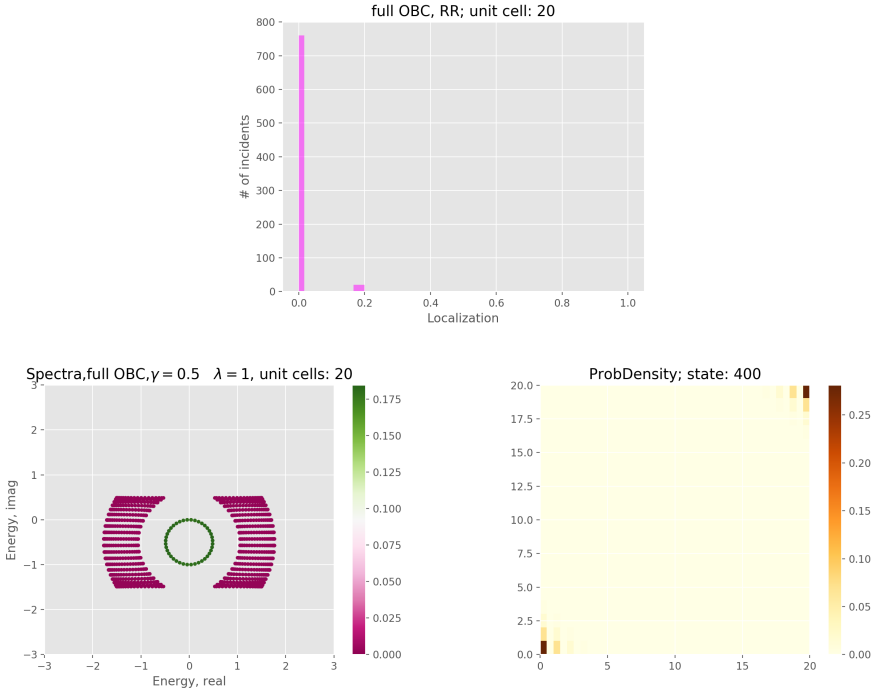

Figure 6.3: *On the top, the histogram of all eigenstates from the real space Hamiltonian for system size $L = 20$ with $\gamma = 0.5$ and $\lambda = 1$ hopping constants. On the bottom left, we see the complex energy spectrum of that real space Hamiltonian in fully OBC and is coded by its histogram values in color. On its right, the density profile of a state from the circle in the energy spectrum plot, which are the most localized states in the system as we see in the histogram given by the bar near the value* 0.2.

II.2 Investigation of the hopping constants

As next I have calculated the energy spectra for $\lambda = -1$ in the non-Hermitian term instead of $\lambda = 1$ (see Fig.(6.4)). I have got the same spectral form and the same IPR values as the previous case. However, when we check all the density profiles of the most localized states they are localized now at the opposite two corners. We still have the same number of corner localized states since the system is still in the same phase with the condition $|\gamma/\lambda| < 1$ and strength of the hopping constants. That means the sign of the nH λ term might be controlling the localization to the corners.

II.3 Number of corner localized states

I diagonalized the Hamiltonian for 5 different system sizes, 20, 40, 60, and 80 unit cells, and counted the number of most localized states based on the IPR values, e.g. the states in the circle on the fully OB spectrum. The number scales two times the system size given in Fig.(6.6), which is consistent with the result on the paper in Ref.[3]. Afterward, I plotted the probability density profile to see where the states are localized (see on Fig.(6.7)). For the system sizes up to around 40 unit cells, the profile looks like what we

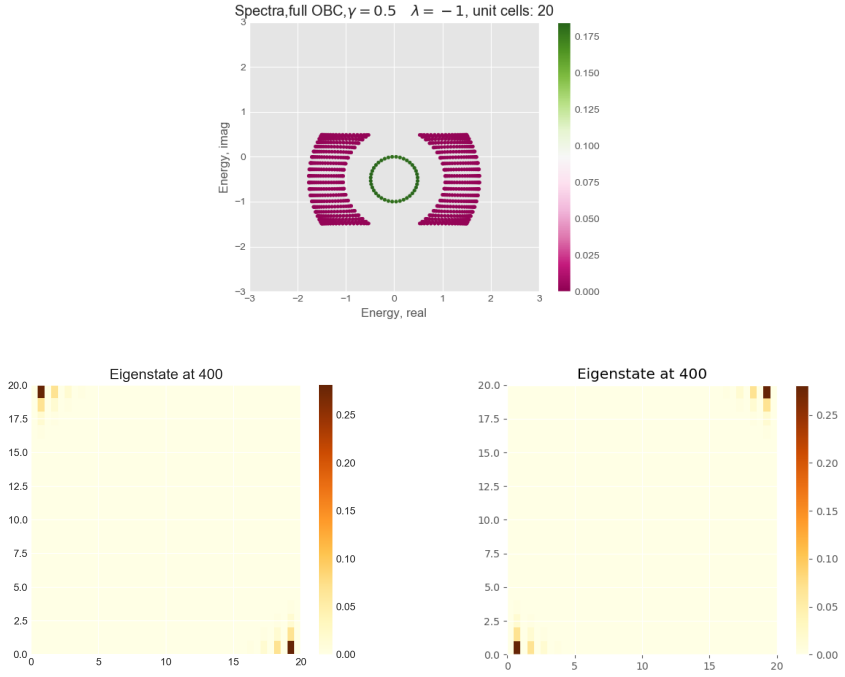

Figure 6.4: *On the top, the energy spectra when I changed the sign of the nH hopping term λ to $-\lambda$. On the bottom left, the density profile of a most localized eigenstate of the Hamiltonian when nH term with $\lambda = 1$ vs. on the right, the density profile of a most localized state of the Hamiltonian when nH term with $\lambda = -1$.*

expect, e.g. the states are at the opposite corners equally dense localized. However, for the bigger system sizes, one of the two corner densities is higher than the other. This contradicts the inversion symmetry of the system. We believe that the diagonalization procedure of the python library for non-Hermitian Hamiltonian could be the reason, why the states are not equally localized at both corners for bigger system sizes.

II.4 The Wyckoff position of the system

$\left|\psi_\Gamma^{L,R}\right\rangle$ is the left and right eigenstate of the non-Hermitian Bloch Hamiltonian at the high symmetry point Γ. Then the eigenvalue of the C_2 operator at Γ can be found as following:

$$\left\langle\psi_\Gamma^{L,R}\right| C_2 \left|\psi_\Gamma^{L,R}\right\rangle = -1 \tag{6.17}$$

I get the same eigenvalues for both left and right eigenvectors at each high symmetry points. The corresponding Wyckoff position of the particular system is then found as in the table (6.1) below.

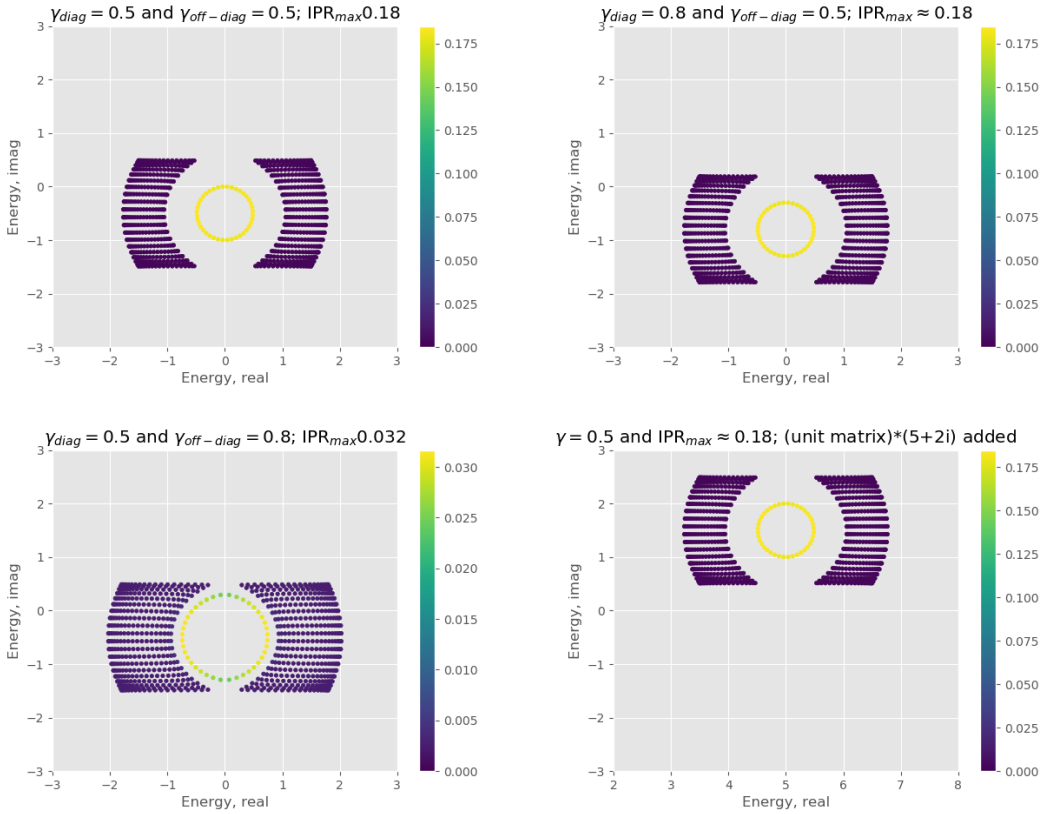

Figure 6.5: *Changing the hopping parameters. On the top left, the energy spectrum is with the usual parameter strengths we calculated throughout the study, $\gamma = 0.5$ and $\lambda = 1$. On the top and right, when we change the diagonal γ term, which is nH dissipation term, the energy spectrum as a whole shifts along the imaginary energy axis. On the bottom left, we change the off-diagonal γ term the energy spectrum as the whole expands and especially the radius of the circle expands, which is expected from the Ref.[3]. On the bottom right, this is a clear result. When we add a complex number to the diagonal term then the energy spectrum shifts simply on the complex plane.*

Table 6.1: *C_2 eigenvalues at high symmetry points and corresponding Wyckoff position*

k points / Wyckoff positions	$\Gamma = (0,0)$	$M = (\pi,\pi)$	$X = (\pi,0)$	$Y = (0,\pi)$
$(0, \frac{1}{2})$ (p-orbital)	-1	1	-1	1

Additionally, when I hermitized the non-Hermitian Hamiltonian as $H_{hermitized} = (H + H^{\dagger})/2$ and computed the eigenvalues of that hermitized Hamiltonian I get the same eigenvalues and therefore the same Wyckoff position as in the Table (6.1).

In the model, we have 2 sites in one unit cell, and on the probability density map, I plot the length of the 2 sites along the x-direction and the other site along the y-direction. I plot also the density profile in square form, e.g., if $L = 20$ is the number of the unit cells

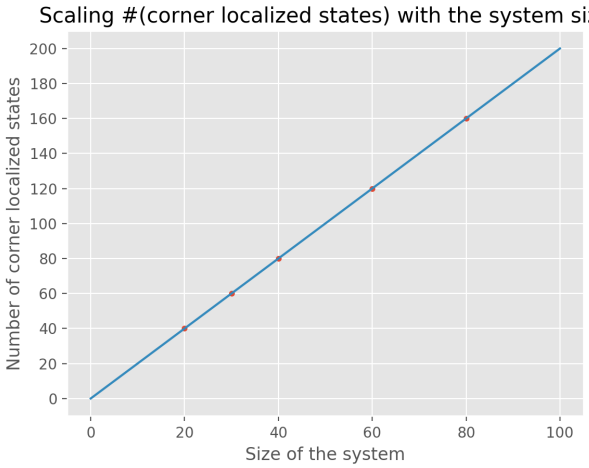

Figure 6.6: *Number of the corner localized states as system size increases. We see here a linear trend. I fitted the pionts with linear equation.*

on the L^2 profile, which has $2 \cdot 20 = 40$ number of sites in x-direction and 20 sites in the y-direction. On the probability density maps of the model, for example in Fig.(6.3), we see every second pixel is filled, which means due to the inversion symmetry the electron probability density is sitting on this particular site of the unit cell, which is its Wyckoff position.

II.5 The quantization of the Wess-Zumino term

In my calculation only for the C_4- type symmetry the WZ integral is quantized in $\{0, 1/2\}$. For the mirror type symmetries the integrals for the two extensions the same, meaning that the integral can take any value in the circle $[0, 1]$. The explicit analytical calculations and results are given in Appendix B.

II.6 Hermitization and probability density profile of its boundary states

We hermitize the model in the following way and get

$$\frac{H(\vec{k}) + H^{\dagger}(\vec{k})}{2} = \lambda(\sin k_x)\sigma_z + (\gamma + \lambda \cos k_y)\sigma_y + \lambda(\sin k_y)\sigma_x \tag{6.18}$$

The corresponding energy spectrum is given in Fig.(6.9) and we see that the most localized states are across the bulk energy gap and going into the bulk region. As we removed the onsite dissipation term $-i\gamma$ and nH λ term the skin states are now localized at the edges instead of localizing at the corners.

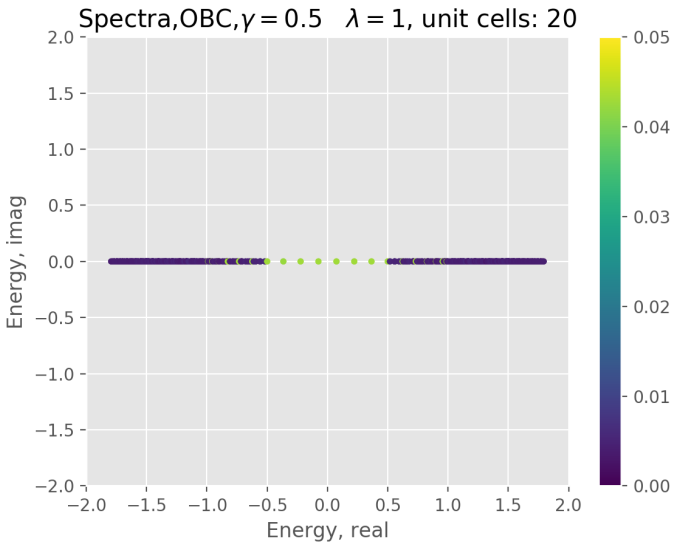

Figure 6.9: *Energy spectrum for the hermitized model with its histogramm values color-coded.*

Here we do not have the corner states any more. The electron densities are edge like localized. Every 2 states are degenerate and each of them is at the opposite edges localized. We see on the Fig.(6.10) discrete densities, this is due to the Wyckoff position. One unit cell has two sites and the electron density can be found where the Wyckoff position lays.

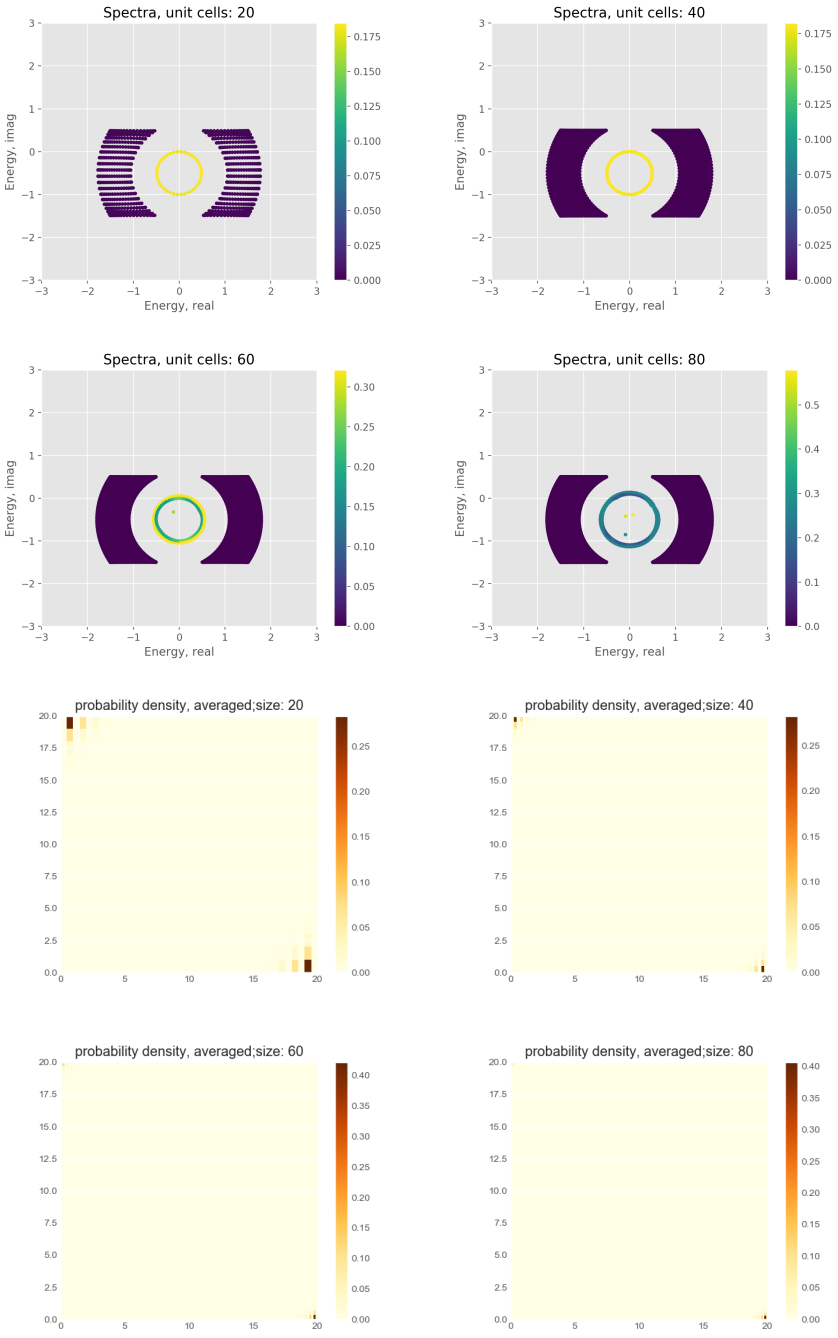

Figure 6.7: *The top 4 plots are energy spectra for the systems with different system sizes L =20, 40, 60, and 80 unit cells. The corner localized states which can be seen on the circle in the spectra scale 2 times the system size L. The bottom 4 plots are the corresponding probability density profiles averaged over all corner localized states in the system.*

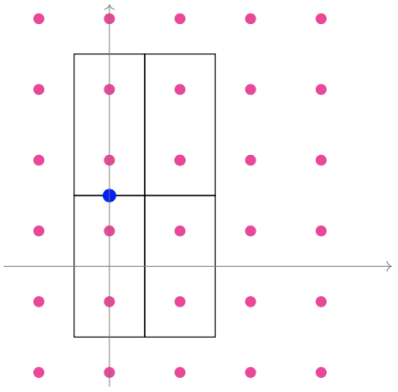

Figure 6.8: *The blue point is the Wyckoff position at* $(0, 1/2)$*. This point is repeated from unit cell to the unit cell, which are not marked on the figure.*

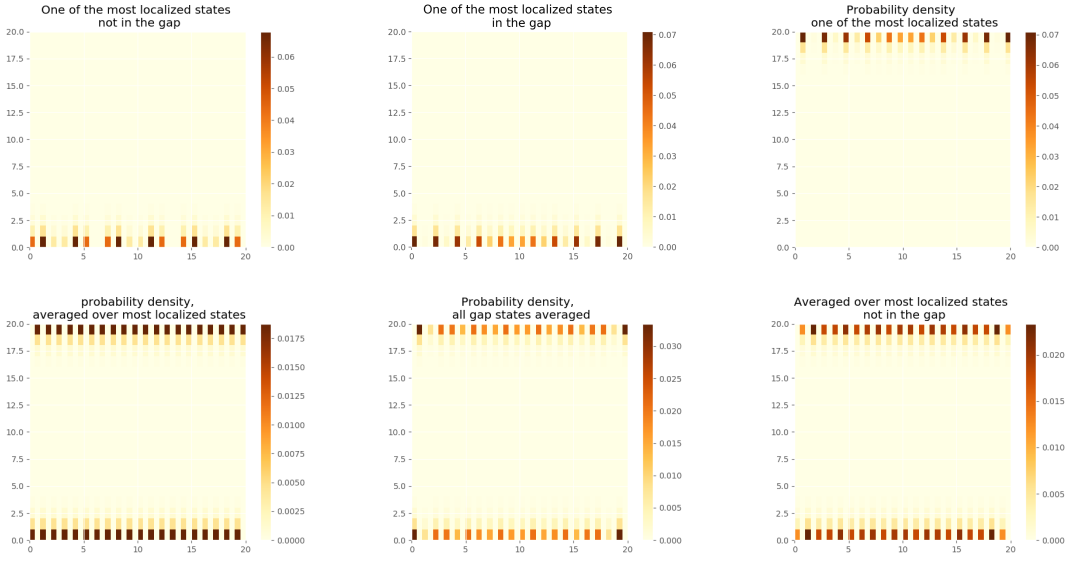

Figure 6.10: *Probability density of the most localized states from the hermitized model. On the top left is the density of states of one of the most localized states and this is a state which hast its energy in the middle of bulk states. On top in the middle and on the left, these states have also the same IPR but have more against the edge corners localized. On the bottom left the most localized states are averaged by the number of the states. We can see by its color the states have almost the same probability density. On the bottom middle, the probability density of the gap states are averaged and we see the tendency is against the corner. On the bottom right, this is the averaged probability density of the states whose energy is in the middle of the bulk states.*

II.7 Random perturbation under various symmetrization and magnitude

I systematically perturbed the system with small symmetry respecting and not symmetry respecting Hamiltonian and saw how the various perturbations change the spectra. The perturbation with a magnitude smaller than the 10^{-10} is numerically not detectable. Thus the perturbations are done with bigger magnitudes.

We expect the spectrum change to respect the magnitude of the random perturbation and the symmetries of the system. Especially we know from the chiral states in 2D Hermitian topological systems that the chiral states do not easily localize like the proper one-dimensional systems (Anderson localization [109]). But to localize such states one should break the symmetry and needs certain strength of perturbation. Thus we study here from what strength and symmetry the corner states disappear or distort. Corner states mean we have to focus on the circle spectrum and its IPR values. The perturbations are done either to the Bloch Hamiltonian and then Fourier transformed or directly to the real space Hamiltonian perturbed. Each case is described in captions. The rest of the perturbations can be found in Appendix E.

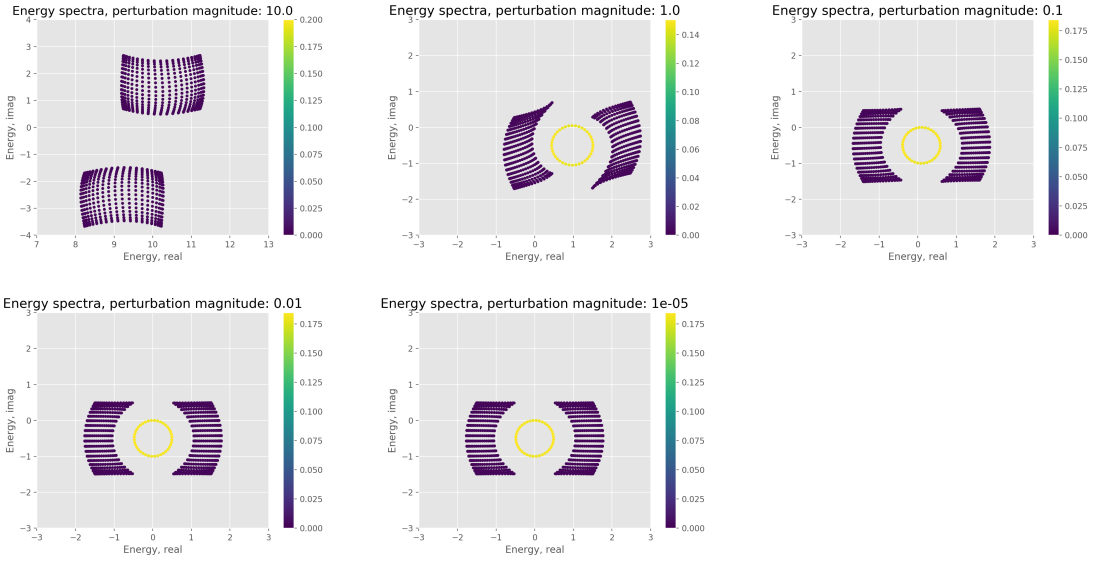

Figure 6.11: *Real valued perturbation. Reciprocal space. C2 perturbation with different magnitudes times always same random matrix*

Reciprocal space perturbation When we perturb the system onto Bloch Hamiltonian the spectrum can vary very much because the size of the Hamiltonian is only 2x2 and thus depends only on 4 values. The perturbing Hamiltonians are taken randomly and then they are symmetrized under desired symmetries. That is the reason why the perturbing Hamiltonian can take additional symmetries very easily.

With C_2 symmetric Bloch Hamiltonian perturbing spectra can be various and I think because of the above reason.

With C_4 symmetric Bloch Hamiltonian perturbing spectra generally keep well its spectra up to the magnitude 0.4 which is around the magnitude of the system which is $\gamma = 0.5$ and $\lambda = 1$. Complex perturbation keeps better and can persist around order of $1i$.

Real space perturbation Real space perturbations with complex amplitudes up to 0.6 keep the circles with different matrices. C_2 real space perturbations with magnitude 1 keep quite well.

Full matrix perturbation up to 0.01 is fine. Diagonal perturbation up to 1 keeps very well. This is exactly the Anderson delocalization in topological systems.

II.8 WZ-integrals and gap sizes of the system with the various hopping constants and their interrelations

From the figure (6.14) we see that the WZ term is indeed quantized to the $\mathbb{Z}_2$ values which is consistent with the topological phase based on the hopping parameter relations $|\gamma/\lambda|$ (that comes from the analytical calculation in its reference paper) and minimal energy gap of the system (w.r.t. the real energy, because there the line gap is closing). At the critical phase $|\gamma/\lambda| = 1$ the WZ integral looks not to be stable and takes random value between 0 and 0.5.

Now we look at the plot fig.(6.13) of WZ terms in varying nH λ values in $[0, 2]$, where $\gamma = 0.5$. When nH λ is zero the WZ integral is accordingly equals zero which confirms that the WZ term is only not zero when there are corner localized states. Because we have seen that in hermitized version of the Hamiltonian the corner states vanish and edge like localized states appear.

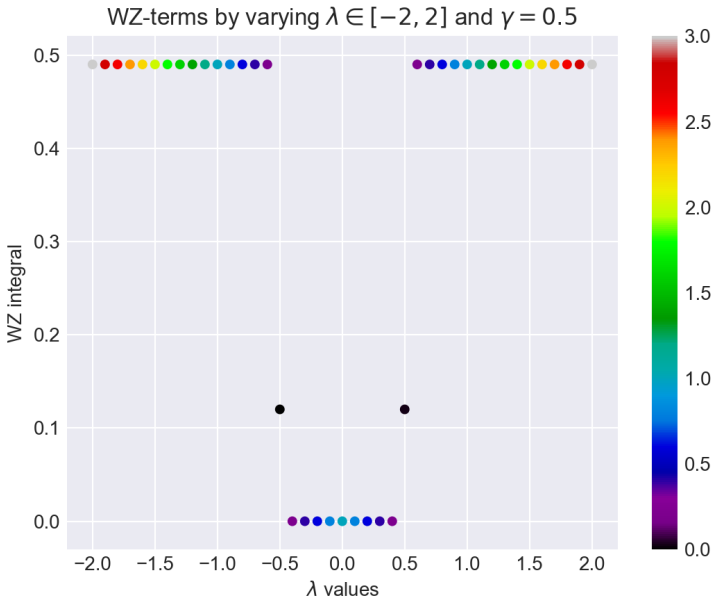

Figure 6.12: *This are WZ integral values by changing the λ's in the whole system. The gap sizes are with respect to the minimal gaps in the real energy Bloch-band.*

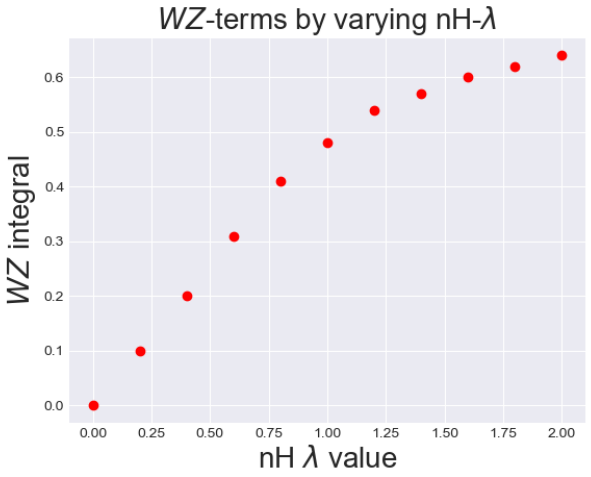

Figure 6.13: *These are the WZ integral values by changing the nH λ term. Here $\gamma = 0.5$.*

When we vary only the nH λ and γ and compute the WZ integrals, we have the WZ term is only quantized when the symmetry is retained (see fig.(6.14)). By breaking the C_4-type symmetry the WZ-terms are not any more quantized. However still having non-zero nH λ terms the WZ is not zero, while nH λ is zero the integral is again quantized and becomes zero telling there are no corner states. So we clearly see the roles of non-Hermiticity and C_4-type symmetry in the system.

In Fig.(6.15) on the left we can check if there is topological phase transition by varying

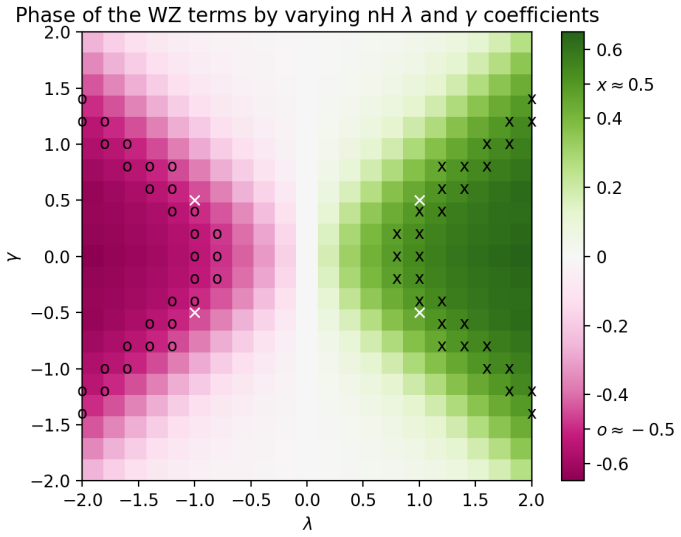

Figure 6.14: *WZ phase by varying nH γ and λ coefficients. The WZ term is indeed a smooth quantity taking values in circle $[0, 1]$. By varying nH γ and λ we break the C_4-type symmetry and in the result the WZ term is not quantized any more. The x and o points are the values where the WZ integrals take values near 0.5. The white x four points are where the WZ integral is quantized and the C_4-type symmetry is of course retained point. The whole line is white when $\lambda = 0$ says the integrals take completely zero values without corner states.*

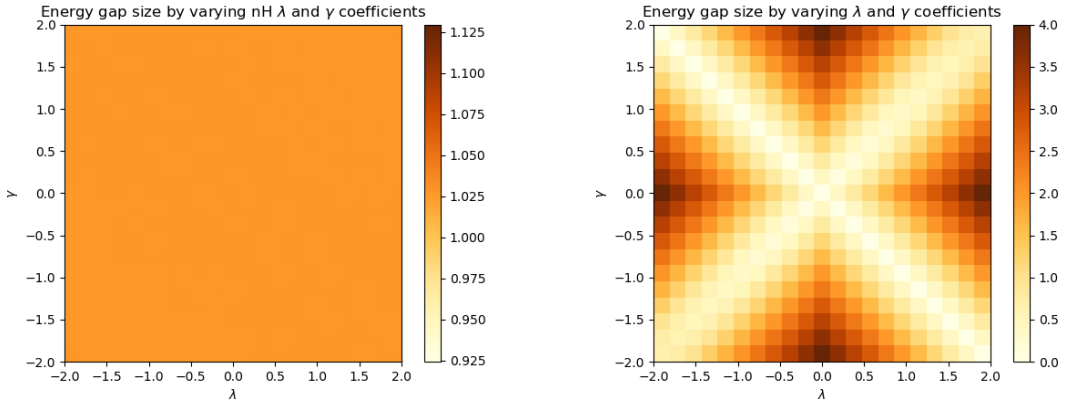

Figure 6.15: *On the left energy gap sizes by varying non-Hermitian γ and λ coefficients. They do not change. On the right energy gap sizes by changing the whole λ and γ values in the system.*

the nH terms in system through closing the energy gap. However, we do not observe any phase transition that occurs by closing the energy gap. The corner states are protected by 4 fold type rotation symmetry, but there are no system phase transition. By changing the whole γ and λ values on Fig.(6.15) on the right there are gap closing when the ratio $|\gamma/\lambda| = 1$.

III Discussion for the 2D model with second order skin effect

A higher-order nH skin effect model was studied [3]. Its extended Hermitian Hamiltonian model is a prototypical Hermitian higher-order boundary state model. The number of the corner localized skin states of the nH Hamiltonian scale twice with the system size L.

The energy spectra with the different boundary conditions were reproduced. We see a fully gapped system in fully PBC and point gap topology was observed in the spectrum of fully OBC. When the topological phase transition occurs $|\gamma/\lambda| = 1$ the real part of the energy gap closes and reopens in the trivial phase. In this model onsite dissipation term determines the energy shift along the imaginary axis.

The corner states sitting on the opposite corners (due to the inversion symmetry) in the probability density profile are the energy eigenstates in the spectrum of circle in fully OBC. The nH λ term pushes the boundary states to the corner. If this term is zero the boundary states are localized at one edge of the 4 edges. By changing the sign of nH λ term the eigenstates localize to the opposite corners, meaning that the sign determines on which corner they are localized.

The topological invariant Wess-Zumino integral for the corner localized phase was introduced in the study of Ref.[3]. This term was investigated for the above model in detail with its nH hopping strengths, energy gap size, and the system spatial symmetries by changing the system hopping parameters in various ways.

We know that topological two distinct phases can occur by adding symmetry constraint. Like that in this model by keeping the ratio of the nH part of the γ and λ parameters the same as the other parameters we have the so-called symmetry enhanced topology (see Fig.(6.15) on the left) so that we have corner states phase and the topological Wess-Zumino invariant is quantized to the $\{0, 1/2\}$(see Fig.(6.14)), i.e. there are corner states it is $1/2$ and when not 0. While varying the whole parameters (Fig.(6.15 on the right) in the system there is complete topological phase transition occurs by closing the energy gap and opening again after the phase transition.

Additionally, instabilities in linear algebra libraries in python could be observed when we calculated the exceptional points in xOByPB and $|\gamma/\lambda| = 1$ case and also by increasing the size of the system the spectrum and density profile did not look as expected for the system size starting from $L = 60$.

If the spectrum under periodic BC fill an area, so we have a skin effect under open BC in nH systems as in the work of Ref.[8] was found. We indeed have finite area in the energy spectrum and also skin states.

Chapter 7

The 3rd model - 3D model with third order skin effect

I Introduction

The model is given by the following Hamiltonian [3]

$$\begin{aligned} H(\boldsymbol{k}) = i\lambda(\sin k_y)\sigma_x + i(\gamma + \lambda\cos k_y)\sigma_y \\ +i\lambda(\sin k_x)\sigma_z + (\gamma + \lambda\cos k_x)\tau_z \\ +\lambda(\sin k_z)\tau_y + (\gamma + \lambda\cos k_z)\tau_x \end{aligned} \tag{7.1}$$

Its extended Hermitian Hamiltonian is also the prototypical 3D higher order topological system.

$$H(\boldsymbol{k}) = \begin{pmatrix} \gamma + \lambda e^{ik_x} & \gamma + \lambda e^{-ik_z} & \gamma + \lambda e^{ik_y} & 0 \\ \gamma + \lambda e^{ik_z} & -\gamma - \lambda e^{-ik_x} & 0 & \gamma + \lambda e^{ik_y} \\ -\gamma - \lambda e^{-ik_y} & 0 & \gamma + \lambda e^{-ik_x} & \gamma + \lambda e^{-ik_z} \\ 0 & -\gamma - \lambda e^{-ik_y} & \gamma + \lambda e^{ik_z} & -\gamma - \lambda e^{ik_x} \end{pmatrix} \tag{7.2}$$

The symmetries of the system for the extended Hermitian Hamiltonian and its nH Hamiltonian are given by

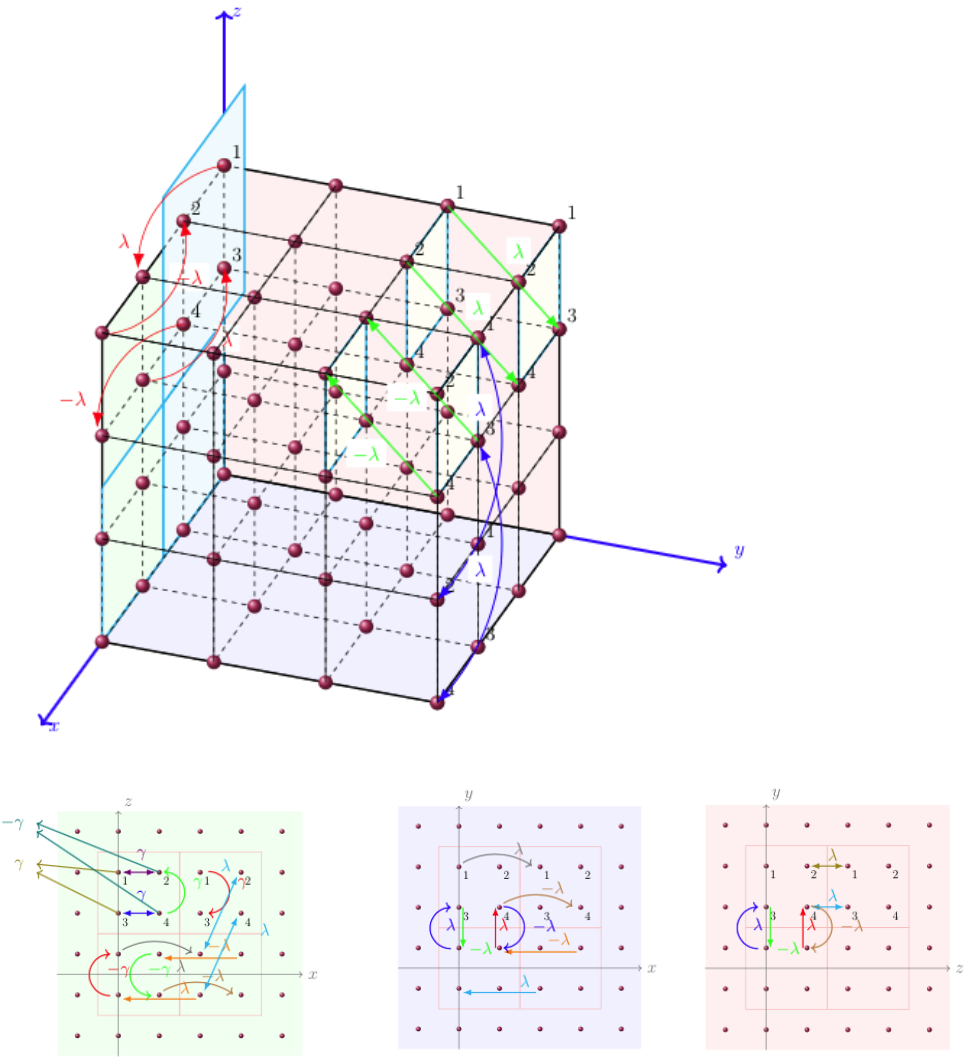

Figure 7.1: *The hopping directions of 3D higher order non-Hermitian model can be seen. One unit cell is here given by the blue plane numbered with the 4 numbers, 1,2,3,and 4. The number of the balls in the unit cell represent the number of degree of freedom. In the 3D plot the red, blue, and green arrows represent the hoppings in all 3 directions. On the light green, blue, and red 2D planes we can see the 2D projections, i.e. xz, xy, and zy, of the hopping strengths and onsite terms. The 3D figure is based on Ref.[110]*

$$(\rho_y\sigma_y\tau_y)\tilde{H}(\boldsymbol{k})(\rho_y\sigma_y\tau_y)^{-1} = \tilde{H}(-\boldsymbol{k}) \tag{7.3}$$

$$(\sigma_y\tau_y)H^{\dagger}(\boldsymbol{k})(\sigma_y\tau_y)^{-1} = -H(-\boldsymbol{k}) \tag{7.4}$$

$$(\rho_x\sigma_z)\tilde{H}(k_x,k_y,k_z)(\rho_x\sigma_z)^{-1} = \tilde{H}(-k_x,k_y,k_z) \tag{7.5}$$

$$(\rho_x\sigma_x)\tilde{H}(k_x,k_y,k_z)(\rho_x\sigma_x)^{-1} = \tilde{H}(k_x,-k_y,k_z) \tag{7.6}$$

$$(\rho_y\tau_y)\tilde{H}(k_x,k_y,k_z)(\rho_y\tau_y)^{-1} = \tilde{H}(k_x,k_y,-k_z) \tag{7.7}$$

$$\sigma_z H^{\dagger}(k_x,k_y,k_z)\sigma_z^{-1} = H(-k_x,k_y,k_z) \tag{7.8}$$

$$\sigma_x H^{\dagger}(k_x,k_y,k_z)\sigma_x^{-1} = H(k_x,-k_y,k_z) \tag{7.9}$$

$$\tau_y H^{\dagger}(k_x,k_y,k_z)\tau_y^{-1} = -H(k_x,k_y,-k_z) \tag{7.10}$$

II Results

II.1 Energy spectra under various boundary conditions

The energy spectra under different boundary conditions and in 2 different phases are plotted on Fig.(7.3). The non-trivial topological phase is on the upper row with the hopping constants $\gamma = 0.5$ and $\lambda = 1$ and lower row with the $\gamma = 1.5$ and $\lambda = 1$ in trivial phase. In the trivial phase we have every where imaginary and real line gaps. In the non-trivial phase first 2 conditions have line gap and in fully OBC we see the point gap suggesting to have skin states. The states sitting on the point gaps have the biggest IPR values. The most localized states are not too separated from the bulk states in IPR values. But the reason could be the system size is small and only $L = 10$. For bigger system size the calculation in python is very slow.

In Fig.(7.2) we see the number of the most localized states scaling with the system size. It is a linear trend as expected from the paper Ref.[3].

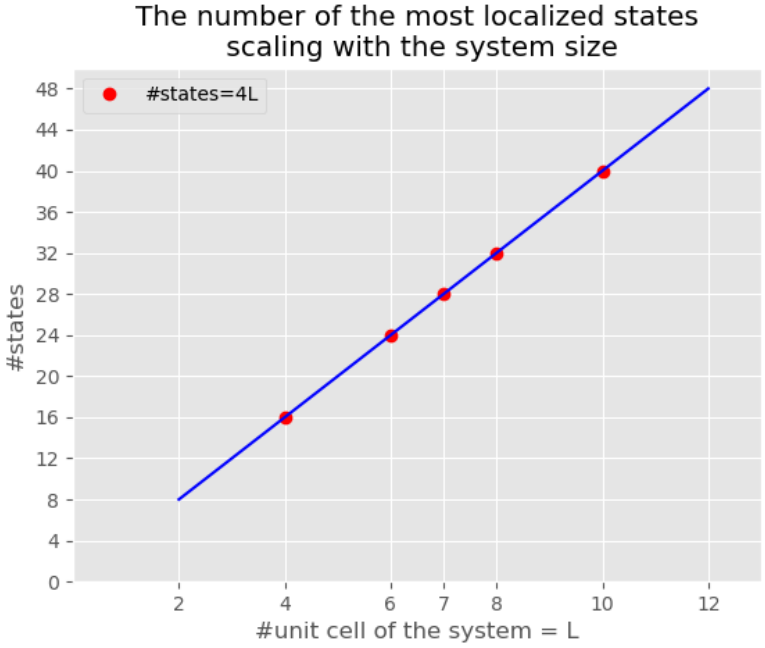

Figure 7.2: *Scaling of number of the most localized states by changing the system size. We also see a linear trend. The points were fitted with a linear function.*

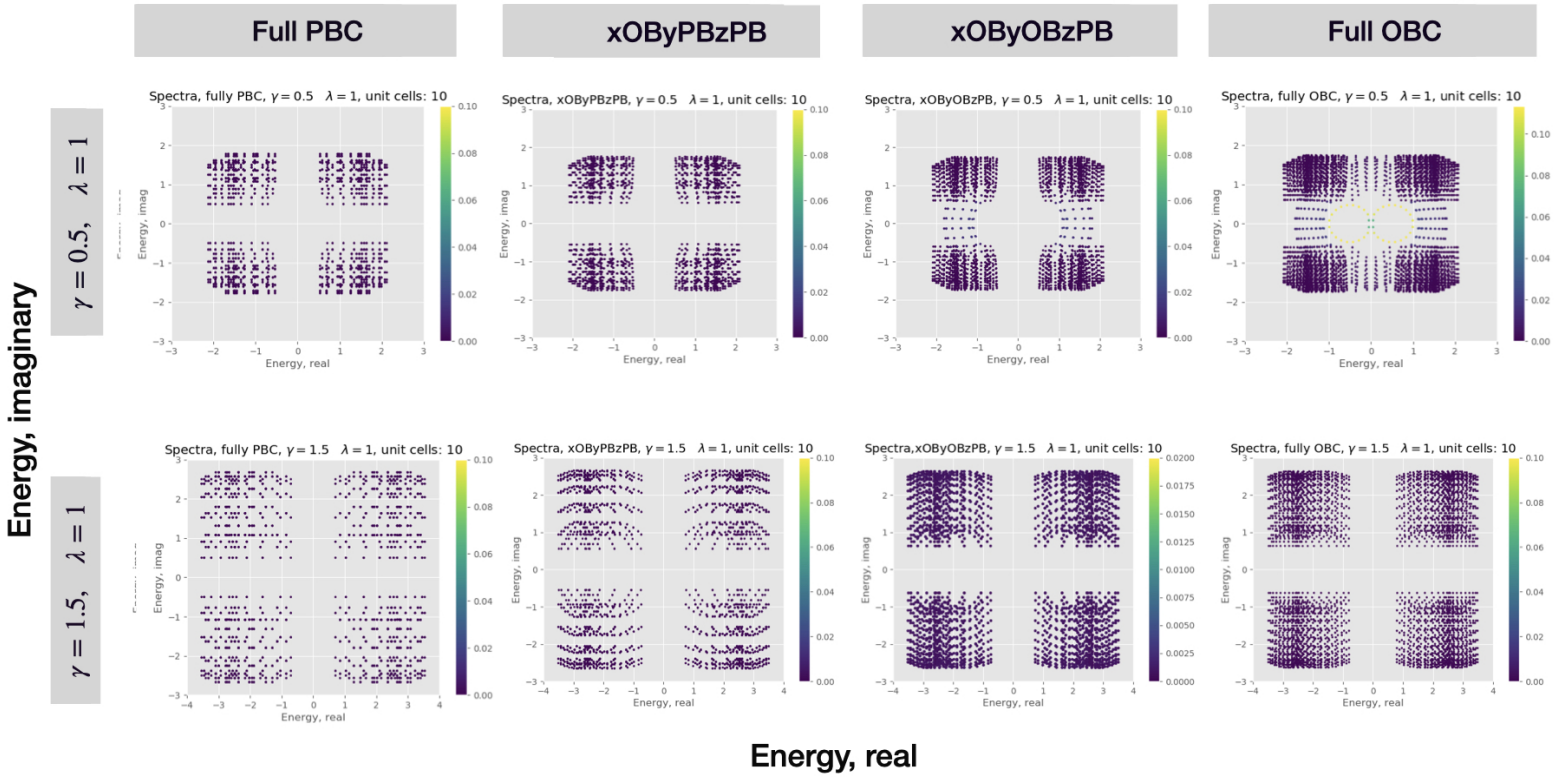

Figure 7.3: *The energy spectra for different boundary conditions are plotted with their histogramm values in color code. In the most of the cases and in fully PBC, the system has real and imaginary line gaps. That means the system does not have nodal phase and therefore no exceptional points in fully PBC. In fully OBC the system has point gap suggesting there are skin states. The spectra are plotted for 2 diferent cases, topologically non-trivial on upper row, when $\gamma = 0.5$ and $\lambda = 1$ and trivial phases on lower row, when $\gamma = 1.5$ and $\lambda = 1$.*

II.2 Hermitization

We hermitize the model to see what are the nH terms and plot the spectra for the unit cells 4 and 10 are in fully OBC in Fig.(7.4). Especially the terms with k_y are completely nH and the terms with k_z are completely Hermitian. We see on the spectrum the more localized states can be found in the gap of the bulk states and some can be found into the bulk spectrum. The Hermitian part of the Hamiltonian is given by

$$H_{Hermi}(\boldsymbol{k}) = \frac{(H(\boldsymbol{k}) + H^{\dagger}(\boldsymbol{k}))}{2} = (\gamma + \lambda \cos k_x)\tau_z + \lambda(\sin k_z)\tau_y + (\gamma + \lambda \cos k_z)\tau_x \tag{7.11}$$

The hermitized Hamiltonian is not inversion symmetric and not pseudo inversion symmetric. From here already we can say that the WZ term for the hermitized Hamiltonian is zero because the one-dimensional winding number should vanish for the WZ term to be defined. Or we can compute a 1D winding number to see if it equals zero and this is not done. We plotted the energy dispersion along with the "high symmetry points", although our system is not inversion symmetric and thus actually not "high" symmetry points. As we have seen on the energy spectrum in fully PBC here also the dispersion should be fully gapped. If we look at the real and imaginary spectra of the nH Hamiltonian, the Hermitized spectrum corresponds to the real spectrum of the nH spectrum. This is due to the commutation of the corresponding Hamiltonians. More precisely the nH Hamiltonian is a normal matrix: $H_{Hermi}H = HH_{Hermi} \Rightarrow HH^{\dagger} = H^{\dagger}H$. The commutation was also numerically checked.

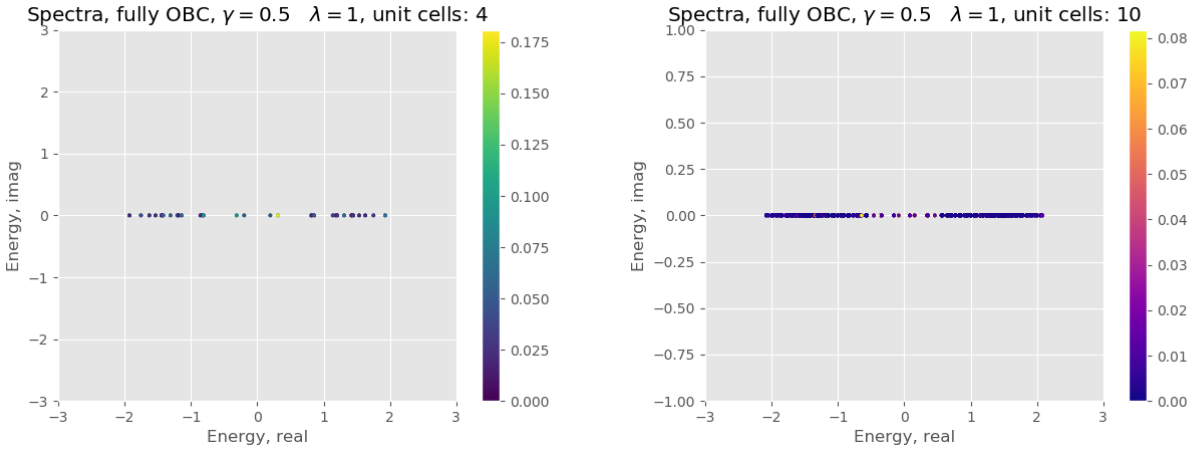

Figure 7.4: *3D hermitized. The number of the most localized states are difficult to determine, because the IPR values are slowly passaging and no discrete values. However the values are approximately linearly dependent to the system size. The most localized states are also spreading over the bulk gap and going into the bulk spectrum.*

Figure 7.5: *Energy bands for nH Hamiltonian along high symmetry lines. Above two plots are the real and imaginary part of the energy. The bottom plot is the energy band for the hermitized Hamiltonian of the above one. As we see the real part of the energy band for nH Hamiltonian is exactly the same as the band for the hermitized model,* $(H + H^{\dagger})/2$ *and* H *is the nH Hamiltonian. Lower band of the real energy band corresponds to the lower energy band of imaginary energy and upper real corresponds to the upper imaginary bands.*

Because the hermitized Hamiltonian 2 dimensional we can look at the probability density profile (see Fig.(7.7) in the middle with the green heading). The most localized states are localized only along the edges.

II.3 Energy spectra for the 2D OBC by keeping 3rd $k = const$ values

Energy spectra are plotted for cuts along xy-plane, xz-plane, and yz-plane OBC and keeping the third k-value some constant in $[0, 2\pi]$ in Fig.(7.6 and 7.7). These energy spectra are in all cases line gapped. Although there are a few states that are very well localized and they are shown probability density profiles (PDP) on the right.

First, we look at the case with OB along xy and $k_z = 3\pi/7$. The energy is real line gapped and for different values of k_z the energy spectrum is only broader or narrower along with the real energy, but the line gap never closes. The most localized states of the

system are at the 2 opposite corners localized and all best-localized states are divided into 2 opposite corner localized.

Then the spectrum along yz open and k_x at TRIM point π (the same results will apply for $k_x = 0$) is both real and imaginary energy line gapped. There are only 4 states that are exponentially localized at the neighboring 2 corners. All 4 are at the opposite neighboring corners localized. When we take a non-TRIM point then each of these 4 states is localized on one corner so that the probability density is twice as much as at TRIM. The next most localized states are at the edges localized which are not shown in Fig.(7.6).

For the case of OB along with xz directions we look at the 3 different cases, one just at fixed k_y value (see Fig.(7.7) the row with the blue heading), the other eliminating the k_y value (with the yellow heading), and the hermitized version (with the green heading). The energy spectrum for the model without k_y terms looks very similar to the previous 2D model in the previous chapter 6. So the states are localized at the corners. For the other two cases, the most localized states are at the edges localized.

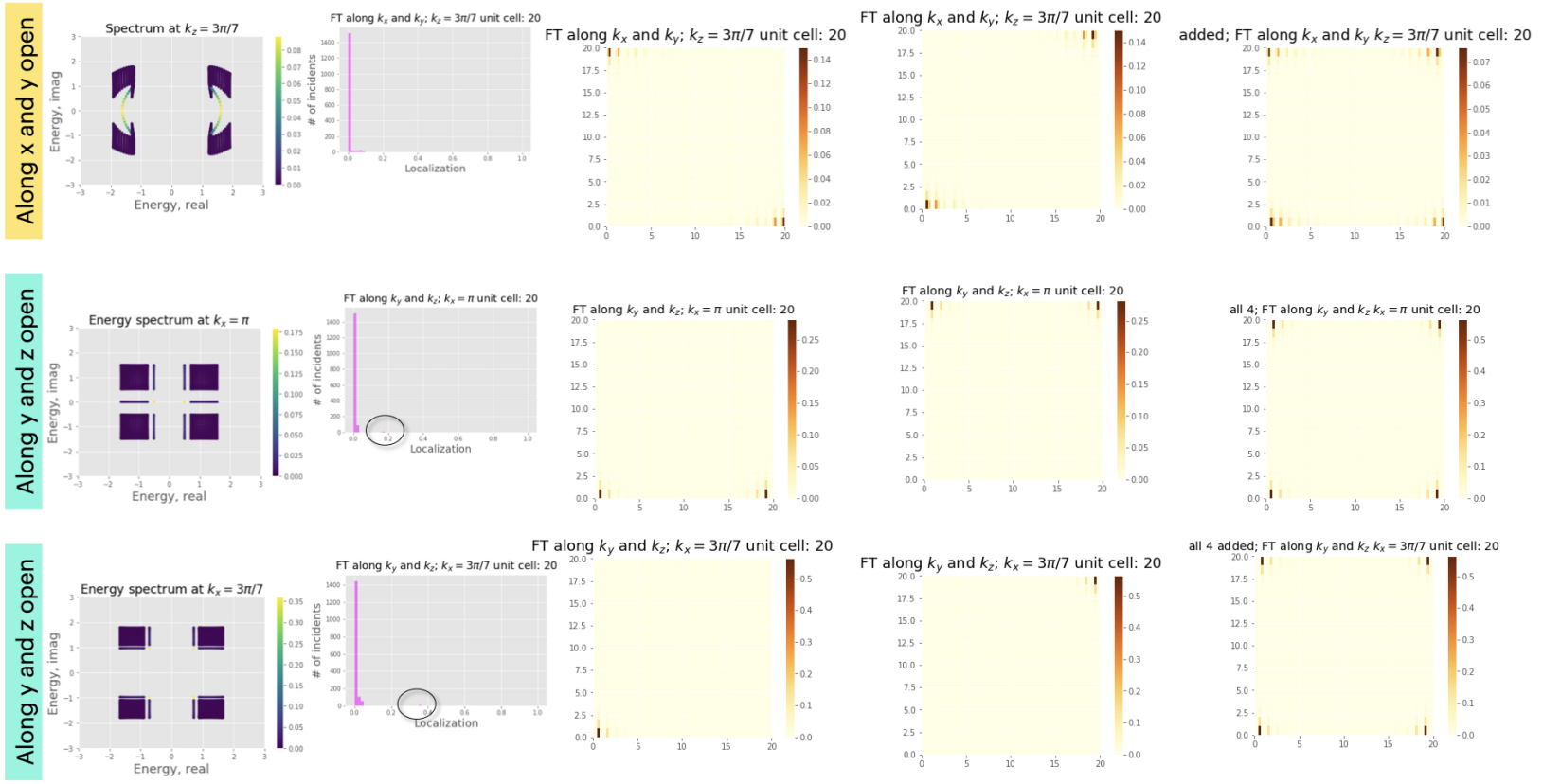

Figure 7.6: *In the first row we see the energy spectrum for $xyOB$ and k_z value is constant and we choose. Its histogram and the most localized states are taken for the Prob.density profile. All most localized states are added and averaged on the very right. The same plots were done for the boundaries along $yzOB$. Here $k_x = \pi$ TRIM was taken which has different localization of the eigenstates. There were only 4 states very well localized which is showed by the circle on the histogramm. These 4 states were localized at 2 neighboring corners. When $k_x = 3\pi/7$ were taken the states are only at one corner localized and all 4 states were localized at each of the 4 corners.*

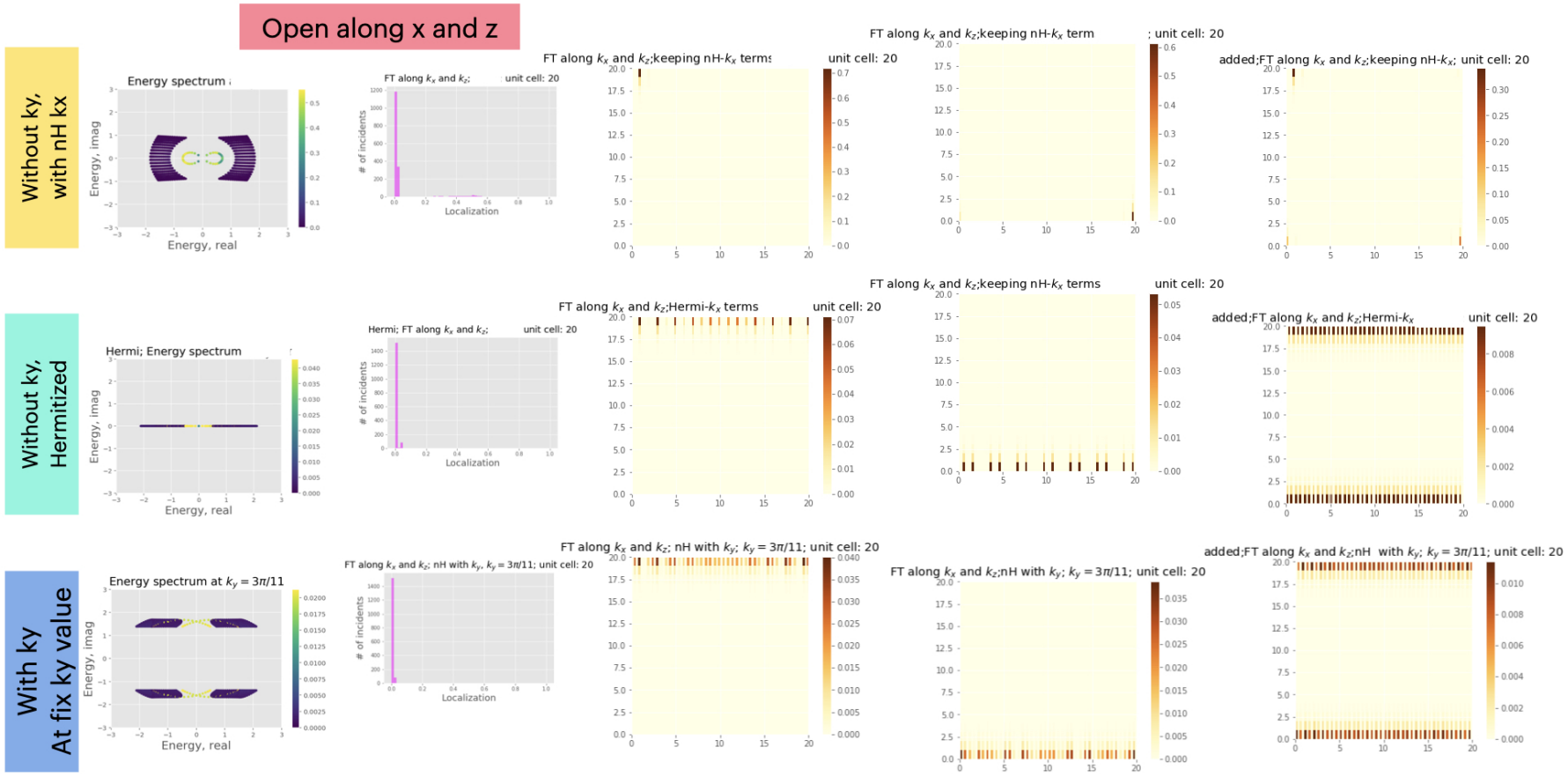

Figure 7.7: *Here we see the energy spectra (20 unit cells), its histogramms and their most localized states prob.density profiles for the $xzOB$ case by taking 3 different cases (from top to bottom) with the hopping constants. Two examples of most localized states were taken to show in order to see where the states are localized. The most localized states were added and averaged and we see on the very right. Because the k_y is completely nH the spectrum for the hermitized case doesnot depend on constant k_y value. The case on the top were taken for removing the nH k_y terms.*

II.4 WZ integral analysis under its symmetries

To prove the WZ integral equals zero the symmetry relation of the third dimension is always needed. From the 2D model we know that the pseudo mirror symmetry does not quantize the WZ term, so is true for a 3D model if we have the pseudo mirror symmetry along the integration direction and not the third dimension which is kept constant.

I could also choose the constant Hamiltonian of the extension without the symmetry operator the same as the one with the symmetry operator. In that case, we can not prove anything, so it is necessary to choose a different constant Hamiltonian so that we have different extensions. In the 2D case, it is important to choose a different constant Hamiltonian, except being non-symmetric under the system Hamiltonian, to get the difference in the integer value and not just zero, so that the integral can be quantized.

The extensions with the symmetry operators are chosen to be the same extension does not imply the same as the extension without symmetry operators yet. This specific choice and the resulting conclusion that the WZ integral equals zero could not be found if we would not have the symmetry relations.

The analytical calculation can be found in Appendix C. In the following table, I tabulated all the analytical (third row) and numerical (fifth row) results. We get everywhere zero as expected. By constructing the real space Hamiltonian along the third direction I am also getting 0 for all 3 directions which are not tabulated.

II.5 Numerical check of the integral values

Table 7.1: *Analysis of symmetries for the WZ integration and its numerical comparison.*

symmetry	integral over	integral/quantization	at_	numerical nonsymm
$(\sigma_y\tau_y)H^\dagger(\boldsymbol{k})(\sigma_y\tau_y)^{-1} = -H(\boldsymbol{k})$	k_x, k_y	0	$k_x = \pi$	0
			$k_x = 0$	0
			$k_x = 3\pi/7$	0
	k_y, k_z	0	$k_x = \pi$	0
			$k_x = 0$	0
			$k_x = 3\pi/7$	0
	k_x, k_z	0	$k_x = \pi$	0
			$k_x = 0$	0
			$k_x = 3\pi/7$	0
$\sigma_z H^\dagger(k_x, k_y, k_z)\sigma_z^{-1} = H(-k_x, k_y, k_z)$	k_x, k_y	0	$k_x = 0$	
			$k_x = \pi$	
	k_y, k_z		$k_x = 0$	
		0	$k_x = \pi$	
	k_x, k_z	0	$k_x = 0$	
			$k_x = \pi$	
$\sigma_x H^\dagger(k_x, k_y, k_z)\sigma_x^{-1} = H(k_x, -k_y, k_z)$	k_x, k_y	0	$k_x = 0$	
			$k_x = \pi$	
	k_y, k_z	0	$k_x = 0$	
			$k_x = \pi$	
	k_x, k_z		$k_x = 0$	
		0	$k_x = \pi$	
$\tau_y H^\dagger(k_x, k_y, k_z)\tau_y^{-1} = -H(k_x, k_y, -k_z)$	k_x, k_y		$k_x = 0$	
		0	$k_x = \pi$	
	k_y, k_z	0	$k_x = 0$	
			$k_x = \pi$	
	k_x, k_z	0	$k_x = 0$	
			$k_x = \pi$	

III Discussion for the 3D model with third order skin effect

I could reproduce the energy spectra for the model like in its Ref.[3]. Also the number of the corner localized states scale with its size in $\mathcal{O}(4L)$ as expected.

In order WZ to be defined the 1D winding number should be zero which I mentioned in the introduction of chapter 6. That means I had to calculate first the 1D winding number and if this is zero we can investigate the WZ term for the system. The nH system has no proper inversion symmetry. That means the 1D winding number is not automatically zero. However, we can also look at the probability density profile and in most cases we see that most of the well localized states are at the edges (very few states are corner localized).

Let us look at the hermitized version of the model, which is a 2D model (x and z plane, see Fig.(7.7)). We have seen on the probability density profile of Hermitian model there are edge states meaning that the 1D winding number could be non-zero. Thus in this case the WZ term should not be defined.

Numerically I am getting everywhere zero for the case when third dimension k dependent or open. The edge states could be the reason why I am getting zero everywhere.

I investigated the WZ terms analytically with its spatial symmetries which is explicitly calculated in Appendix B. I got that having mirror type symmetries the integral either quantized to $\{0, 1/2\}$ or the integral can be totally 0.

Then if we look at the surface probability density profiles then there are edge localized states except the corner localized ones. That could be the reason why we get zero everywhere, because the WZ term is defined when there are no edge localized states.

Chapter 8

The 4th model - exceptional topological insulator model

I Introduction

The exceptional topological insulator (ETI) model [111] is given by the following Hamiltonian

$$H(\boldsymbol{k}) = (\cos k_x + \cos k_y + \cos k_z - M)\tau_z\sigma_0 + \lambda(\sin k_x\tau_x\sigma_x + \sin k_y\tau_x\sigma_y + \sin k_z\tau_x\sigma_z) + [\sin\alpha\tau_0 + \cos\alpha\tau_z](\boldsymbol{B}\cdot\boldsymbol{\sigma}) + i\delta\tau_x\sigma_0 \tag{8.1}$$

Here τ_i and σ_j are the regular Pauli matrices. The Hermitian part of that model (and without the Zeeman field), this is when $\boldsymbol{B} = \delta = 0$, is already very well known 3D Weyl system, i.e. 3D TI, for $1 < |M| < 3$ and trivial phase when $|M|$ reaches values 1 or 3. M is the control parameter for the inversion between s and p orbitals, and λ is the spin-orbit coupling term. $\boldsymbol{B}$ stands for the Zeeman field and for the further discussions we will take $\boldsymbol{B} = (B, B, B)^T$. The α is a term which controls the g factor for the s and p orbitals. When $\alpha = \pi/2$ the g factors are the same and when $\alpha = 0$ then they have opposite signs. [111]

The Hermitian topological insulating phase has single gapless Dirac nodes on its surface BZ and two of them on two different surfaces. After adding the nH term $i\delta\tau_x\sigma_0$ the system becomes defective at energy $E = 0$ due to the exceptional degeneracy of two eigenvectors only are linearly independent (out of 4). Without the Zeeman field the system is isotropic. After introducing the Zeeman field in $(1, 1, 1)$ direction with the $\alpha = 0, \pi/2$ values the system acquires $2\pi/3$ rotational symmetry w.r.t. the field axis. [111]

In its paper Ref.[111] the system is discussed by setting the parameters $\delta = \lambda = 1$ and $M = 3$ where the system is non-trivial. With that parameters the bulk spectrum has completely point gap and also there is a point gap w.r.t the zero energy. For example, at $M = 2.3$, $\lambda = 1$, and $\delta = 0.5$ besides 6 point gap in the bulk spectrum there is a line gap w.r.t. the zero energy. We are interested in the case of previous parameters.

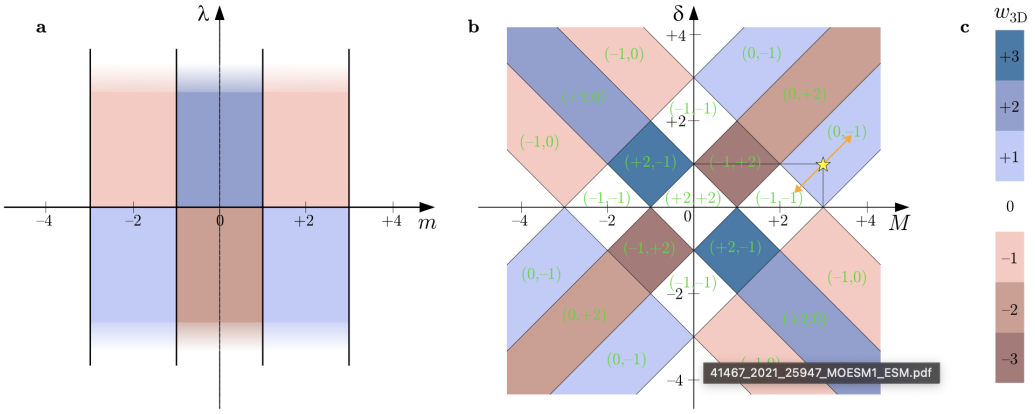

Figure 8.1: *The figure was taken from ref.[111]. The phase diagram of the system parameters. The w_{3D} numbers are the 3D topological invariant. The green numbers on the δ and M plane are the w_{3D}^{LL}, w_{3D}^{UR} numbers, see in supplementary materials in ref.[111].*

After introducing the Zeeman field (with $\alpha = \pi/2$) there is a single Fermi point in the surface BZ at the momentum $k_x = k_y = 0$. Appearance of a single Fermi point is not possible due to the Fermion doubling theorem for nH models in proper 2D. However the surface states are not strictly 2D, but it is surface of the 3D model.

Changing the parameter α from $\alpha = \pi/2$ to $\alpha = 0$ the exceptional point moves from the point gap region to the bulk spectral area which has analogies with the Dirac nodes in 3D TI [112].

II Results

II.1 Energy spectrum with different BC

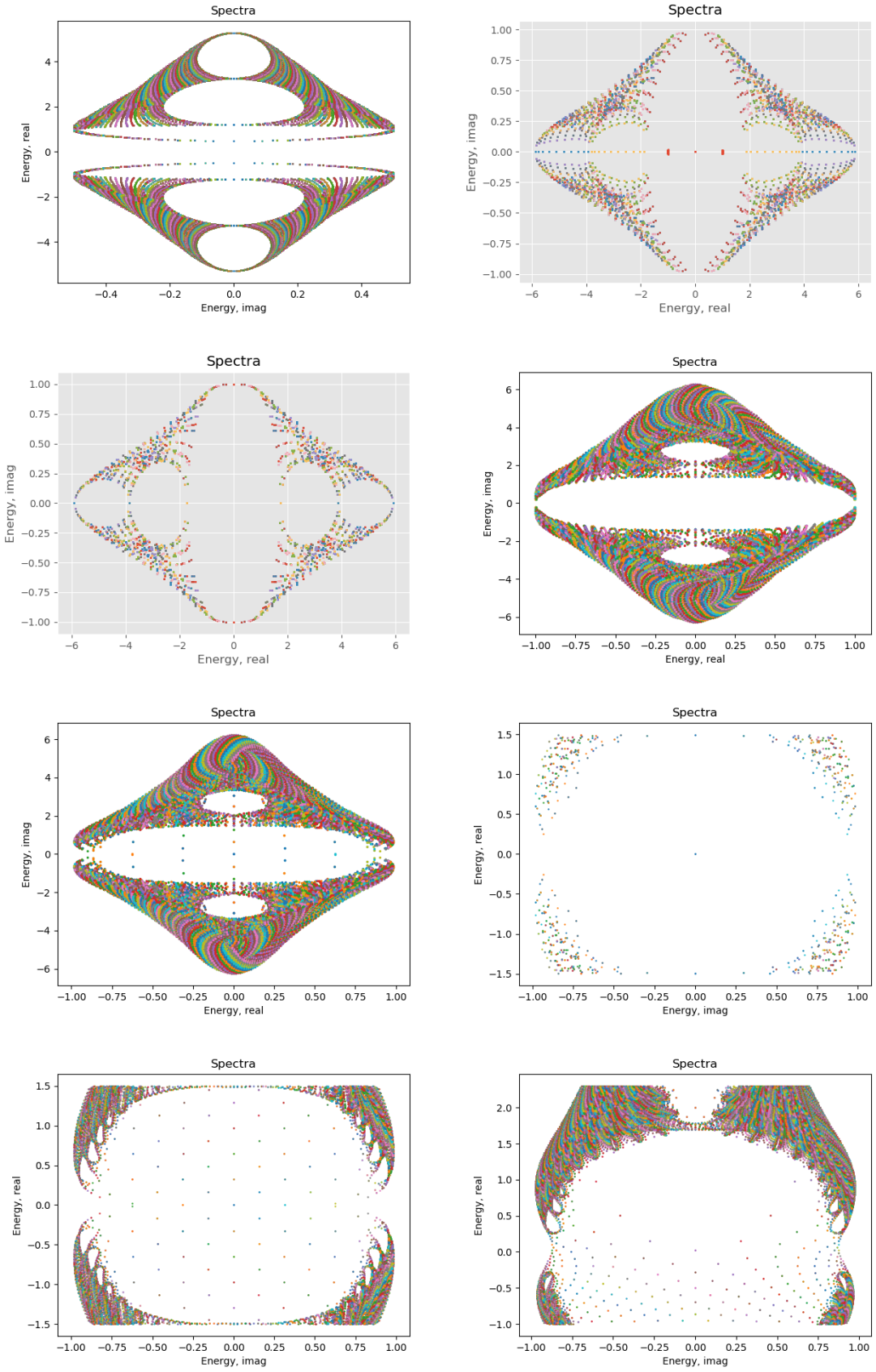

Figure 8.2: *ETI spectra, in z ribbon geometry, OBC and PBC with and without the magnetic field.*

$$\begin{bmatrix} -i(\gamma+\lambda cos(k_x))+\lambda sin(k_x) & \lambda sin(k_z) & -i(\gamma+\lambda cos(k_y))+\lambda sin(k_y) & 0 \\ \lambda sin(k_z) & -i(\gamma+\lambda cos(k_x))+\lambda sin(k_x) & 0 & -i(\gamma+\lambda cos(k_y))+\lambda sin(k_y) \\ i(\gamma+\lambda cos(k_y))+\lambda sin(k_y) & 0 & -i(\gamma+\lambda cos(k_x))-\lambda sin(k_x) & \lambda sin(k_z) \\ 0 & i(\gamma+\lambda cos(k_y))+\lambda sin(k_y) & \lambda sin(k_z) & -i(\gamma+\lambda cos(k_x))-\lambda sin(k_x) \end{bmatrix}$$

$$\begin{aligned} H(\boldsymbol{k}) = & -i(\gamma+\lambda\cos(k_x))I\otimes I+\lambda\sin(k_x)\sigma_z\otimes I \\ & +(\gamma+\lambda\cos(k_y))\sigma_y\otimes I+\lambda\sin(k_y)\sigma_z\otimes I \\ & +\lambda\sin(k_z)I\otimes\sigma_x \end{aligned} \tag{8.2}$$

$$WZ[H]-(WZ[H])^*=\frac{1}{24\pi^2}\oint dk_xdk_ydt\epsilon_{ijk}tr[H^{-1}\partial_iHH^{-1}\partial_jHH^{-1}\partial_kH-(H^{-1}\partial_iHH^{-1}\partial_jHH^{-1}\partial_kH)^*] \tag{8.3}$$

II.2 WZ integral for each plane

Let us investigate the system at TRIM points. At $k_z = \pi$ and $\boldsymbol{B} = 0$ the Hamiltonian looks in the following way:

$$H(\boldsymbol{k}) = (\cos k_x + \cos k_y - 1 - M)\tau_z\sigma_0 + \lambda(\sin k_x \tau_x\sigma_x + \sin k_y \tau_x\sigma_y) + i\delta\tau_x\sigma_0 \qquad (8.4)$$

and from my code at $M = 2$ and $\delta = 1$ for the WZ term it gives me exploded value. For ribbon geometric Hamiltonian the term is also zero. The WZ term at TRIM points is always zero for every value of M and δ. If not TRIM then it is just some values in $[0, 1]$.

Table 8.1: *The WZ integration for the extension of 2D model into 3D version.*

symmetry	integral over	integral/quantization	at_	numerical nonsymm
$\sigma_y H(k_x, k_y)\sigma_y^{-1} = H(-k_x, -k_y)$	k_x, k_y	we expect 0 without kz term	$k_z = 0$ $k_z = \pi$ or without	0.027
$\sigma_z H^\dagger(k_x, k_y, k_z)\sigma_z^{-1} = -H(-k_x, k_y, k_z)$		otherwise nonzero	$k_z = 2\pi/5$	$-0.02 - 7.93 \cdot 10^{-6}i$
$\sigma_x H^\dagger(k_x, k_y, k_z)\sigma_x^{-1} = -H(k_x, -k_y, k_z)$			$k_z = 4\pi/13$	$-0.05 + 0.026i$
$\sigma_x H^T(k_x, k_y, k_z)\sigma_x^{-1} = H(-k_x, k_y, k_z)$	k_y, k_z	0 by pseudo mirror w.r.t. k_x	$k_x = \pi$	$-5.41 \cdot 10^{-6}i$
$\sigma_z H^T(k_x, k_y, k_z)\sigma_z^{-1} = H(k_x, -k_y, k_z)$		except TRIM points	$k_x = 0$	0
$-i\sigma_y H^\dagger(k_x, k_y, k_z) = H(-k_y, k_x, k_z)$			$k_x = 3\pi/7$	0
			$k_x = 5\pi/17$	0
$\tau_y H(k_x, k_y, k_z)\tau_y^{-1} = H(k_x, k_y, -k_z)$	k_x, k_z	0 by pseudo mirror w.r.t. k_y	$k_y = \pi$	$-0.0013i$
		except TRIM points	$k_y = 0$	0
			$k_y = 3\pi/7$	0
			$k_y = 3\pi/13$	0

Table 8.2: *The WZ integration with different constant Hamiltonian and evolution of the spectra of H_{WZ} depending on t. The constant Hamiltonians does not have C_4-type symmetry and various under other symmetries. The symmetries are listed below the tables with the corresponding numbers.*

H_{const}	symmetry	spectral evolution	numerical WZ integral
I	(18)True (21)True (22)True (25)True (26)True (29)False	shrinks to one point on the real axis.	$-0.167 - 0.005i$
σ_x	(18)False (21)True (22)False (25)True (26)False (29)False	shrinks to 2 points on the real axis with complex axis line gap.	-0.5
σ_y	(18)True (21)True (22)True (25)True (26)True (29)False	shrinks to 2 points on the real axis with complex axis line gap.	-0.5
σ_z	(18)True (21)False (22)True (25)False (26)True (29)False	shrinks to 2 points on the real axis with complex axis line gap.	0.5
$\begin{pmatrix} -0.5 & 0.5i \\ -0.5i & 0.5 \end{pmatrix}$	(18)False (21)False (22)True (25)False (26)True (29)False	shrinks to 2 points on the real axis with complex axis line gap.	0.5
$\begin{pmatrix} 0.75 & -0.75 \\ 0.75 & 0.75 \end{pmatrix}$	(18)True (21)False (22)False (25)True (26)True (29)True	shrinks to complex 2 points with real axis line gap.	-1.523i

Table 8.3: *The WZ integration with different constant Hamiltonian and evolution of the spectra of H_{WZ} depending on t. The case with constant Hamiltonians without all system symmetries.The symmetries are listed below the tables with the corresponding numbers.*

H_{const}	symmetry	spectral evolution	numerical WZ integral
$\begin{pmatrix} -0.15+0.05i & 0.05+0.15i \\ 0.05-0.15i & 0.15+0.05i \end{pmatrix}$	(18)False (21)False (22)False (25)False (26)False (29)False	shrinks to complex 2 points with complex axis line gap.	0.391
$\begin{pmatrix} -0.08-0.08i & 0.08+0.25i \\ 0.08-0.25i & 0.08-0.08i \end{pmatrix}$	(18)False (21)False (22)False (25)False (26)False (29)False	shrinks to complex 2 points with complex axis line gap.	0.239
$\begin{pmatrix} -0.08i+0.08 & 0.08i-0.25 \\ 0.08i+0.25 & 0.08i+0.08 \end{pmatrix}$	(18)False (21)False (22)False (25)False (26)False (29)False	shrinks to complex 2 points with real axis line gap.	-0.125-0.338j
$\begin{pmatrix} 0.25+0.25i & 0.25-0.25i \\ -0.25-0.25i & 0.25-0.25i \end{pmatrix}$	(18)False (21)False (22)False (25)False (26)False (29)False	shrinks to complex 2 points with real axis line gap.	0
$\begin{pmatrix} -0.33 & -0.33+0.33i \\ -0.33-0.33i & 0.33 \end{pmatrix}$	(18)False (21)False (22)False (25)False (26)False (29)False	shrinks to 2 points on the real axis with complex axis line gap.	0.164
$\begin{pmatrix} -0.5 & -0.5 \\ -0.5 & 0.5 \end{pmatrix}$	(18)False (21)False (22)False (25)False (26)False (29)False	shrinks to 2 points on the real axis with complex axis line gap.	0

$$\sigma_y H(k_x, k_y)\sigma_y^{-1} = H(-k_x, -k_y) \quad \text{eq.(18)}$$
$$\sigma_z H^\dagger(k_x, k_y)\sigma_z^{-1} = -H(-k_x, k_y) \quad \text{eq.(21)}$$
$$\sigma_x H^\dagger(k_x, k_y)\sigma_x^{-1} = -H(k_x, -k_y) \quad \text{eq.(22)}$$
$$\sigma_x H^T(k_x, k_y)\sigma_x^{-1} = H(-k_x, k_y) \quad \text{eq.(25)}$$
$$\sigma_z H^T(k_x, k_y)\sigma_z^{-1} = H(k_x, -k_y) \quad \text{eq.(26)}$$
$$-i\sigma_y H^\dagger(k_x, k_y) = H(-k_y, k_x) \quad \text{eq.(29)}$$

Table 8.4: *ETI model,WZ term with or wihtout B field. When no B field there is no restrictions on the constant Hamiltonian and therefore the WZ terms are real. When we do have B field I guess there exists some symmetry and there are certains restrictions on the H_{const} and therefore some complex integral values for the wrong chosen H_{const}. In order to get real numbers I have to experiment by taking different H_{const} or I have to know the symmetry explicitly.*

H_{const}	integral over	at	α	without B field	with B field
$\text{kron}(\sigma_x, \sigma_x)$	ky and kz	$k_x = \pi$	$\pi/2$	0.00039	0.00043
$\text{kron}(\sigma_x, \sigma_x)$	ky and kz	$k_x = \pi$	0	0.00039	0.0004-0.0041j
$\text{kron}(\sigma_x, \sigma_x)$	ky and kz	$k_x = 0$	$\pi/2$	-0.5	-0.5
$\text{kron}(\sigma_x, \sigma_x)$	ky and kz	$k_x = 0$	0	-0.5	$-0.49 + 0.11j$
$\text{kron}(\sigma_x, \sigma_x)$	kx and kz	$k_y = \pi$	$\pi/2$	3.4e-06	0
$\text{kron}(\sigma_x, \sigma_x)$	kx and kz	$k_y = \pi$	0	3.4e-06	0.12-0.06j
$\text{kron}(\sigma_x, \sigma_x + \sigma_z)$	kx and kz	$k_y = 0$	$\pi/2$	singular matrix od. 0	-0.02-0.08j
$\text{kron}(\sigma_x, \sigma_x + \sigma_z)$	kx and kz	$k_y = 0$	0	singular matrix od. 0	0.06-0.02j
$\text{kron}(\sigma_x, \sigma_x)$	kx and ky	$k_z = \pi$	$\pi/2$	0	0
$\text{kron}(\sigma_x, \sigma_x)$	kx and ky	$k_z = \pi$	0	0	2.2e-05-0.004j
$\text{kron}(\sigma_x, \sigma_x)$	kx and ky	$k_z = 0$	$\pi/2$	0	0
$\text{kron}(\sigma_x, \sigma_x)$	kx and ky	$k_z = 0$	0	0	0.31+0.39j

III Discussion for the ETI model

I could reproduce the energy spectra for different boundary conditions. Since the system has exceptional topology the energy spectrum in fully periodic boundary should have a point gap and thus the system is intrinsically non-Hermitian. In this case, it is guaranteed to have skin modes according to the "universal skin effect" of Ref.[8].

The main result of my project on that model is the numerical calculation of the WZ integrals. The challenge of calculating the WZ term in my way is that how to choose the H_{const} for my extending Hamiltonian $H_{WZ} = H(\boldsymbol{k})(1-t) + tH_{const}$.

In its Ref.[3] H_{const} is the Hamiltonian for the vacuum. That sounds consistent with my assumption that the H_{const} should not possess the WZ quantizing symmetry. In the 2D model also the H_{const} should break the C_4-type symmetry so that my integral was 0.5 otherwise it takes different values.

Then I calculated for each surface the WZ term for the 3D ETI model. I systematically calculated the WZ terms for some possible symmetric constant Hamiltonian to calculate the WZ terms. It is important to notice that the constant Hamiltonian should not close the energy gap during interpolation to the system Hamiltonian, i.e. the ETI Hamiltonian. The numerical results are tabulated.

I did not check if the 1D winding number is zero. If this is not zero the WZ term is anyways not defined.

On the other side, I got many 0.5 values for the integral which is consistent with my analytical results where the term should be quantized to $\{0, 1/2\}$. And also with the fact that the WZ term should be non-zero when the system has corner localized states. To properly investigate I should know the symmetry explicitly when the system has a non-zero Zeeman field.

Chapter 9

General conclusion

My goal of the project was to investigate how the non-Hermitian Hamiltonians could recover the bulk boundary correspondence, which is generally broken in nH systems. Since the topology of the systems is deeply connected with the symmetries it was important to understand the symmetry interrelations within the models.

I numerically investigated 4 different models in 2D and 3D. The first model was a 2D reciprocal non-Hermitian nodal system, called the π-flux model. The system has no symmetries in presence of non-Hermitian diagonal hoppings. The system has exceptional topology so that the skin effect is guaranteed by the "universal skin effect" of Ref.[8]. In that model, the skin effect was predicted by the 1D winding number along with k_y ribbon geometry. And the bulk boundary correspondence could be recovered with the SVD spectrum which was proposed for the recovery of BBC in Ref.[1].

In my second model, I had to reproduce the quantization of the geometrical WZ term which can be quantized in presence of spatial symmetries. I could reproduce the result and the term should be quantized to $\{0, 1/2\}$ in presence of C_4-type symmetries. Following, I investigated the interrelation of the WZ term with the symmetry of the system and topological phase transition by looking at the energy gap evolution by varying system parameters. All results were consistent and my conclusion was C_4-type symmetry is the symmetry that causes the symmetry enhanced topology. Only in presence of C_4-type symmetry, the WZ term was quantized and not for the edge state phase.

My third and fourth models were 3D systems and I continuously studied the WZ terms for these models. The WZ term is for 2D systems defined. However, like the 1D winding numbers, we could use it as a weak topological invariant. I analytically studied the term in the presence of spatial symmetries for the third dimension. In that case, the term can take just a value in the circle $[0, 1]$, or 0 or it can be quantized to $\{0, 1/2\}$ in presence of

mirror type symmetries with respect to third dimension. All analytical results are given on the decision tree below in Fig.(9.1 and 9.2).

I get for the third model everywhere zero for the WZ integrals and that could come from the fact that there are edge states localized at the surface probability density profile. The explicit symmetries should be determined in presence of Zeeman field. However, I get for some H_{const} choices $WZ = 0.5$ which could be because of the quantization of the WZ term.

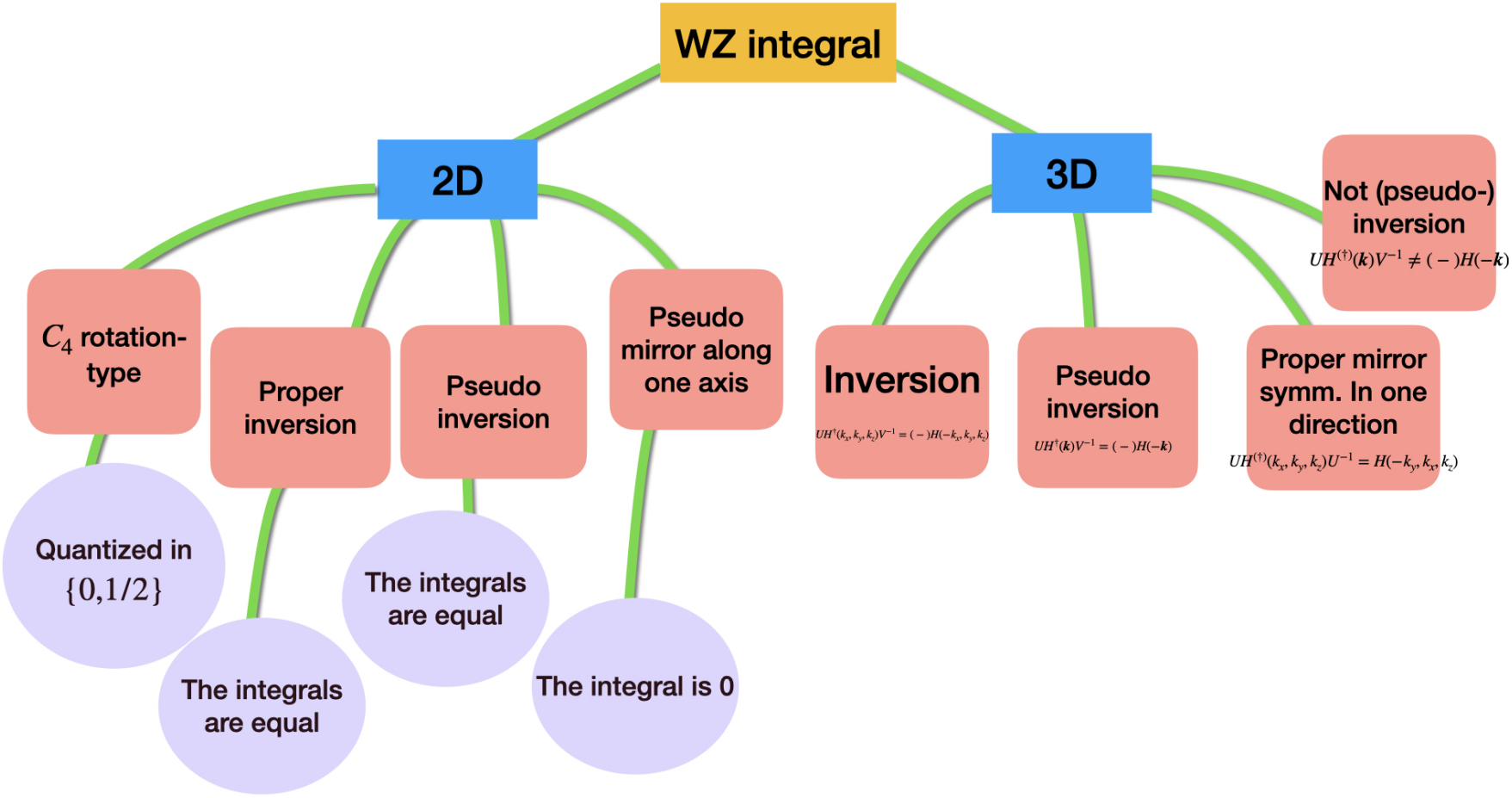

Figure 9.1: *Decision tree for the WZ integral.*

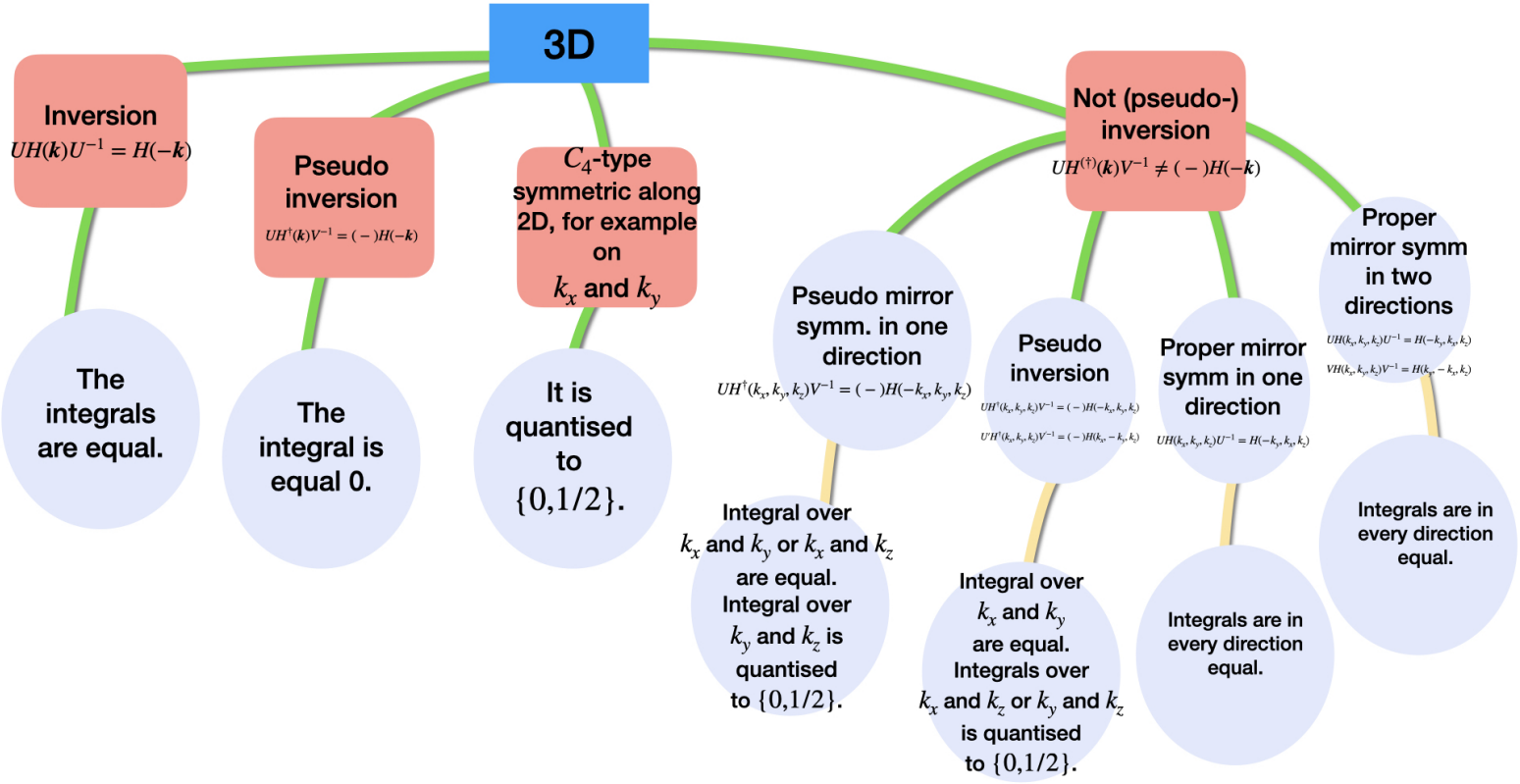

Figure 9.2: *Decision tree for the WZ integral for the 3D case. 9.1*

Appendix A

Winding number expression

The expression for the phase as trace is derived here:

$$\partial_k \ln \det H(k) = \mathrm{Tr}[H^{-1}(k)\partial_k H(k)] \tag{A.1}$$

$$\partial_k \ln \det H(k) \equiv \lim_{\epsilon \to 0} \frac{\ln \det H(k+\epsilon) - \ln \det H(k)}{\epsilon} \tag{A.2}$$

$$\begin{aligned} &\det[H(k) + \epsilon \partial_k H(k)] + O(\epsilon^2) \\ &\quad = \det H(k) \det[I + \epsilon H^{-1}(k)\partial_k H(k)] + O(\epsilon^2) \\ &\quad = \det H(k)[]1 + \epsilon \mathrm{Tr}\{H^{-1}(k)\partial_k H(k)]\} + O(\epsilon^2) \end{aligned} \tag{A.3}$$

using the approximation $\ln(1+x) = x + O(x^2)$ we obtain the eq.(A.1). [75]

Appendix B

Quantization of the Wess-Zumino term for 2D models

To make my calculations simpler I wrote the system Hamiltonian H in eq.(6.1) explicitly and also taking its Hermitian conjugate with the rotated reciprocal axes

$$H(\vec{k}) = \begin{pmatrix} -i\gamma - i\lambda\cos k_x + \lambda\sin k_x & -i\gamma - i\lambda\cos k_y + \lambda\sin k_y \\ i\gamma + i\lambda\cos k_y + \lambda\sin k_y & -i\gamma - i\lambda\cos k_x - \lambda\sin k_x \end{pmatrix} \tag{B.1}$$

$$\begin{aligned} H^{\dagger}(k_y, -k_x) &= \begin{pmatrix} -i\gamma - i\lambda\cos k_y + \lambda\sin k_y & -i\gamma - i\lambda\cos k_x - \lambda\sin k_x \\ i\gamma + i\lambda\cos k_x - \lambda\sin k_x & -i\gamma - i\lambda\cos k_y - \lambda\sin k_y \end{pmatrix}^{\dagger} \\ &= \begin{pmatrix} i\gamma + i\lambda\cos k_y + \sin k_y & -i\gamma - i\lambda\cos k_x + \lambda\sin k_x \\ i\gamma + i\lambda\cos k_x - \sin k_x & i\gamma + i\lambda\cos -k_y - \lambda\sin k_y \end{pmatrix} \end{aligned} \tag{B.2}$$

For an extension $H_{WZ}(k_x, k_y, t)$ we can introduce another extension by applying the rotation matrices $H'_{WZ}(k_x, k_y, t) = UH^{\dagger}_{WZ}(k_y, -k_x, t)V^{-1}$ for $t \in [0, 1]$ and here $H(k_x, k_y, t = 0)$ is the system Hamiltonian rotated once backward and $H'(k_y, -k_x, t = 0)$ takes the same form as the original Hamiltonian. The WZ integrals for the above two extensions are given by:

$$\begin{aligned} WZ[H_{WZ}] &= \int_{T^2 x[0,1]} tr\left[(H_{WZ})^{-1} dH_{WZ}\right]^3 \\ &= \oint_{T^2 x[0,1]} \frac{d^2 k dt}{24\pi^2} \epsilon^{ijk} tr((H_{WZ})^{-1}\partial_i H_{WZ}(H_{WZ})^{-1}\partial_j H_{WZ}(H_{WZ})^{-1}\partial_k H_{WZ}) \end{aligned} \tag{B.3}$$

$$
\begin{aligned}
WZ[H'_{WZ}] &= \int_{T^2x[0,1]} tr\left[(H'_{WZ})^{-1}dH'_{WZ}\right]^3 \\
&= \oint_{T^2x[0,1]} \frac{d^2kdt}{24\pi^2}\epsilon^{ijk}tr((H'_{WZ})^{-1}\partial_i H'_{WZ}(H'_{WZ})^{-1}\partial_j H'_{WZ}(H'_{WZ})^{-1}\partial_k H'_{WZ})
\end{aligned}
\tag{B.4}
$$

I write the trace here explicitly. For convenience, I use for the extended Hamiltonian $H_{WZ}(k_x, k_y, t) = H(k_x, k_y, t)$ and for the system Hamiltonian just $H(k_x, k_y, t = 0) = H(k_x, k_y)$:

$$
\begin{aligned}
&tr\{(UH^\dagger(k_y,-k_x)V^{-1})^{-1}\partial_i U(H^\dagger(k_y,-k_x)V^{-1}) \\
&\quad (UH^\dagger(k_y,-k_x)V^{-1})^{-1}\partial_j(UH^\dagger(k_y,-k_x)V^{-1}) \\
&\quad (UH^\dagger(k_y,-k_x)V^{-1})^{-1}\partial_k(UH^\dagger(k_y,-k_x)V^{-1})\} = \\
&tr\{VH^{\dagger-1}(k_y,-k_x)U^{-1}U\partial_i H^\dagger(k_y,-k_x)V^{-1} \\
&\quad VH^{\dagger-1}(k_y,-k_x)U^{-1}U\partial_j(H^\dagger(k_y,-k_x)V^{-1} \\
&\quad VH^{\dagger-1}(k_y,-k_x)U^{-1}U\partial_k H^\dagger(k_y,-k_x)V^{-1}\} = \\
&tr\{VH^{\dagger-1}(k_y,-k_x)\partial_i H^\dagger(k_y,-k_x) \\
&\quad H^{\dagger-1}(k_y,-k_x)\partial_j(H^\dagger(k_y,-k_x) \\
&\quad H^{\dagger-1}(k_y,-k_x)\partial_k H^\dagger(k_y,-k_x)V^{-1}\}
\end{aligned}
\tag{B.5}
$$

Since U and V matrices are independet of k_x, k_y and t, I can switch ∂_{ijk} with U and V.

By the cyclic permutation of the matrices in the trace we get rid of the V matrices and I use the fact that Hermitian conjugation and inversion of a matrix can be exchanged. Then take the Hermitian conjugation out of the all matrices and doing once again cyclic

permutation we get:

$$\begin{aligned}
&tr\{(\partial_k H(k_y,-k_x)\\
&\quad H^{-1}(k_y,-k_x)\partial_j(H(k_y,-k_x)\\
&\quad H^{-1}(k_y,-k_x)\partial_i H(k_y,-k_x)H^{-1}(k_y,-k_x))^\dagger\} =\\
&(tr\{\partial_k H(k_y,-k_x)\\
&\quad H^{-1}(k_y,-k_x)\partial_j H(k_y,-k_x)\\
&\quad H^{-1}(k_y,-k_x)\partial_i H(k_y,-k_x)H^{-1}(k_y,-k_x)\})^* =\\
&(tr\{H^{-1}(k_y,-k_x)\partial_k H(k_y,-k_x)\\
&\quad H^{-1}(k_y,-k_x)\partial_j(H(k_y,-k_x)\\
&\quad H^{-1}(k_y,-k_x)\partial_i H(k_y,-k_x)\})^* =\\
&tr\{H^{-1}(k_y,-k_x)\partial_k H(k_y,-k_x)\\
&\quad H^{-1}(k_y,-k_x)\partial_j H(k_y,-k_x)\\
&\quad H^{-1}(k_y,-k_x)\partial_i H(k_y,-k_x)\}
\end{aligned} \tag{B.6}$$

Because the overall integral is a value in $[0,1]$, we can leave out the complex conjugation. The minus sign from the partial derivative w.r.t. $-k_x$ multiplies with the minus sign from substitution $-d(-k_x)$ and one minus sign from the integral limits gives us overall negative sign for the integral. Now, the order of the derivatives changed and if we look at the indices closer the new order of ϵ tensor is: $\epsilon'^{ijk} = -\epsilon^{ijk}$. Finally, we can resubstitute k'_x and k_y in the Hamiltonian functions and accordingly change the derivatives. This results in switching the 2 indices in the "new" ϵ tensor.

The order of the derivatives w.r.t. the sign of epsilon tensor (I just write here the indices and they are the transpose of the signs of ϵ):

$$\begin{aligned}
&\epsilon^{123}\partial_3\partial_2\partial_1\\
&\epsilon^{312}\partial_2\partial_2\partial_3\\
&\epsilon^{231}\partial_1\partial_3\partial_2\\
&\epsilon^{132}\partial_2\partial_3\partial_1\\
&\epsilon^{213}\partial_3\partial_1\partial_2\\
&\epsilon^{321}\partial_1\partial_2\partial_3
\end{aligned} \tag{B.7}$$

Additionally, if I switch 2 indices the ϵ tensor gives us by definition one minus sign.

$$\begin{aligned} WZ[H'_{WZ}] = -\int_0^1 \int_o^{2\pi} \int_o^{2\pi} \frac{d^2k'dt}{24\pi^2} \epsilon'^{ijk} tr\{H^{-1}(k'_x,k_y)\partial_i H(k'_x,k_y) \\ H^{-1}(k'_x,k_y)\partial_j (H(k'_x,k_y) \\ H^{-1}(k'_x,k_y)\partial_k H(k'_x,k_y)\} = -WZ[H_{WZ}] \end{aligned} \tag{B.8}$$

$$\begin{aligned} WZ[H_{WZ}] = \int_0^1 \int_o^{2\pi} \int_o^{2\pi} \frac{d^2kdt}{24\pi^2} \epsilon^{ijk} tr\{H^{-1}(k_x,k_y,t)\partial_k H(k_x,k_y,t) \\ H^{-1}(k_x,k_y,t)\partial_j (H(k_x,k_y,t) \\ H^{-1}(k_x,k_y,t)\partial_i H(k_x,k_y,t)\} \end{aligned} \tag{B.9}$$

Conclusion for the WZ term analysis

In my calculation only for the C_4- type symmetry the WZ integral is quantized in $\{0, 1/2\}$. For the mirror type symmetries the integrals for the two extensions the same, meaning that the integral can take any value in the circle $[0, 1]$.

Appendix C

Quantization of Wess-Zumino term in presence of spatial symmetries for 3D models

To prove the WZ integral equals to zero the symmetry relation of the third dimension is always needed. From the 2D model we know that the pseudo mirror symmetry does not quantize the WZ term, so is true for 3D model if we have the pseudo mirror symmetry along the integration direction and not third dimension which is kept constant.

I could also choose the constant Hamiltonian of the extension without the symmetry operator the same as the one with the symmetry operator. In that case we can not prove anything, so it is necessary to choose a different constant Hamiltonian, so that we have different extensions. In the 2D case it is important to choose a different constant Hamiltonian, except being non-symmetric under the system Hamiltonian, too in order to get the difference the integer value and not just zero, so that the integral can be quantized.

The extensions with the symmetry operators are just chosen to be the same extension does not imply the same as the extension without symmetry operators yet. This specific choice and the resulting conclusion that the WZ integral equals zero could not be found if we would not have the symmetry relations. I think that means the choice does not contradict the generality. As we have chosen U and V operators to show the relation

In the following I calculate if the WZ term is quantized along the xy-plane for the pseudo mirror symmetry w.r.t. the x axis by integrating the WZ integral over k_x and k_y. I show how the WZ integral of the extended Hamiltonian without symmetry operators applied

is related to the integral of a Hamiltonian by building a different extension using the symmetry operators.

$$WZ[H'_{WZ}(k_x,k_y,k_z,t)] = WZ[\sigma_z H^\dagger(-k_x,k_y,k_z,t)\sigma_z^{-1}] \tag{C.1}$$

$$\begin{aligned}= \int_0^1\int_0^{2\pi}\int_0^{2\pi}\frac{dk_x dk_y dt}{24\pi^2}\epsilon^{ijk} tr\{&(\sigma_z H^\dagger(-k_x,k_y,k_z,t)\sigma_z^{-1})^{-1}\partial_i(\sigma_z H^\dagger(-k_x,k_y,k_z,t)\sigma_z^{-1})\\ &(\sigma_z H^\dagger(-k_x,k_y,k_z,t)\sigma_z^{-1})^{-1}\partial_j(\sigma_z H^\dagger(-k_x,k_y,k_z,t)\sigma_z^{-1})\\ &(\sigma_z H^\dagger(-k_x,k_y,k_z,t)\sigma_z^{-1})^{-1}\partial_k(\sigma_z H^\dagger(-k_x,k_y,k_z,t)\sigma_z^{-1})\}\end{aligned}$$

$$\begin{aligned}= \int_0^1\int_0^{2\pi}\int_0^{2\pi}\frac{dk_x dk_y dt}{24\pi^2}\epsilon^{ijk} tr\{&(H^\dagger(-k_x,k_y,k_z,t))^{-1}\partial_i H^\dagger(-k_x,k_y,k_z,t)\\ &((H^\dagger(-k_x,k_y,k_z,t))^{-1}\partial_j H^\dagger(-k_x,k_y,k_z,t)\\ &((H^\dagger(-k_x,k_y,k_z,t))^{-1}\partial_k H^\dagger(-k_x,k_y,k_z,t)\}\end{aligned} \tag{C.2}$$

$$\begin{aligned}= \int_0^1\int_0^{2\pi}\int_0^{2\pi}\frac{dk_x dk_y dt}{24\pi^2}\epsilon^{ijk} tr\{&[(H(-k_x,k_y,k_z,t))^{-1}\partial_k H(-k_x,k_y,k_z,t)\\ &((H(-k_x,k_y,k_z,t))^{-1}\partial_j H(-k_x,k_y,k_z,t)\\ &((H(-k_x,k_y,k_z,t))^{-1}\partial_i H(-k_x,k_y,k_z,t)]^\dagger\}\end{aligned} \tag{C.3}$$

$$\begin{aligned}= \int_0^1\int_0^{2\pi}\int_0^{2\pi}\frac{dk'_x dk_y dt}{24\pi^2}\epsilon^{ijk}(-1) tr\{&(H(k'_x,k_y,k_z,t))^{-1}\partial_k H(k'_x,k_y,k_z,t)\\ &((H(k'_x,k_y,k_z,t))^{-1}\partial_j H(k'_x,k_y,k_z,t)\\ &((H(k'_x,k_y,k_z,t))^{-1}\partial_i H(k'_x,k_y,k_z,t)\}\end{aligned} \tag{C.4}$$

$$\begin{aligned}= \int_0^1\int_0^{2\pi}\int_0^{2\pi}\frac{dk'_x dk_y dt}{24\pi^2}\epsilon^{ijk} tr\{&(H(k'_x,k_y,k_z,t))^{-1}\partial_i H(k'_x,k_y,k_z,t)\\ &((H(k'_x,k_y,k_z,t))^{-1}\partial_j H(k'_x,k_y,k_z,t)\\ &((H(k'_x,k_y,k_z,t))^{-1}\partial_k H(k'_x,k_y,k_z,t)\}\end{aligned} \tag{C.5}$$

$$= WZ[H_{WZ}(k'_x,k_y,k_z,t)] \tag{C.6}$$

Here H_{WZ} is the extended Hamiltonian and H'_{WZ} is if we apply the symmetry operator once back to the system Hamiltonian H and extend it with the same extension and finally apply again the symmetry operators to the transformed extended Hamiltonian in order to get a different extension using the symmetry of the system. We see that the WZ term is not quantized, because we get the same integral as not rotated one.

The integral over k_x and k_z would give the exact same result.
In the following I integrate the same extension over k_y and k_z.

$$WZ[H'_{WZ}(k_x,k_y,k_z,t)] = WZ[\sigma_z H^\dagger(-k_x,k_y,k_z,t)\sigma_z^{-1}] \tag{C.7}$$

$$\begin{aligned}= \int_0^1\int_0^{2\pi}\int_0^{2\pi} \frac{dk_y dk_z dt}{24\pi^2}\epsilon^{ijk} tr\{&(\sigma_z H^\dagger(-k_x,k_y,k_z,t)\sigma_z^{-1})^{-1}\partial_i(\sigma_z H^\dagger(-k_x,k_y,k_z,t)\sigma_z^{-1})\\ &(\sigma_z H^\dagger(-k_x,k_y,k_z,t)\sigma_z^{-1})^{-1}\partial_j(\sigma_z H^\dagger(-k_x,k_y,k_z,t)\sigma_z^{-1})\\ &(\sigma_z H^\dagger(-k_x,k_y,k_z,t)\sigma_z^{-1})^{-1}\partial_k(\sigma_z H^\dagger(-k_x,k_y,k_z,t)\sigma_z^{-1})\}\end{aligned}$$

$$\begin{aligned}= \int_0^1\int_0^{2\pi}\int_0^{2\pi} \frac{dk_y dk_z dt}{24\pi^2}\epsilon^{ijk} tr\{&(H(-k_x,k_y,k_z,t))^{-1}\partial_k H(-k_x,k_y,k_z,t)\\ &((H(-k_x,k_y,k_z,t))^{-1}\partial_j H(-k_x,k_y,k_z,t)\\ &((H(-k_x,k_y,k_z,t))^{-1}\partial_i H(-k_x,k_y,k_z,t)\}\end{aligned} \tag{C.8}$$

$$\begin{aligned}= -\int_0^1\int_0^{2\pi}\int_0^{2\pi} \frac{dk_y dk_z dt}{24\pi^2}\epsilon^{ijk} tr\{&(H(-k_x,k_y,k_z,t))^{-1}\partial_i H(-k_x,k_y,k_z,t)\\ &((H(-k_x,k_y,k_z,t))^{-1}\partial_j H(-k_x,k_y,k_z,t)\\ &((H(-k_x,k_y,k_z,t))^{-1}\partial_k H(-k_x,k_y,k_z,t)\}\end{aligned} \tag{C.9}$$

$$\neq WZ[H_{WZ}(k_x,k_y,k_z,t)] \tag{C.10}$$

$$\text{except:}\quad WZ[H'_{WZ}(0,k_y,k_z,t)] = -WZ[H_{WZ}(0,k_y,k_z,t)] \tag{C.11}$$

$$\Rightarrow WZ[H_{WZ}(0,k_y,k_z,t)] \in \{0,1/2\} \tag{C.12}$$

$$WZ[H'_{WZ}(\pi,k_y,k_z,t)] = -WZ[H_{WZ}(\pi,k_y,k_z,t)] \tag{C.13}$$

$$\Rightarrow WZ[H_{WZ}(\pi,k_y,k_z,t)] \in \{0,1/2\} \tag{C.14}$$

The integrals are not equal for general k_x and at the TRIM points for k_x the integral is equal to zero. However, I showed in the conclusion part, that the integral of the shape eq.(C.9) us quantized to the following values $\{-1,-\frac{1}{2},0,\frac{1}{2},1\}$.
For the mirror type symmetry w.r.t. y axis the WZ integration over k_x and k_z is also not equal and at the k_y TRIM points the integral is equal to zero. For other values of the k_y the integral is not clear.
We can also show that the integration over k_x and k_y and the other one over k_z and k_y are equal: $WZ[H_{WZ}] = WZ[H'_{WZ}]$.

The pseudo mirror symmetry w.r.t. the z axis is slightly different in form than the other axes, so let us look at the integral explicitly:

$$WZ[H'_{WZ}(k_x,k_y,k_z,t)] = WZ[-\tau_y H^\dagger(k_x,k_y,-k_z,t)\tau_y^{-1}] \tag{C.15}$$

$$\begin{aligned}= \int_0^1\int_0^{2\pi}\int_0^{2\pi} \frac{dk_x dk_y dt}{24\pi^2}\epsilon^{ijk} tr\{&(-1)^6(\tau_y H^\dagger(k_x,k_y,-k_z,t)\tau_y^{-1})^{-1}\partial_i(\tau_y H^\dagger(k_x,k_y,-k_z,t)\tau_y^{-1})\\ &(\tau_y H^\dagger(k_x,k_y,-k_z,t)\tau_y^{-1})^{-1}\partial_j(\tau_y H^\dagger(k_x,k_y,-k_z,t)\tau_y^{-1})\\ &(\tau_y H^\dagger(k_x,k_y,-k_z,t)\tau_y^{-1})^{-1}\partial_k(\tau_y H^\dagger(k_x,k_y,-k_z,t)\tau_y^{-1})\}\end{aligned}$$

$$\begin{aligned}= \int_0^1\int_0^{2\pi}\int_0^{2\pi} \frac{dk_x dk_y dt}{24\pi^2}\epsilon^{ijk} tr\{&(H(k_x,k_y,-k_z,t))^{-1}\partial_k H(k_x,k_y,-k_z,t)\\ &((H(k_x,k_y,-k_z,t))^{-1}\partial_j H(-k_x,k_y,-k_z,t)\\ &((H(k_x,k_y,-k_z,t))^{-1}\partial_i H(-k_x,k_y,-k_z,t)\}\end{aligned} \tag{C.16}$$

$$\begin{aligned}= -\int_0^1\int_0^{2\pi}\int_0^{2\pi} \frac{dk_x dk_y dt}{24\pi^2}\epsilon^{ijk} tr\{&(H(k_x,k_y,-k_z,t))^{-1}\partial_i H(k_x,k_y,-k_z,t)\\ &((H(k_x,k_y,-k_z,t))^{-1}\partial_j H(k_x,k_y,-k_z,t)\\ &((H(k_x,k_y,-k_z,t))^{-1}\partial_k H(k_x,k_y,-k_z,t)\}\end{aligned} \tag{C.17}$$

$$\begin{aligned}= -\int_0^1\int_0^{2\pi}\int_0^{2\pi} \frac{dk_x dk_y dt}{24\pi^2}\epsilon^{ijk} tr\{&(H(k_x,k_y,-k_z,t))^{-1}\partial_i H(k_x,k_y,-k_z,t)\\ &((H(k_x,k_y,-k_z,t))^{-1}\partial_j H(k_x,k_y,-k_z,t)\\ &((H(k_x,k_y,-k_z,t))^{-1}\partial_k H(k_x,k_y,-k_z,t)\}\end{aligned} \tag{C.18}$$

$$\neq WZ[H_{WZ}(k_x,k_y,k_z,t)] \tag{C.19}$$

$$\text{except:}\quad WZ[H'_{WZ}(k_x,k_y,0,t)] = -WZ[H_{WZ}(k_x,k_y,0,t)] \tag{C.20}$$

$$\Rightarrow WZ[H_{WZ}(k_x,k_y,0,t)] \in \{0,1/2\} \tag{C.21}$$

$$WZ[H'_{WZ}(k_x,k_y,\pi,t)] = -WZ[H_{WZ}(k_x,k_y,\pi,t)] \tag{C.22}$$

$$\Rightarrow WZ[H_{WZ}(k_x,k_y,\pi,t)] \in \{0,1/2\} \tag{C.23}$$

Here if I choose the extension as $(1-t)H+tH_{const}$, I will have different integrand in both H'_{WZ} and H_{WZ}. In the integral of H'_{WZ} I will have the following extended Hamiltonian:

$$\tau_y((1-t)(-1)H^\dagger(k_x,k_y,-k_z)+tH^\dagger_{const})\tau_y^{-1} = (-1)(\tau_y((1-t)H^\dagger(k_x,k_y,-k_z)-tH^\dagger_{const})\tau_y^{-1}) \tag{C.24}$$

$$\partial_t(\tau_y((1-t)H^\dagger(k_x,k_y,-k_z)-tH^\dagger_{const})\tau_y^{-1}) = (\tau_y(-H^\dagger(k_x,k_y,-k_z)-H^\dagger_{const})\tau_y^{-1}) \tag{C.25}$$

Instead, if we take $U=-\tau_y$ and $V=\tau_y$, we have in front of H_{const} plus sign and therefore at the TRIM points for k_z the integral is equal zero. For other values of k_z the two extensions are not equal.

Now I integrate over k_y and k_z:

$$WZ[H'_{WZ}(k_x,k_y,k_z,t)] = WZ[-\tau_y H^\dagger(k_x,k_y,-k_z,t)\tau_y^{-1}] \tag{C.26}$$

$$\begin{aligned}
&= \int_0^1 \int_0^{2\pi} \int_0^{2\pi} \frac{dk_y dk_z dt}{24\pi^2} \epsilon^{ijk} tr\{(-1)^6 (\tau_y H^\dagger(k_x,k_y,-k_z,t)\tau_y^{-1})^{-1} \partial_i (\tau_y H^\dagger(k_x,k_y,-k_z,t)\tau_y^{-1}) \\
&\qquad (\tau_y H^\dagger(k_x,k_y,-k_z,t)\tau_y^{-1})^{-1} \partial_j (\tau_y H^\dagger(k_x,k_y,-k_z,t)\tau_y^{-1}) \\
&\qquad (\tau_y H^\dagger(k_x,k_y,-k_z,t)\tau_y^{-1})^{-1} \partial_k (\tau_y H^\dagger(k_x,k_y,-k_z,t)\tau_y^{-1})\}
\end{aligned}$$

$$\begin{aligned}
&= \int_0^1 \int_0^{2\pi} \int_0^{2\pi} \frac{dk_y dk_z dt}{24\pi^2} \epsilon^{ijk} tr\{(H(k_x,k_y,-k_z,t))^{-1} \partial_k H(k_x,k_y,-k_z,t) \\
&\qquad ((H(k_x,k_y,-k_z,t))^{-1} \partial_j H(-k_x,k_y,-k_z,t) \\
&\qquad ((H(k_x,k_y,-k_z,t))^{-1} \partial_i H(-k_x,k_y,-k_z,t)\}
\end{aligned} \tag{C.27}$$

$$\begin{aligned}
&= \int_0^1 \int_0^{2\pi} \int_0^{2\pi} \frac{dk_y dk'_z dt}{24\pi^2} \epsilon^{ijk} tr\{(H(k_x,k_y,k'_z,t))^{-1} \partial_i H(k_x,k_y,k'_z,t) \\
&\qquad ((H(k_x,k_y,k'_z,t))^{-1} \partial_j H(k_x,k_y,k'_z,t) \\
&\qquad ((H(k_x,k_y,k'_z,t))^{-1} \partial_k H(k_x,k_y,k'_z,t)\}
\end{aligned} \tag{C.28}$$

$$\begin{aligned}
&= \int_0^1 \int_0^{2\pi} \int_0^{2\pi} \frac{dk_y dk'_z dt}{24\pi^2} \epsilon^{ijk} tr\{(H(k_x,k_y,k'_z,t))^{-1} \partial_i H(k_x,k_y,k'_z,t) \\
&\qquad ((H(k_x,k_y,k'_z,t))^{-1} \partial_j H(k_x,k_y,k'_z,t) \\
&\qquad ((H(k_x,k_y,k'_z,t))^{-1} \partial_k H(k_x,k_y,k'_z,t)\}
\end{aligned} \tag{C.29}$$

$$= WZ[H_{WZ}(k_x,k_y,k_z,t)] \tag{C.30}$$

By taking the $U = -\tau_y$ and $V = \tau_y$, I could show that the integral is exactly the same as not symmetry applied one.
The integral over k_x and k_z yields the same result, e.g. the integrals are equal.

Let us check now the pseudo inversion symmetry:

$$WZ[H'_{WZ}(k_x,k_y,k_z,t)] = WZ[-(\sigma_y\tau_y)H^\dagger(-\boldsymbol{k},t)(\sigma_y\tau_y)^{-1}] \tag{C.31}$$

$$\begin{aligned}= \int_0^1\int_0^{2\pi}\int_0^{2\pi}\frac{dk_xdk_ydt}{24\pi^2}\epsilon^{ijk}tr\{&(-1)^6((\sigma_y\tau_y)H^\dagger(-\boldsymbol{k},t)(\sigma_y\tau_y)^{-1})^{-1}\partial_i((\sigma_y\tau_y)H^\dagger(-\boldsymbol{k},t)(\sigma_y\tau_y)^{-1})\\ &((\sigma_y\tau_y)H^\dagger(-\boldsymbol{k},t)(\sigma_y\tau_y)^{-1})^{-1}\partial_j((\sigma_y\tau_y)H^\dagger(-\boldsymbol{k},t)(\sigma_y\tau_y)^{-1})\\ &((\sigma_y\tau_y)H^\dagger(-\boldsymbol{k},t)(\sigma_y\tau_y)^{-1})^{-1}\partial_k((\sigma_y\tau_y)H^\dagger(-\boldsymbol{k},t)(\sigma_y\tau_y)^{-1})\}\end{aligned}$$

$$\begin{aligned}= \int_0^1\int_0^{2\pi}\int_0^{2\pi}\frac{dk_xdk_ydt}{24\pi^2}\epsilon^{ijk}tr\{&(H(-\boldsymbol{k},t))^{-1}\partial_kH(-\boldsymbol{k},t)\\ &((H(-\boldsymbol{k},t))^{-1}\partial_jH(-\boldsymbol{k},t)\\ &((H(-\boldsymbol{k},t))^{-1}\partial_iH(-\boldsymbol{k},t)\}\end{aligned} \tag{C.32}$$

$$\begin{aligned}= -\int_0^1\int_0^{2\pi}\int_0^{2\pi}\frac{dk'_xdk'_ydt}{24\pi^2}\epsilon^{ijk}tr\{&(H(k'_x,k'_y,-k_z,t))^{-1}\partial_iH(k'_x,k'_y,-k_z,t)\\ &((H(k'_x,k'_y,-k_z,t))^{-1}\partial_jH(k'_x,k'_y,-k_z,t)\\ &((H(k'_x,k'_y,-k_z,t))^{-1}\partial_kH(k'_x,k'_y,-k_z,t)\}\end{aligned} \tag{C.33}$$

$$\neq WZ[H_{WZ}(k_x,k_y,k_z,t)] \tag{C.34}$$

$$\text{except:}\quad WZ[H'_{WZ}(k_x,k_y,0,t)] = -WZ[H_{WZ}(k_x,k_y,0,t)] \tag{C.35}$$

$$\Rightarrow WZ[H_{WZ}(k_x,k_y,0,t)] \in \{0,1/2\} \tag{C.36}$$

$$WZ[H'_{WZ}(k_x,k_y,\pi,t)] = -WZ[H_{WZ}(k_x,k_y,\pi,t)] \tag{C.37}$$

$$\Rightarrow WZ[H_{WZ}(k_x,k_y,\pi,t)] \in \{0,1/2\} \tag{C.38}$$

If I take $U = -\sigma_y\tau_y$ and $V = \sigma_y\tau_y$ the integrals are not equal for the general k_z, but at the TRIM points for k_z the integral is quantized. The same results yield from the integrals over other two combinations of (k_x, k_y, k_z).

WZ quantization for 3D models with mirror type symmetries

Firstly τ_y and σ_y commute

Secondly H_{const} should not be commuting with the symmetry operators.

Using the pseudo inversion and pseudo mirror symmetry w.r.t the k_z we get the same extension of the Hamiltonian if we choose the end constant Hamiltonian in the following

way:

$$\begin{gathered} WZ[H'] = \\ WZ[-\sigma_y\tau_y((1-t)H^\dagger(-\boldsymbol{k}) + tH'_{const})(\sigma_y\tau_y)^{-1}] = WZ[-\tau_y((1-t)H^\dagger(k_x,k_y,-k_z) + tH''_{const})\tau_y] \\ WZ[(1-t)H(\boldsymbol{k}) - t\tau_y\sigma_y H'_{const}\sigma_y\tau_y] = WZ[(1-t)H(\boldsymbol{k}) - t\tau_y H''_{const}\tau_y] \end{gathered} \tag{C.39}$$

the integral is over k_y and k_z or k_x and k_z and the two extensions are equal in the case of $\sigma_y H'_{const}\sigma_y = H''_{const}$, the primes over the H_{const} are to distinguish the constant Hamiltonians that they are different. For every H'_{const} there is other constant Hamiltonian H''_{const} which is connected in the above way.

From eq. (C.33) we get:

$$WZ[H'(k_z)] = -WZ[H(-k_z)] \tag{C.40}$$

From eq. (C.30) we get:

$$WZ[H'(k_z)] = WZ[H(k_z)] \tag{C.41}$$

From eq.(C.39) we have two terms are the same and get an odd relation:

$$WZ[H'(k_z)] = -WZ[H(-k_z)] = WZ[H(k_z)] \tag{C.42}$$

The relation between 2 extensions is:

$$WZ[H(k_z)] - WZ[H'(k_z)] = n \in \mathbb{Z} \tag{C.43}$$

From eq. (C.41) we see that $n = 0$ and (C.40) in (C.43):

$$WZ[H(k_z)] + WZ[H(-k_z)] = WZ[H(k_z)] - WZ[H(k_z)] = 0 \tag{C.44}$$

Circlic values of WZ terms we get: $WZ[H(k_z)] = -WZ[H(k_z)]$, setting this in eq.(C.44) we get the WZ integral equals zero:

$$\Rightarrow 2WZ[H(k_z)] = 0 \tag{C.45}$$

$$\Rightarrow WZ[H(k_z)] = 0 \text{ or } WZ[H(k_z)] = \frac{1}{2} \tag{C.46}$$

So, due to the both pseudo inversion symmetry and pseudo mirror symmetry w.r.t the k_z we get that the integral is quantized. Additionally it is true for every symmetry, which implies in every WZ integral equals zero.

$$\begin{gathered} WZ[H'] = \\ WZ[\sigma_z((1-t)H^\dagger(-k_x,k_y,k_z)+tH'_{const})\sigma_z^{-1}] = WZ[-\tau_y((1-t)H^\dagger(k_x,k_y,-k_z)+tH''_{const})\tau_y^{-1}] \\ WZ[(1-t)H(k_x,k_y,k_z)+t\sigma_z H'_{const}\sigma_z] = WZ[(1-t)H(k_x,k_y,k_z)-t\tau_y H''_{const}\tau_y] \end{gathered} \tag{C.47}$$

$$\text{From eq. (85) } WZ[H'(k_z)] = -WZ[H(-k_z)] \text{ integral over } k_y \text{ and } k_z \tag{C.48}$$

$$\text{From eq. (101) } WZ[H'(k_z)] = WZ[H(k_z)] \text{ integral over } k_x \text{ and } k_z \text{ or } k_y \text{ and } k_z \tag{C.49}$$

The integral over k_x and k_y results also in $WZ = 0$:

$$\begin{gathered} WZ[H'] = \\ WZ[\sigma_z((1-t)H^\dagger(-k_x,k_y,k_z)+tH'_{const})\sigma_z^{-1}] = WZ[-\sigma_y\tau_y(H^\dagger(-\boldsymbol{k})+tH'_{const})(\sigma_y\tau_y)^{-1}] \\ WZ[(1-t)H(k_x,k_y,k_z)+t\sigma_z H'_{const}\sigma_z] = WZ[(1-t)H(k_x,k_y,k_z)-t\tau_y H''_{const}\tau_y] \end{gathered} \tag{C.50}$$

$$\text{From eq. (77) } WZ[H'] = WZ[H] \text{ integral over } k_x \text{ and } k_y \tag{C.51}$$

$$\text{From eq. (104) } WZ[H'(k_z)] = -WZ[H(-k_z)] \text{ integral over } k_x \text{ and } k_y \tag{C.52}$$

only mirror symmetries:

As shown above every extension with the symmetry operators can be related to the other extensions

- mirror symmetry w.r.t. k_x :
  - ◇ integral over k_x and k_y or k_x and k_z: $WZ[H'] = WZ[H]$

  - ◇ integral over k_y and k_z: $WZ[H'(k_x)] = -WZ[H(-k_x)]$

- mirror symmetry w.r.t. k_y :
  - ◇ integral over k_x and k_y or k_y and k_z: $WZ[H'] = WZ[H]$
  - ◇ integral over k_x and k_z: $WZ[H'(k_y)] = -WZ[H(-k_y)]$

- mirror symmetry w.r.t. k_z :
  - ◇ integral over k_x and k_z or k_y and k_z: $WZ[H'] = WZ[H]$
  - ◇ integral over k_x and k_y: $WZ[H'(k_z)] = -WZ[H(-k_z)]$

To prove the WZ integral equals to zero the symmetry relation of the third dimension is always needed. From the 2D model we know that the pseudo mirror symmetry does not quantize the WZ term, so is true for 3D model if we have the pseudo mirror symmetry along the integration direction and not third dimension which is kept constant.
I could also choose the constant Hamiltonian of the extension without the symmetry operator the same as the one with the symmetry operator. In that case we can not prove anything, so it is necessary to choose a different constant Hamiltonian, so that we have different extensions. In the 2D case it is important to choose a different constant Hamiltonian, except being non-symmetric under the system Hamiltonian, too in order to get the difference the integer value and not just zero, so that the integral can be quantized.
The extensions with the symmetry operators are just chosen to be the same extension does not imply the same as the extension without symmetry operators yet. This specific choice and the resulting conclusion that the WZ integral equals zero could not be found if we would not have the symmetry relations. I think that means the choice does not contradict the generality. As we have chosen U and V operators to show the relation

Appendix D

Plane cuts and its energy spectra and prob.density profiles for the 3rd model

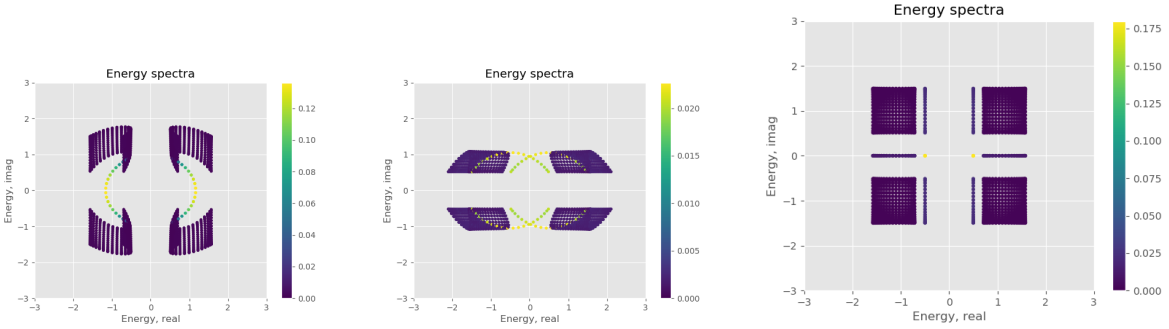

Figure D.1: *cut along xy-plane, xz-plane, and yz-plane*

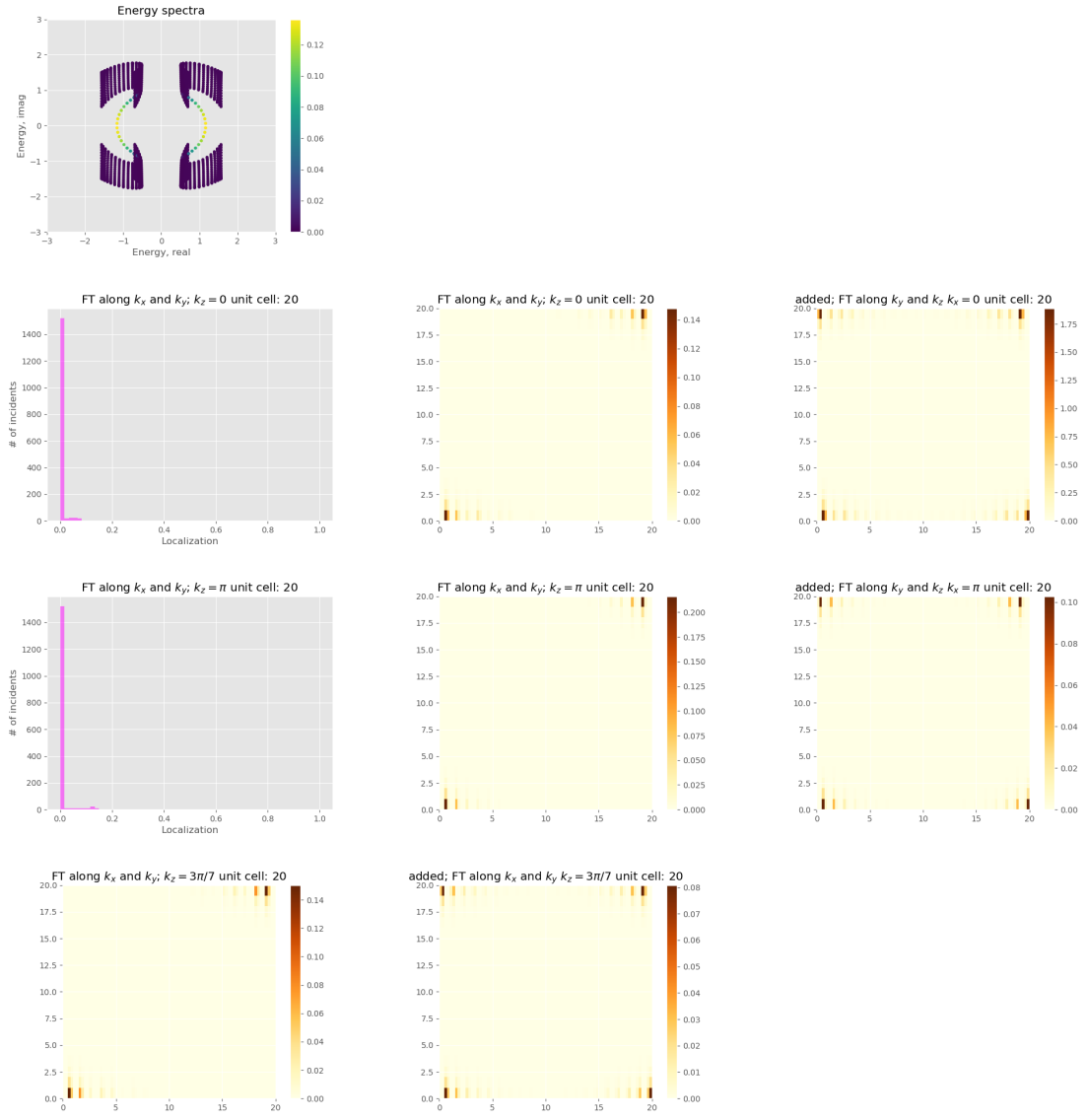

Figure D.2: *cut along xy-plane*

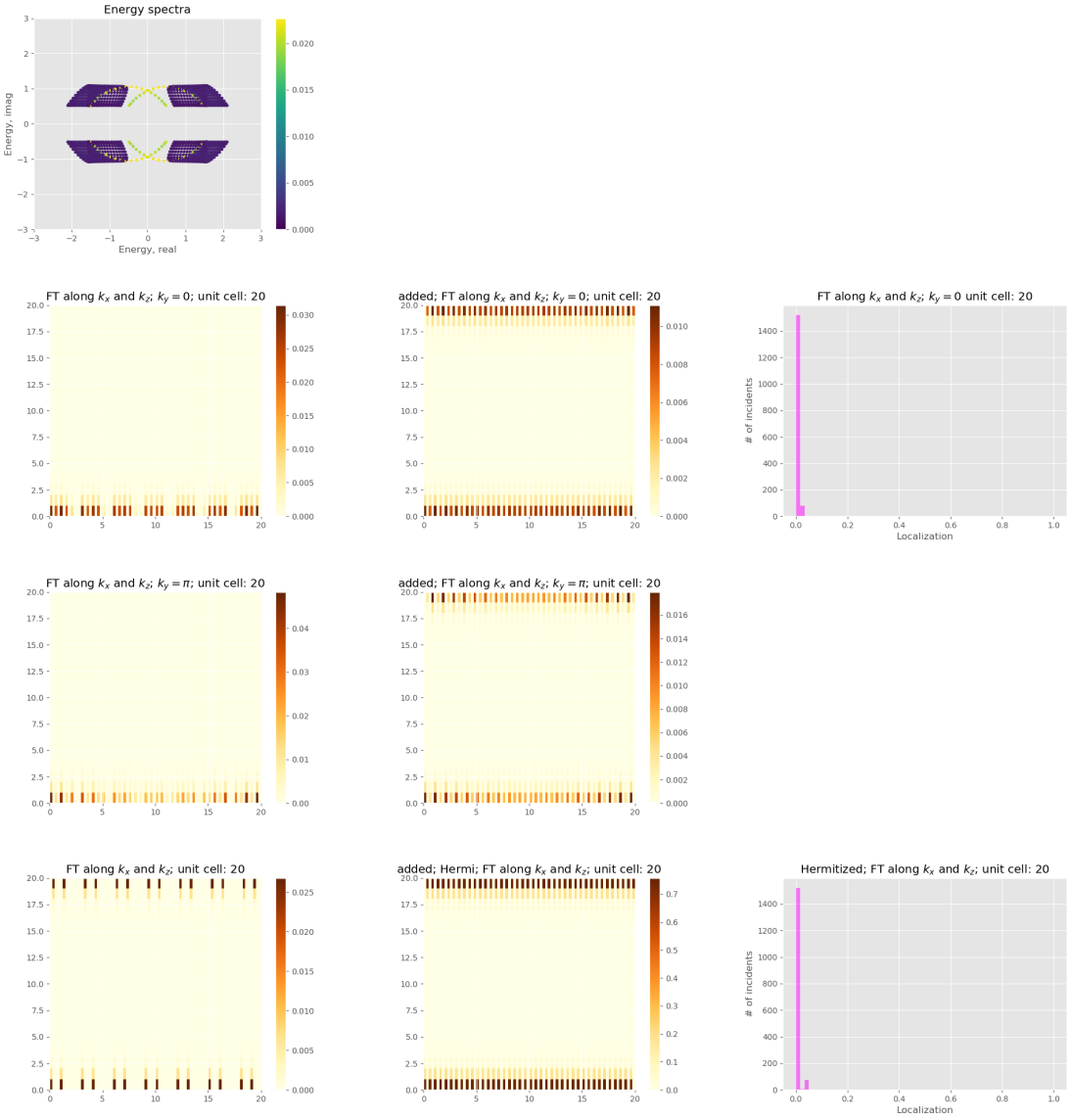

Figure D.3: *cut along xz-plane. Exactly 80 states are at the boundary localized in hermitized model.*

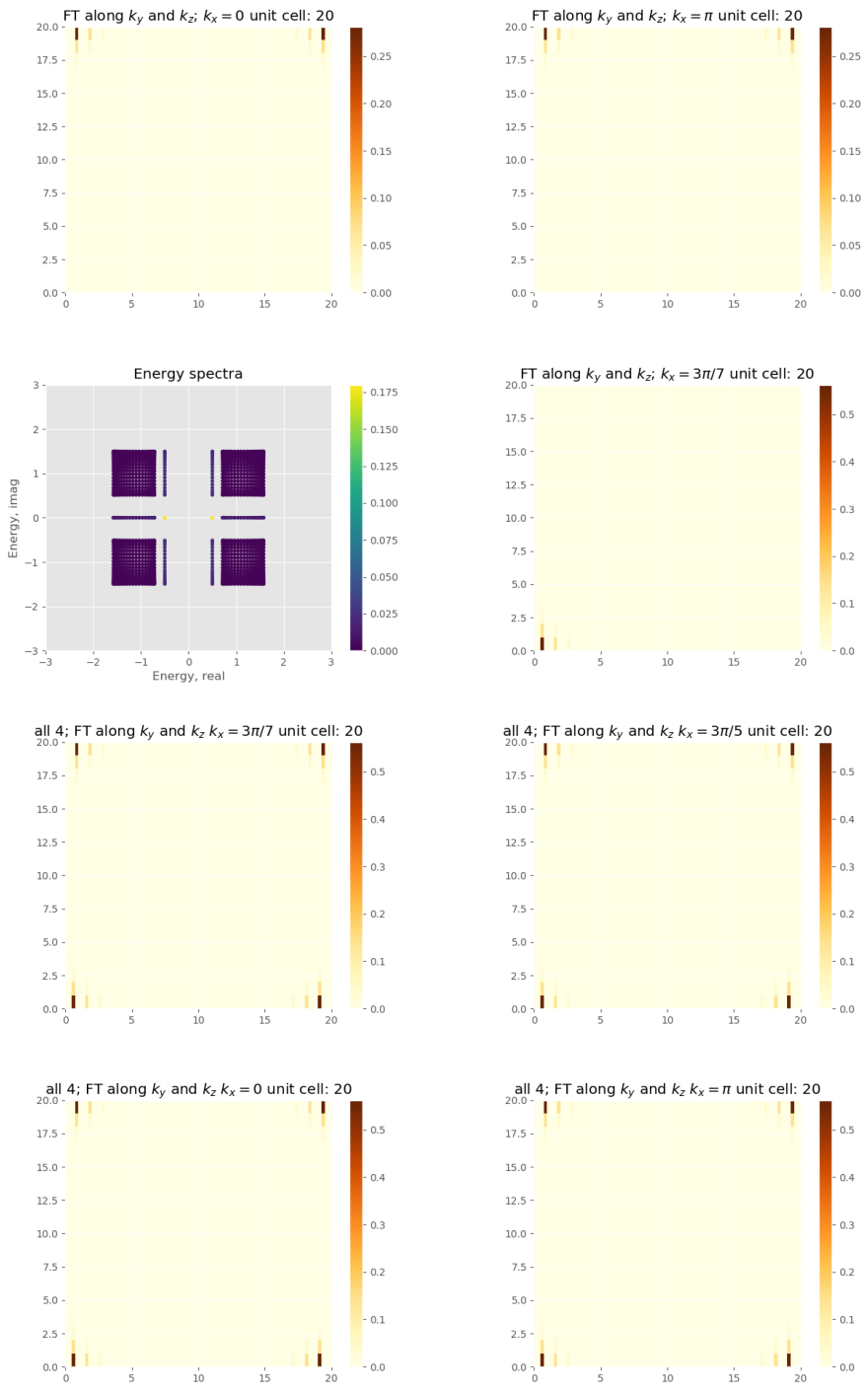

Figure D.4: *cut along yz-plane. I will put them on affinity design.*

Appendix E

Perturbation results for the second model

I systematically perturbed the system with small symmetry respecting and not symmetry respecting Hamiltonian and seen how the various perturbations change the spectra. the perturbation with the magnitude smaller than the 10^{-10} is numerically not detectable. So the perturbations are done with bigger magnitudes.
This Hamiltonian respects four-fold-rotation (C_4) type symmetry in the following form:

$$UH^{\dagger}(g^{-1}\vec{k}) = H(\vec{k}) \tag{E.1}$$

$$-i\sigma_y H^{\dagger}(k_x, k_y) = H(-k_y, k_x) \tag{E.2}$$

$H(\vec{k})$ also respects C_2 spatial inversion symmetry:

$$\sigma_y H(\vec{k})\sigma_y = H(-\vec{k}) \tag{E.3}$$

The Hamiltonian with the C_4 symmetric perturbation is given as following:

$$H(\vec{k}) \longrightarrow H(\vec{k}) + \delta H(\vec{k}) + \delta H^{\dagger}(g^{-1}\vec{k})U + U^{-1}\delta H(g^{-1}g^{-1}\vec{k})U + U^{-1}\delta H^{\dagger}(g^{-1}g^{-1}g^{-1}\vec{k})U^2 \tag{E.4}$$

U is a unitary matrix:

$$U^\dagger = U^{-1} \tag{E.5}$$

Rotate the third term once forward:

$$U(\delta H^\dagger(g^{-1}\vec{k})U)^\dagger = U(U^\dagger \delta H(g^{-1}\vec{k})) = \delta H(\vec{k}) \tag{E.6}$$

Rotate the fourth term once forward:

$$U(U^{-1}\delta H(g^{-1}g^{-1}\vec{k})U)^\dagger = U(U^\dagger H^\dagger(g^{-1}g^{-1}\vec{k})U) = \delta H^\dagger(g^{-1}\vec{k})U \tag{E.7}$$

Rotate the fifth term once forward:

$$U(U^{-1}\delta H^\dagger(g^{-1}g^{-1}g^{-1}\vec{k})U^2)^\dagger = U((U^\dagger)^2 H(g^{-1}g^{-1}g^{-1}\vec{k})U) = U^{-1}\delta H(g^{-1}g^{-1}\vec{k})U \tag{E.8}$$

Here $\delta H(\vec{k})$ is a matrix with 2x2 random entries, that means δH matrix is actually not dependent on $\vec{k}$. U is a matrix for C_4 type symmetry operator on the Bloch Hamiltonian and therefore given as $U = -i\sigma_y$, σ_y is a Pauli matrix.
If we rotate the perturbing Hamiltonian:

$$U\left(\delta H(\vec{k}) + \delta H^\dagger(g^{-1}\vec{k})U + U^{-1}\delta H(g^{-1}g^{-1}\vec{k})U + U^{-1}\delta H^\dagger(g^{-1}g^{-1}g^{-1}\vec{k})U^2\right)^\dagger(g\vec{k}') = \\ = U\delta H(g\vec{k}) + \delta H(\vec{k}) + \delta H^\dagger(g^{-1}\vec{k})U + U^{-1}\delta H(g^{-1}g^{-1}\vec{k})U$$

The g operators on $\vec{k}$ apply after clockwise or anticlockwise rotation.
I have to rotate this actually 4 times to show if the matrix comes in the same state.

The Hamiltonian with the C_2 symmetric perturbation is given as following:

$$H(\vec{k}) \longrightarrow H(\vec{k}) + \delta H(\vec{k}) + \sigma_y \delta H(-\vec{k})\sigma_y \tag{E.9}$$

Here $\delta H(\vec{k})$ is a matrix with 2x2 random entries in the range [0,1]. σ_y is a Pauli matrix and the C_2 symmetry operator on our Bloch Hamiltonian.

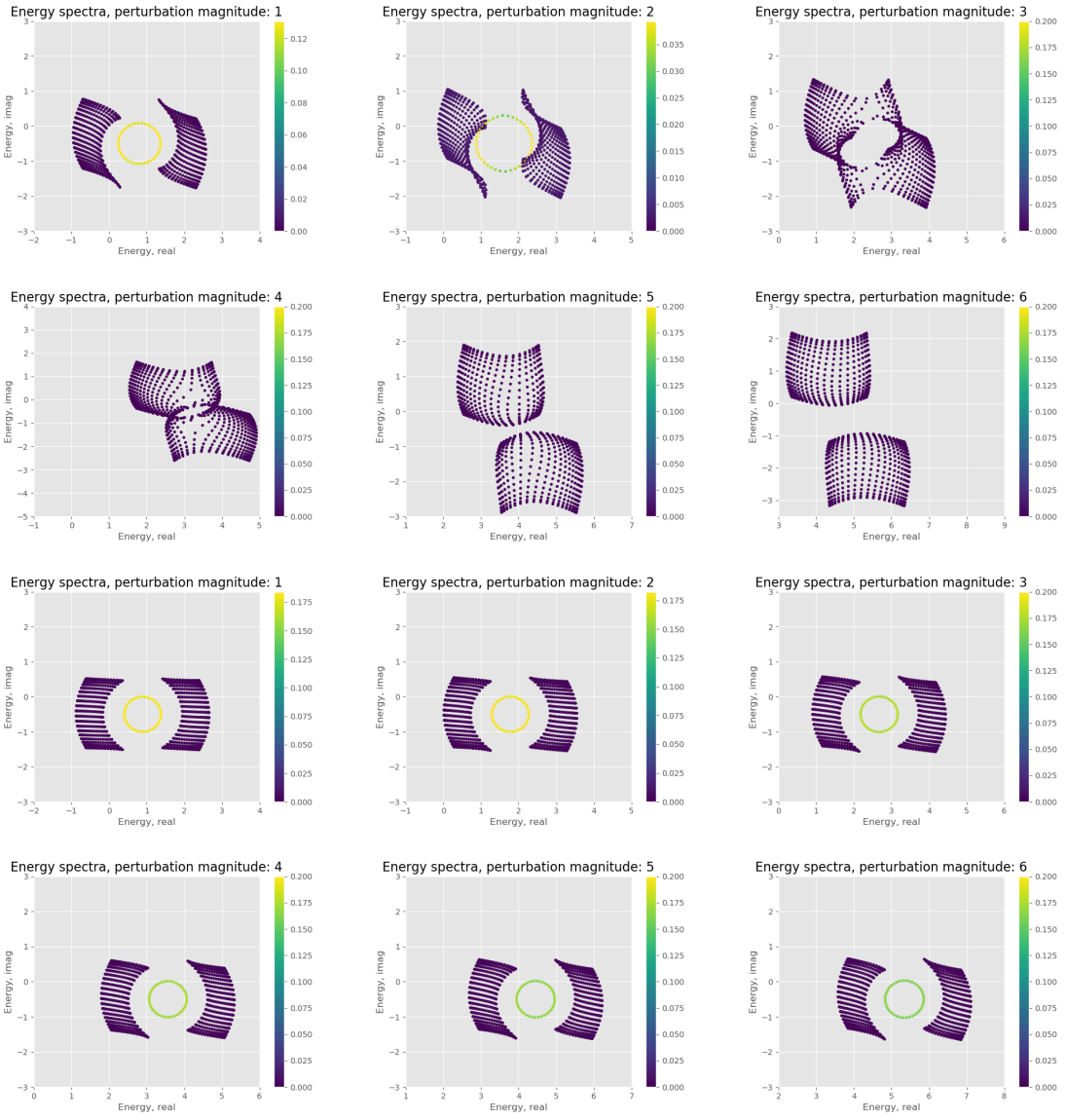

Figure E.1: *Real perturbation. Reciprocal space. C2 perturbation with different magnitudes (1i,2i,3i,4i,5i,6i) times always the same random matrix*

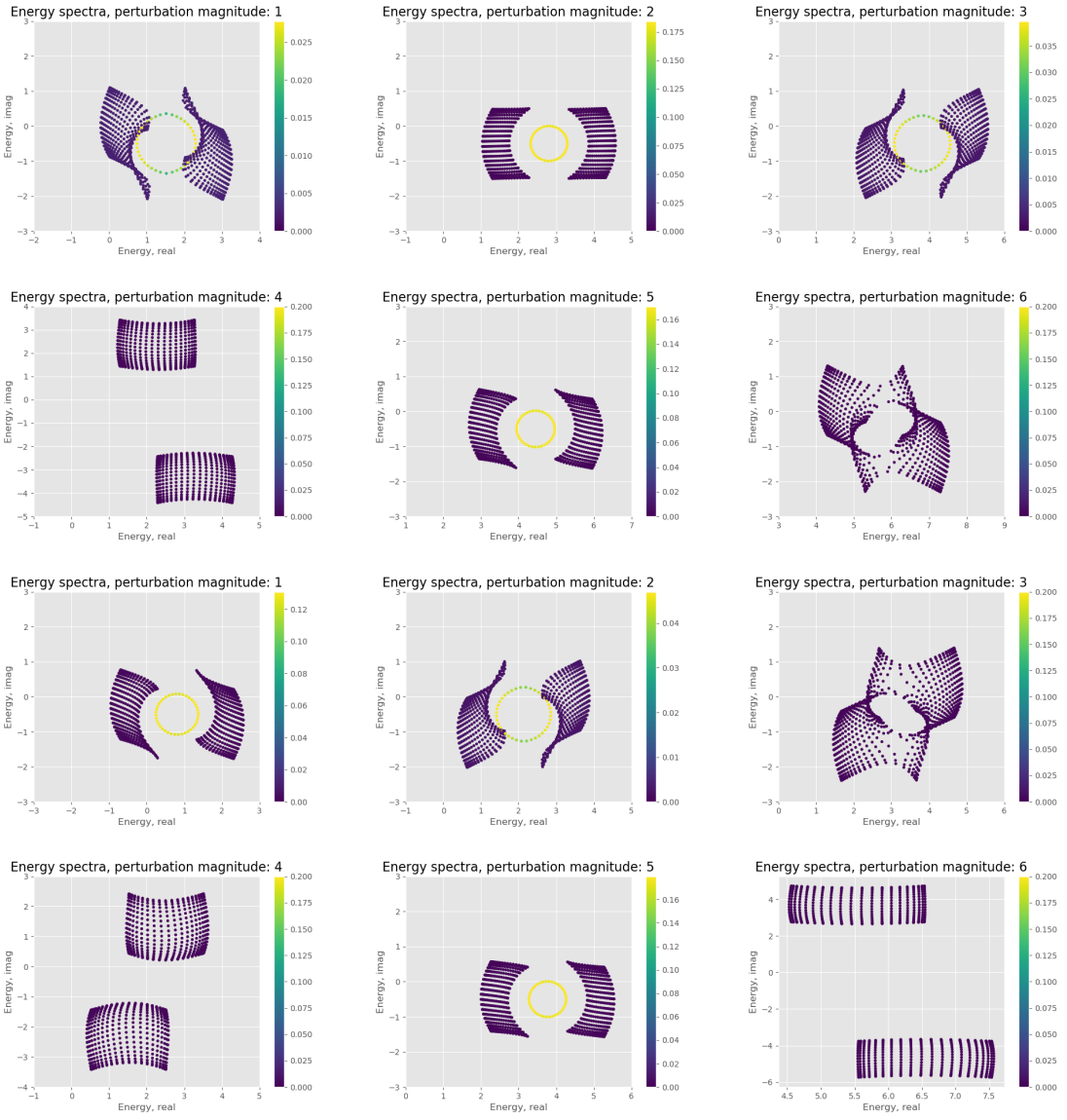

Figure E.2: *Real perturbation. Reciprocal space. C2 perturbation with different magnitudes (1i,2i,3i,4i,5i,6i) times different random matrix*

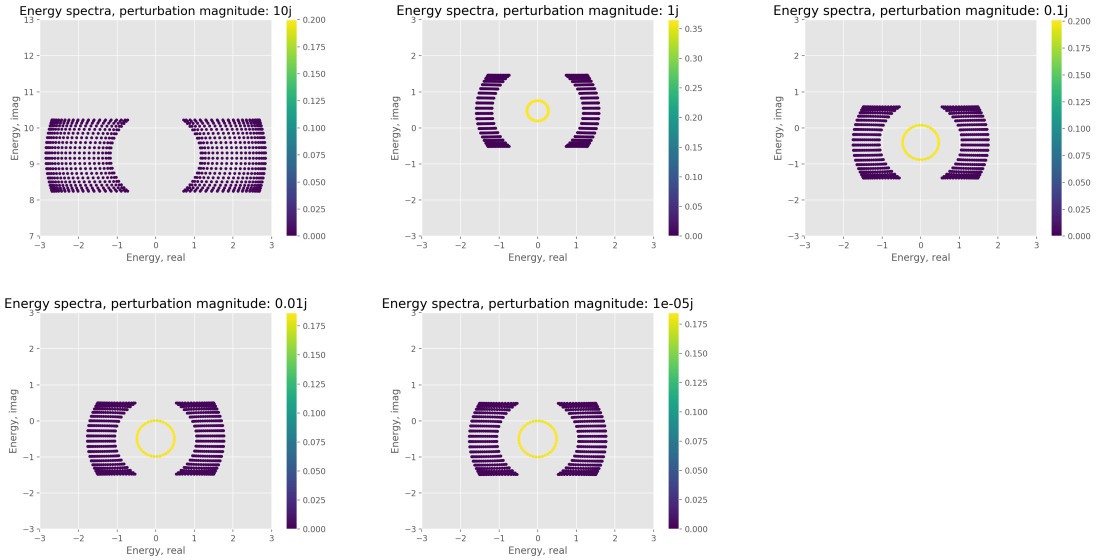

Figure E.3: *Complex perturbation. Reciprocal space. C2 perturbation with different magnitudes times always same random matrix*

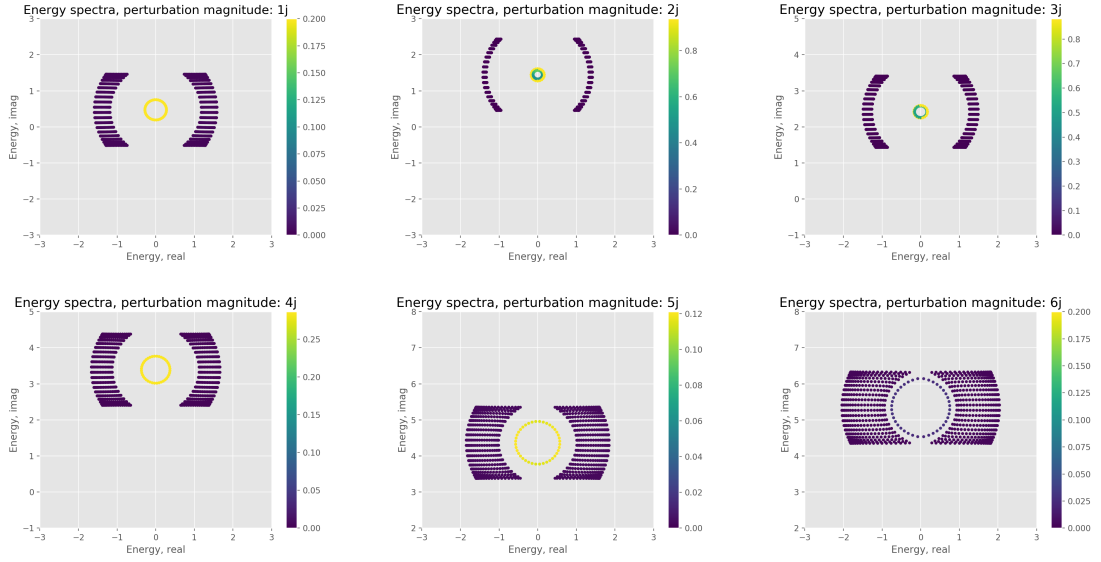

Figure E.4: *Complex perturbation. Reciprocal space. C2 perturbation with different magnitudes (1i,2i,3i,4i,5i,6i) times always the same random matrix*

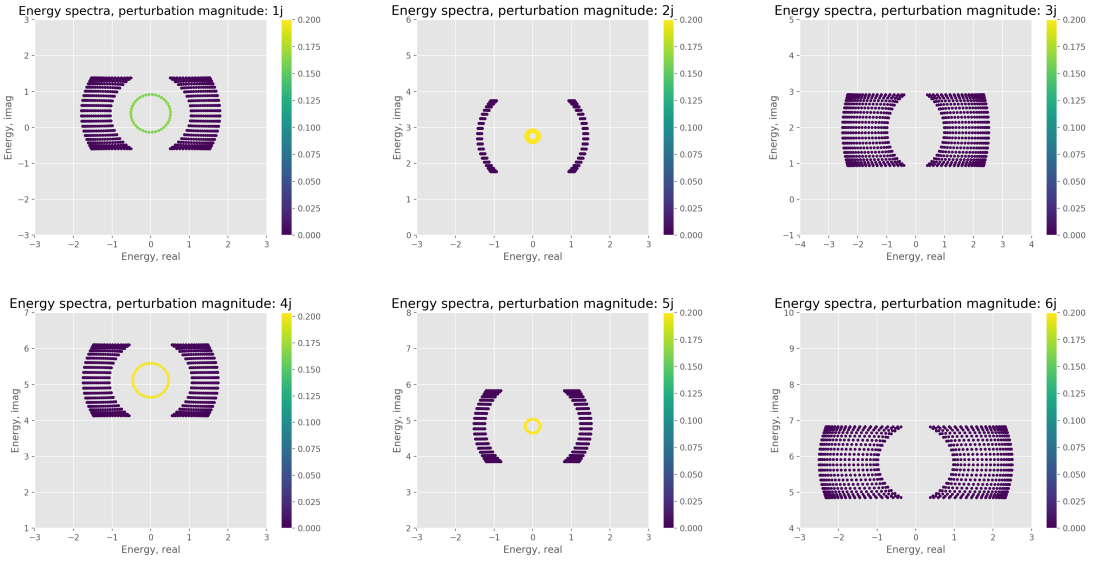

Figure E.5: *Complex perturbation. Reciprocal space. C2 perturbation with different magnitudes (1i,2i,3i,4i,5i,6i) times different random matrix*

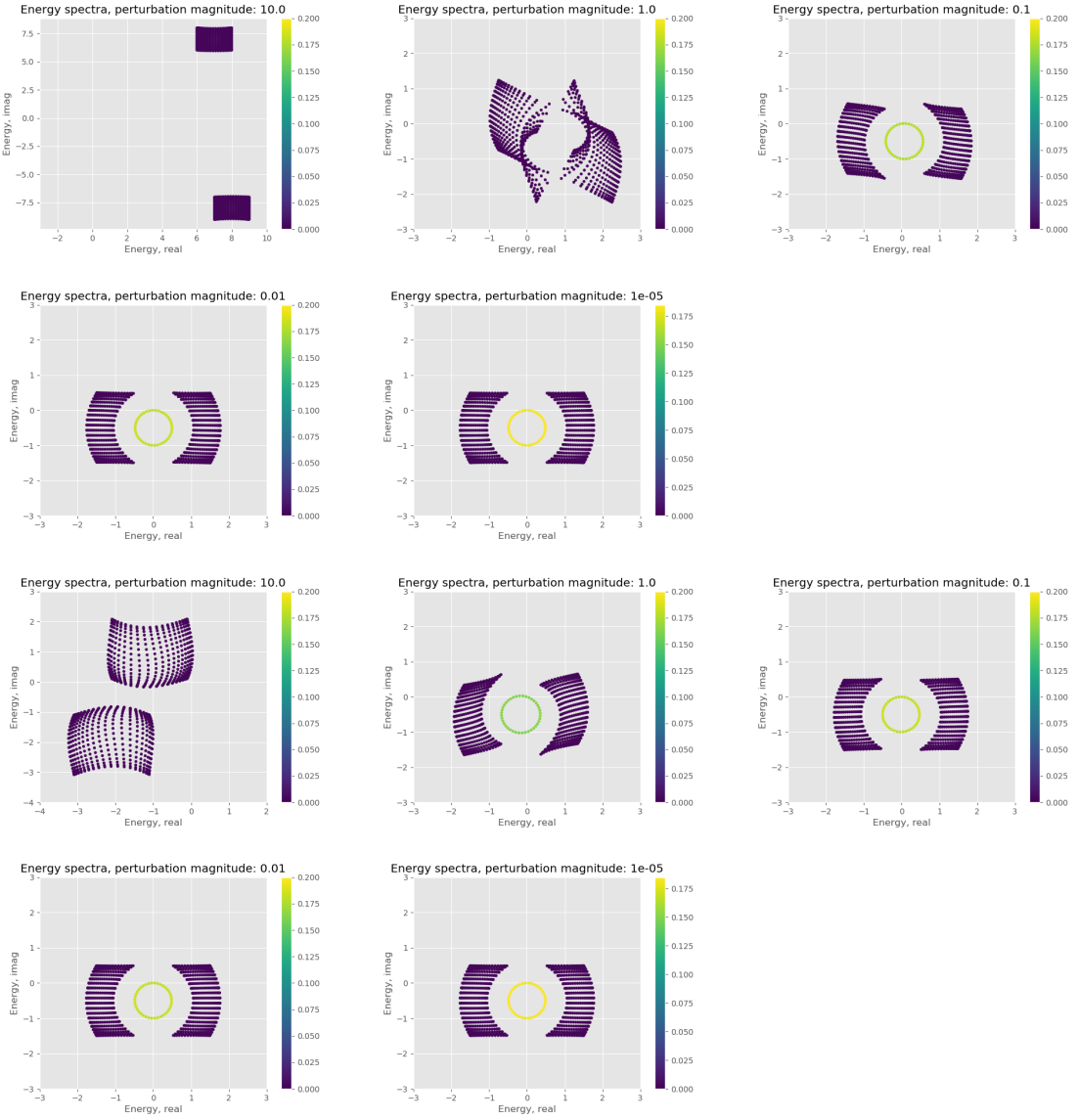

Figure E.6: *Real valued perturbation. Reciprocal space. C4 perturbation with different magnitudes with the same perturbation matrices. First and second plots are both for different random matrices.*

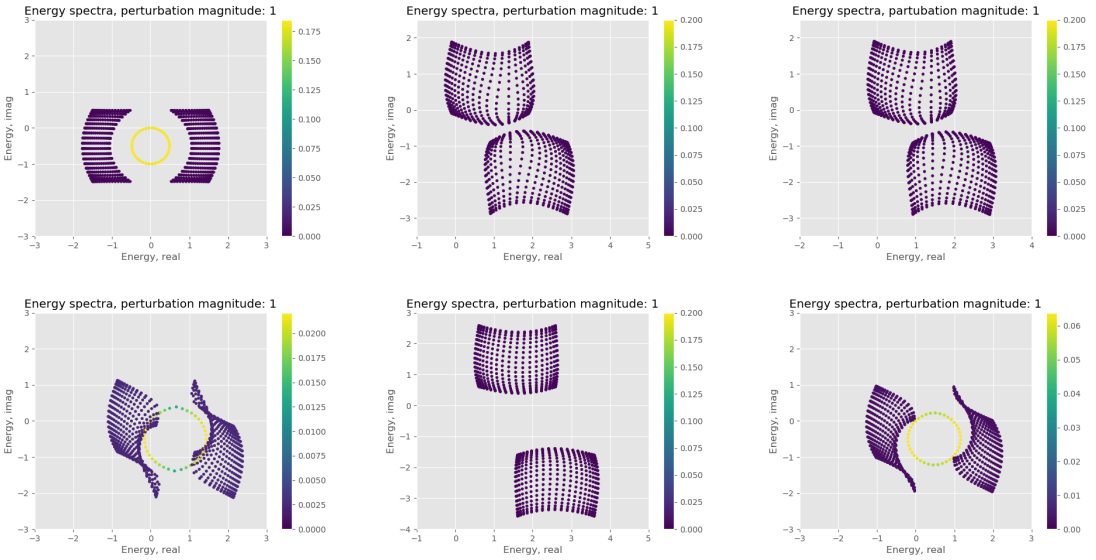

Figure E.7: *Real valued perturbation. Reciprocal space. C4 perturbation magnitude=1 with the different perturbation matrices.*

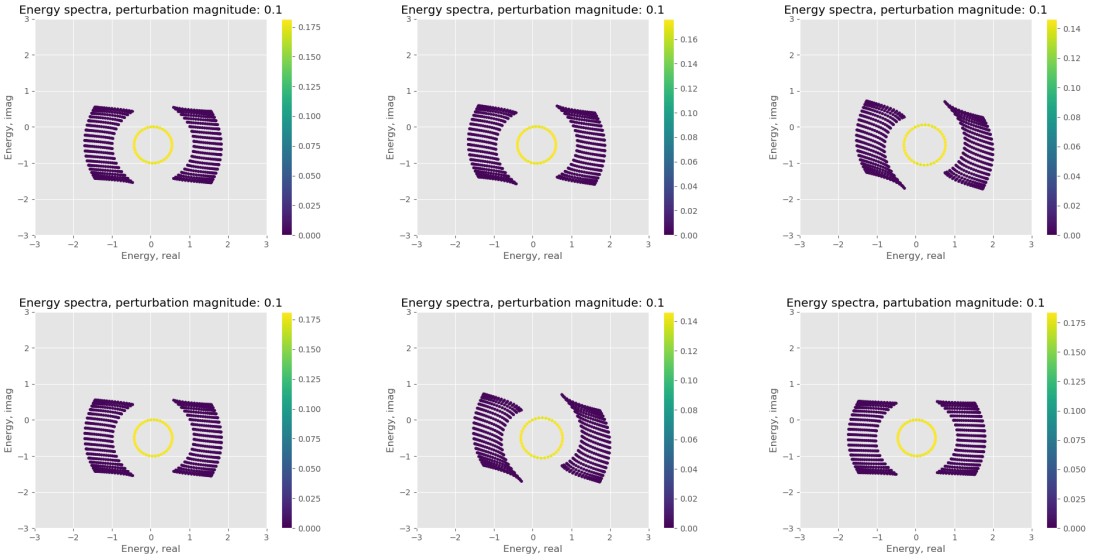

Figure E.8: *Real valued perturbation. Reciprocal space. C4 perturbation magnitude=0.1 with the different perturbation matrices.*

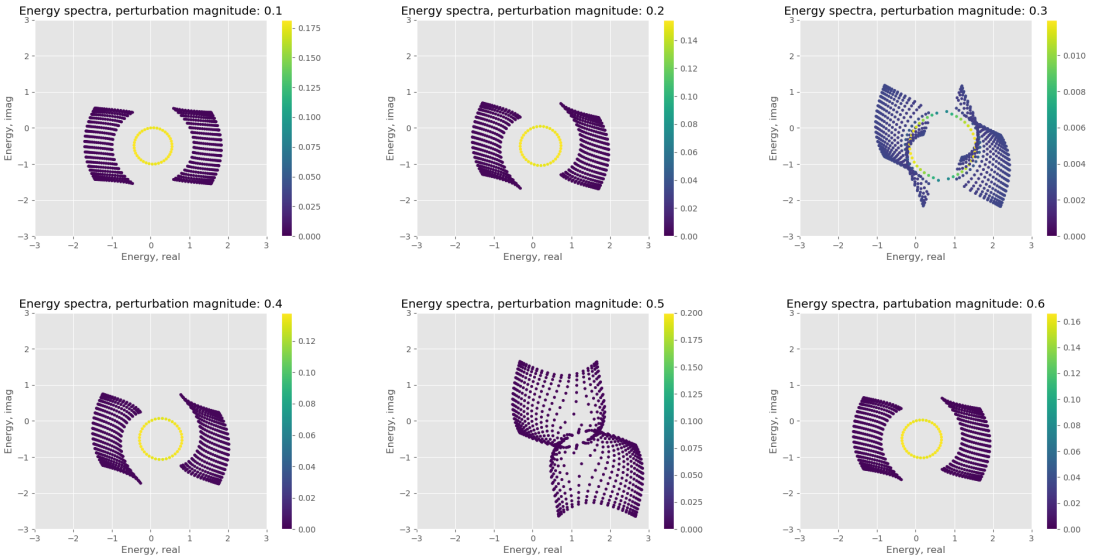

Figure E.9: *Real valued perturbation. Reciprocal space. C4 perturbation magnitude=(0.1, 0.2, 0.3, 0.4, 0.5, 0.6) with the different perturbation matrices.*

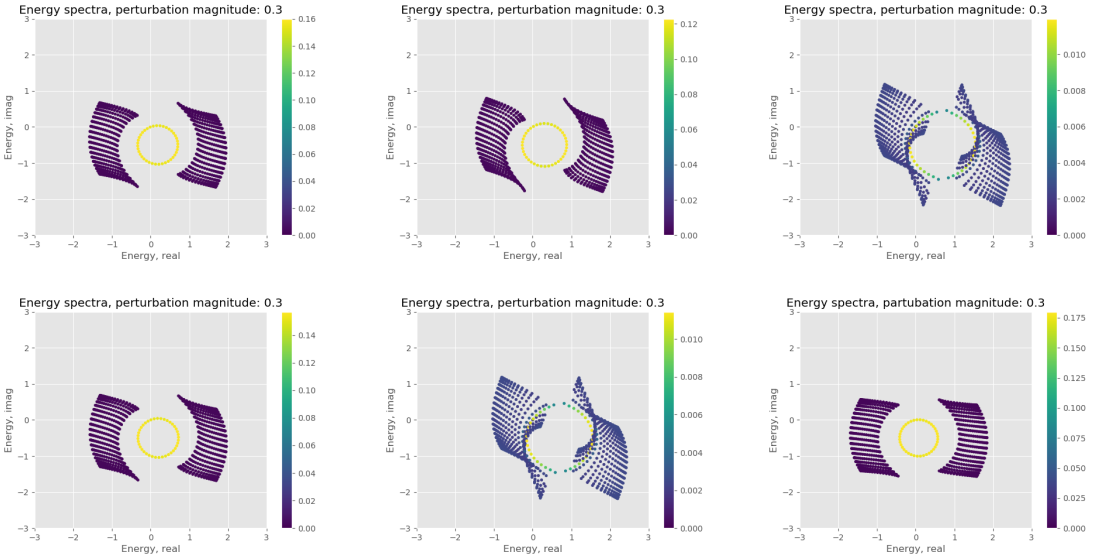

Figure E.10: *Real valued perturbation. Reciprocal space. C4 perturbation magnitude=0.3 with the different perturbation matrices.*

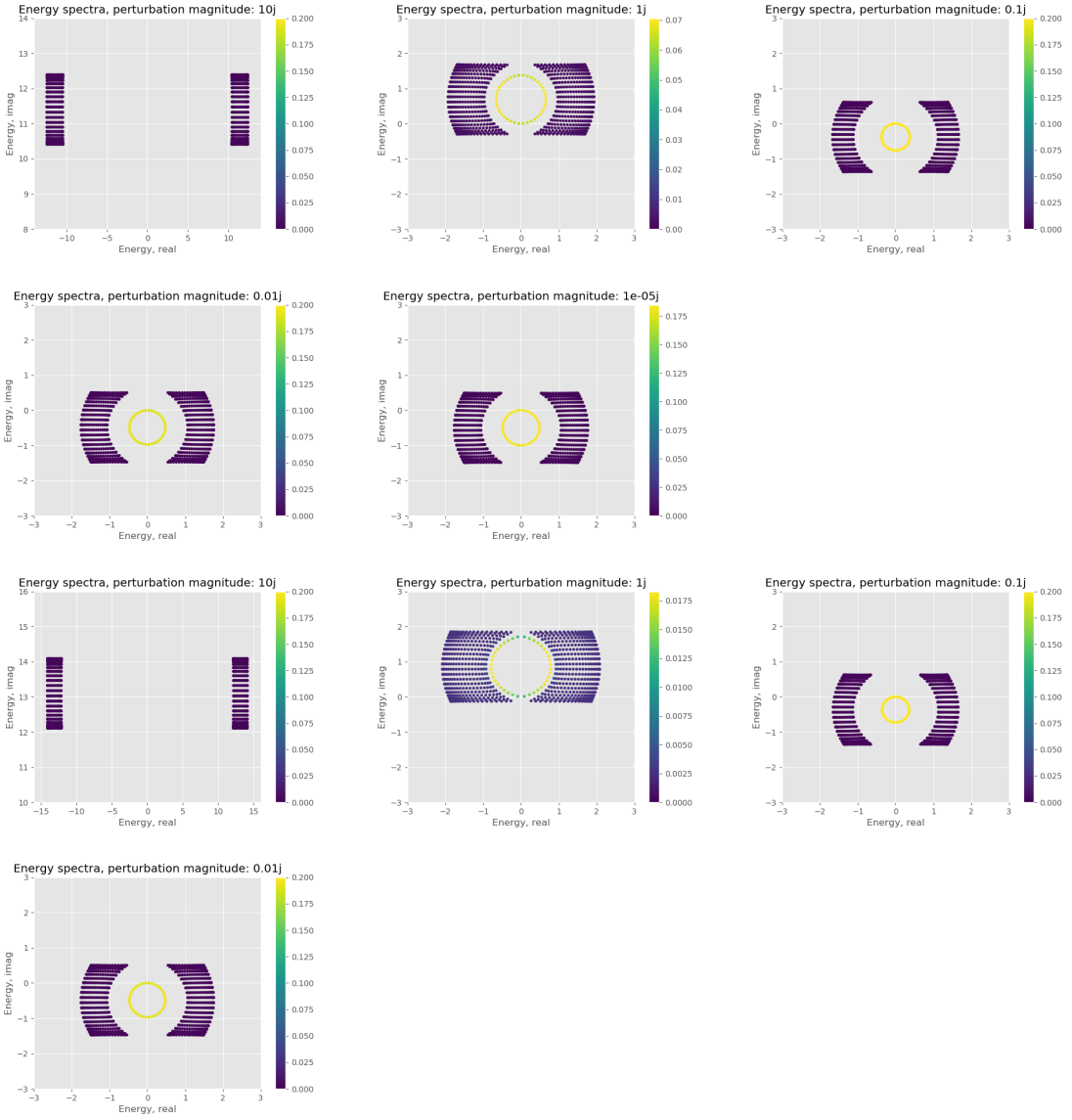

Figure E.11: *Complex valued perturbation. Reciprocal space. C4 perturbation with different magnitudes with the same perturbation matrices. First and second plots are both for different random matrices.*

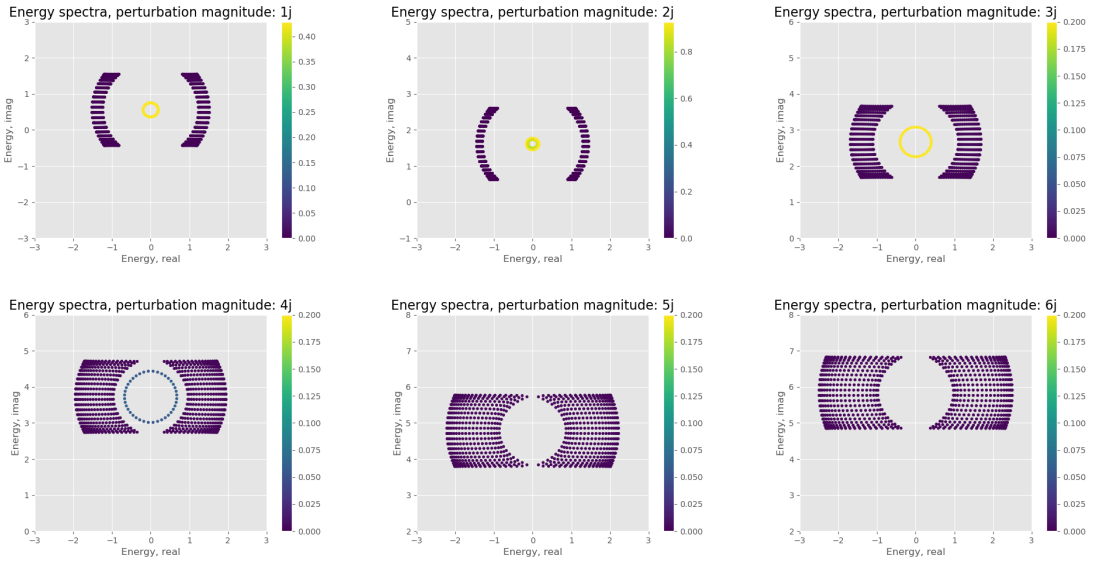

Figure E.12: *Complex perturbation. Reciprocal space. C4 perturbation with different magnitudes (1i,2i,3i,4i,5i,6i) times always the same random matrix. However depending on the random matrix we have corner localized state or not. So let us check also different randoms at magnitude 1j.*

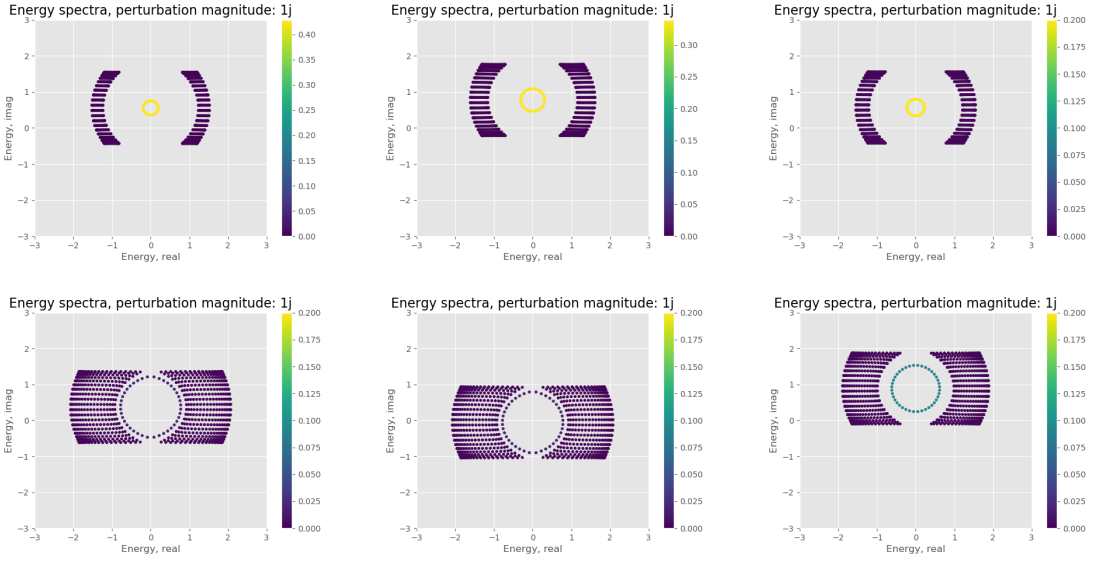

Figure E.13: *Complex perturbation. Reciprocal space. C4 perturbation with different magnitude=1i times different random matrices.*

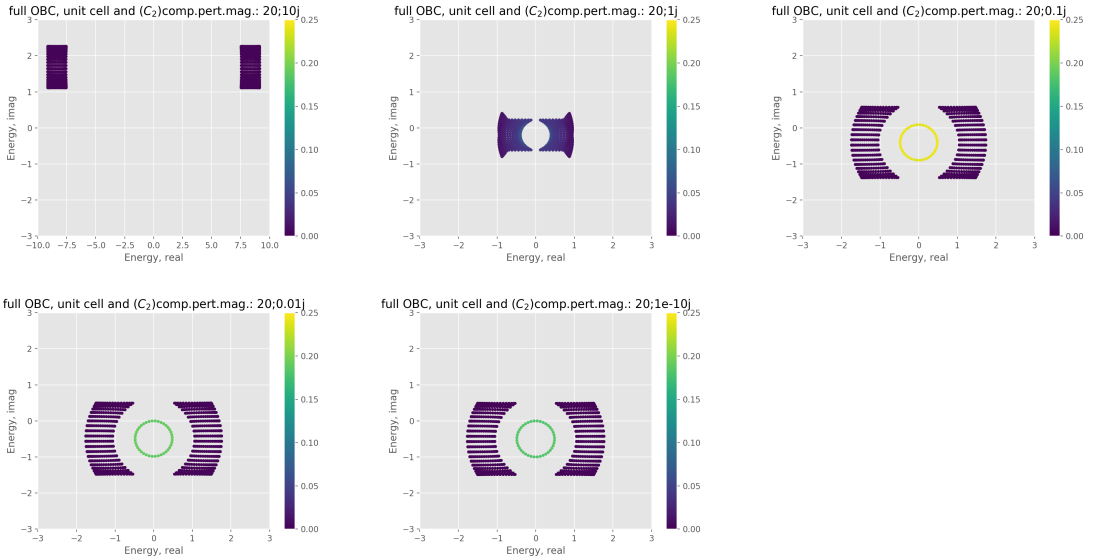

Figure E.14: *Real space. C2 perturbation with pure complex values with different magnitudes and same random matrix. I checked all magnitude=0.1j are fine.*

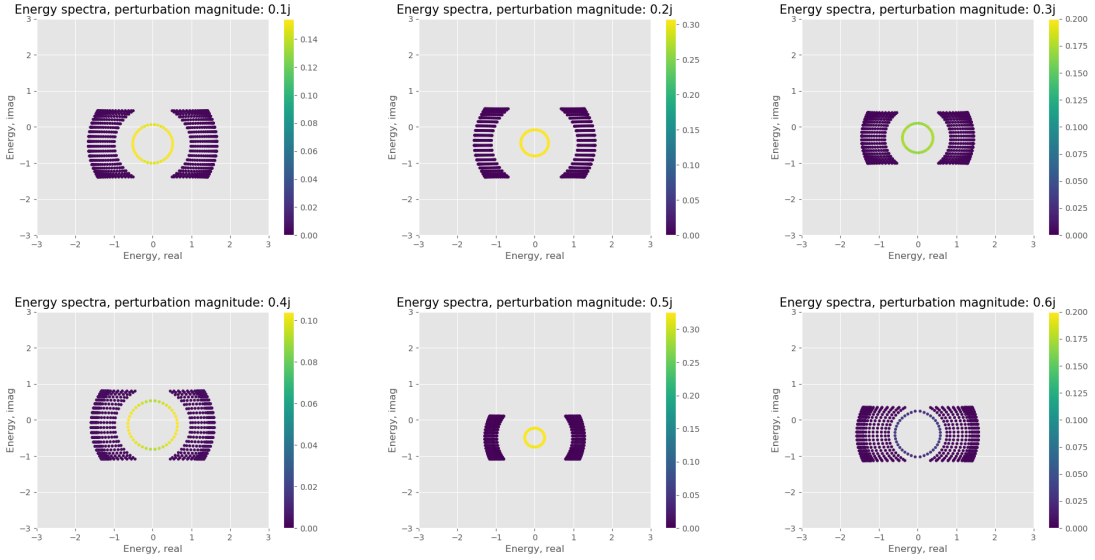

Figure E.15: *Real space. C2 perturbation with pure complex values with different magnitudes and different random matrices. I checked all magnitude=0.1j are fine.*

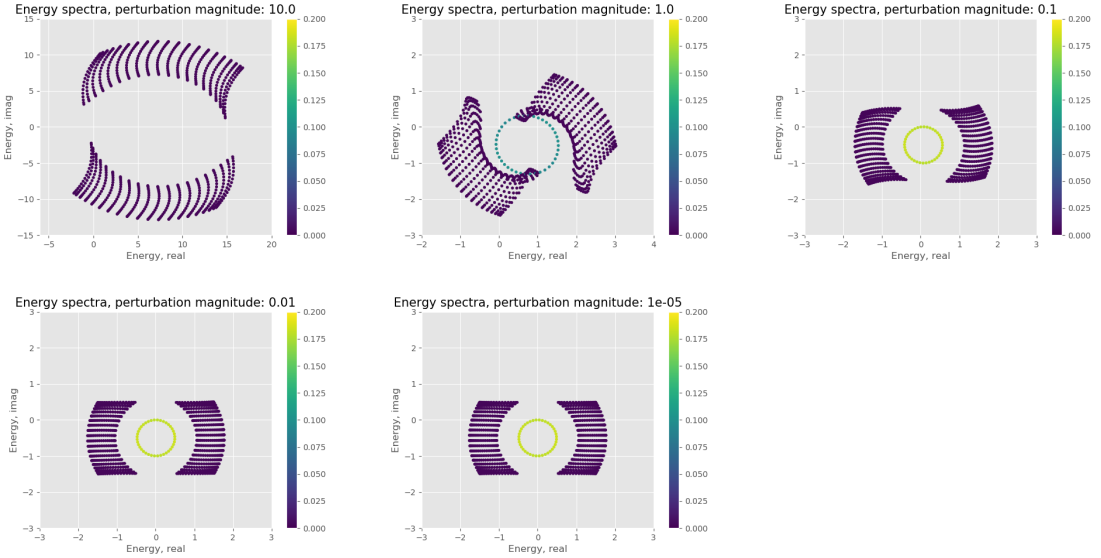

Figure E.16: *Real space. C2 perturbation with real values with different magnitudes. Same random matrices.*

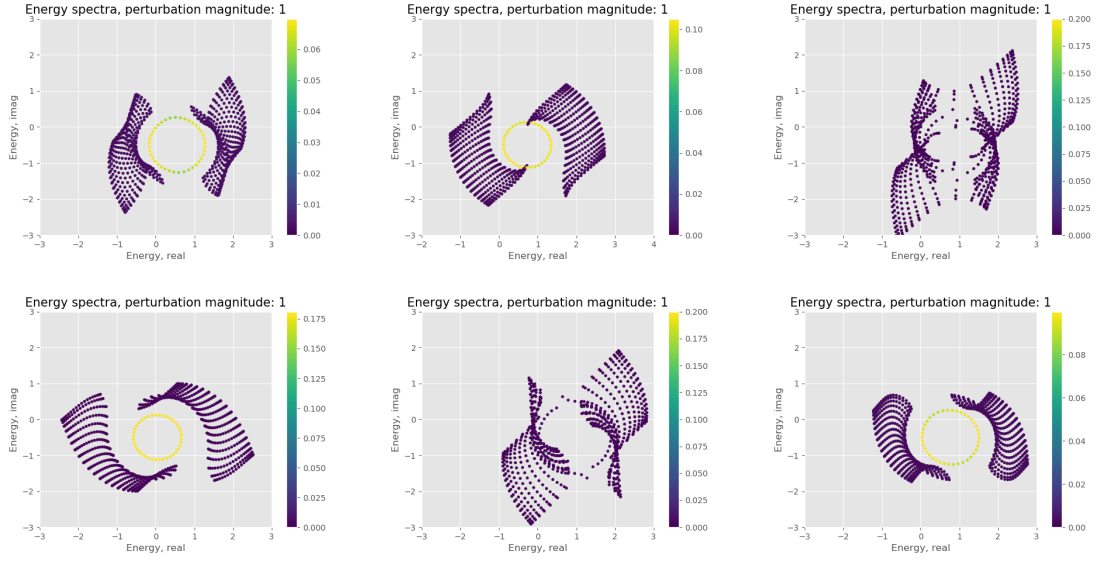

Figure E.17: *Real space. C2 perturbation with real magnitude = 1. Different random matrix.*

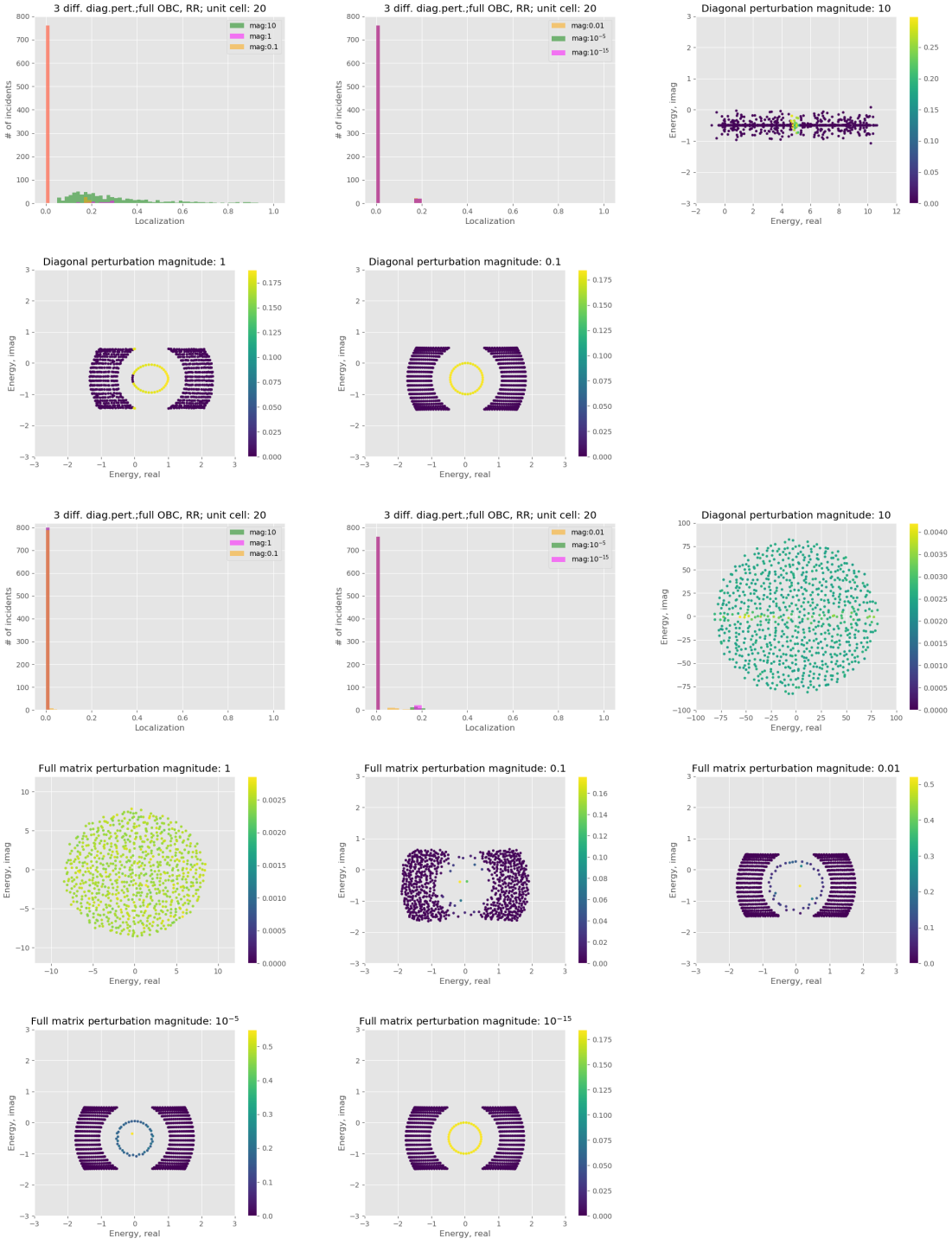

Figure E.18: *random diagonal and random full matrix perturbation with different magnitude and one random matrix.*

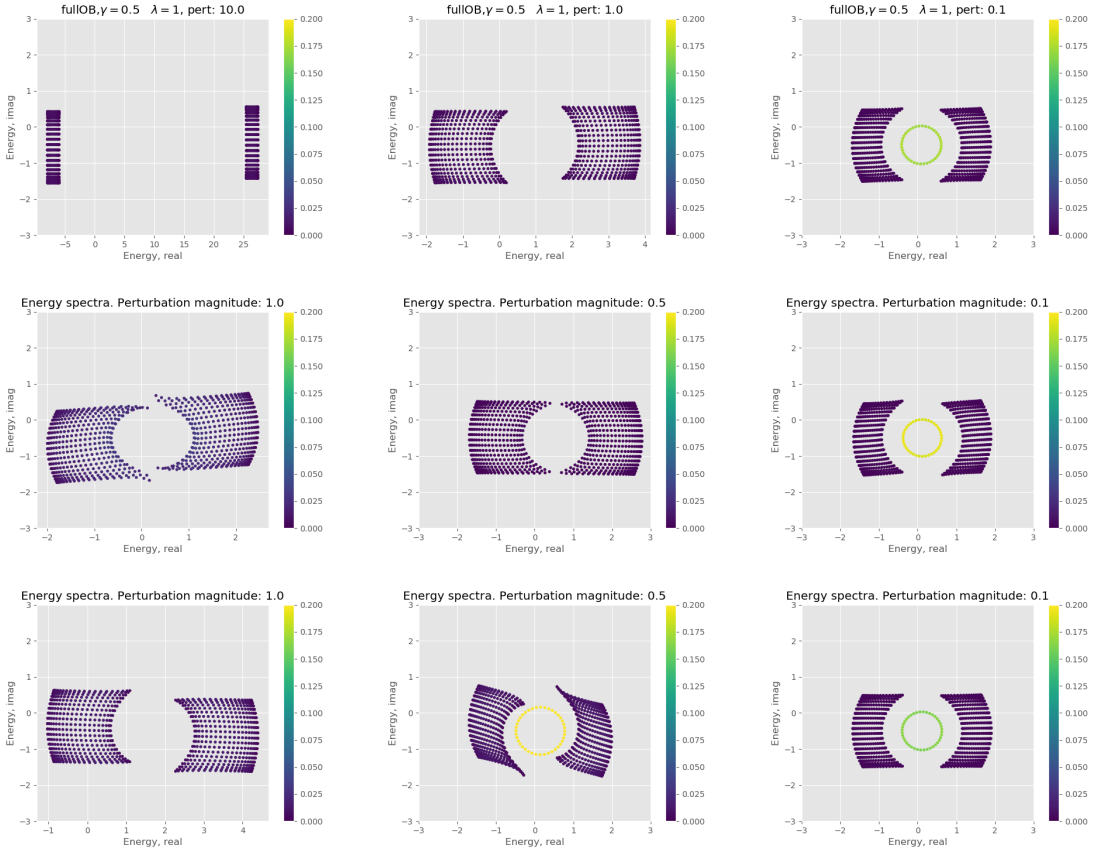

Figure E.19: *Reciprocal space. σ_x symmetric perturbation with different magnitudes and for 3 different random matrices.*

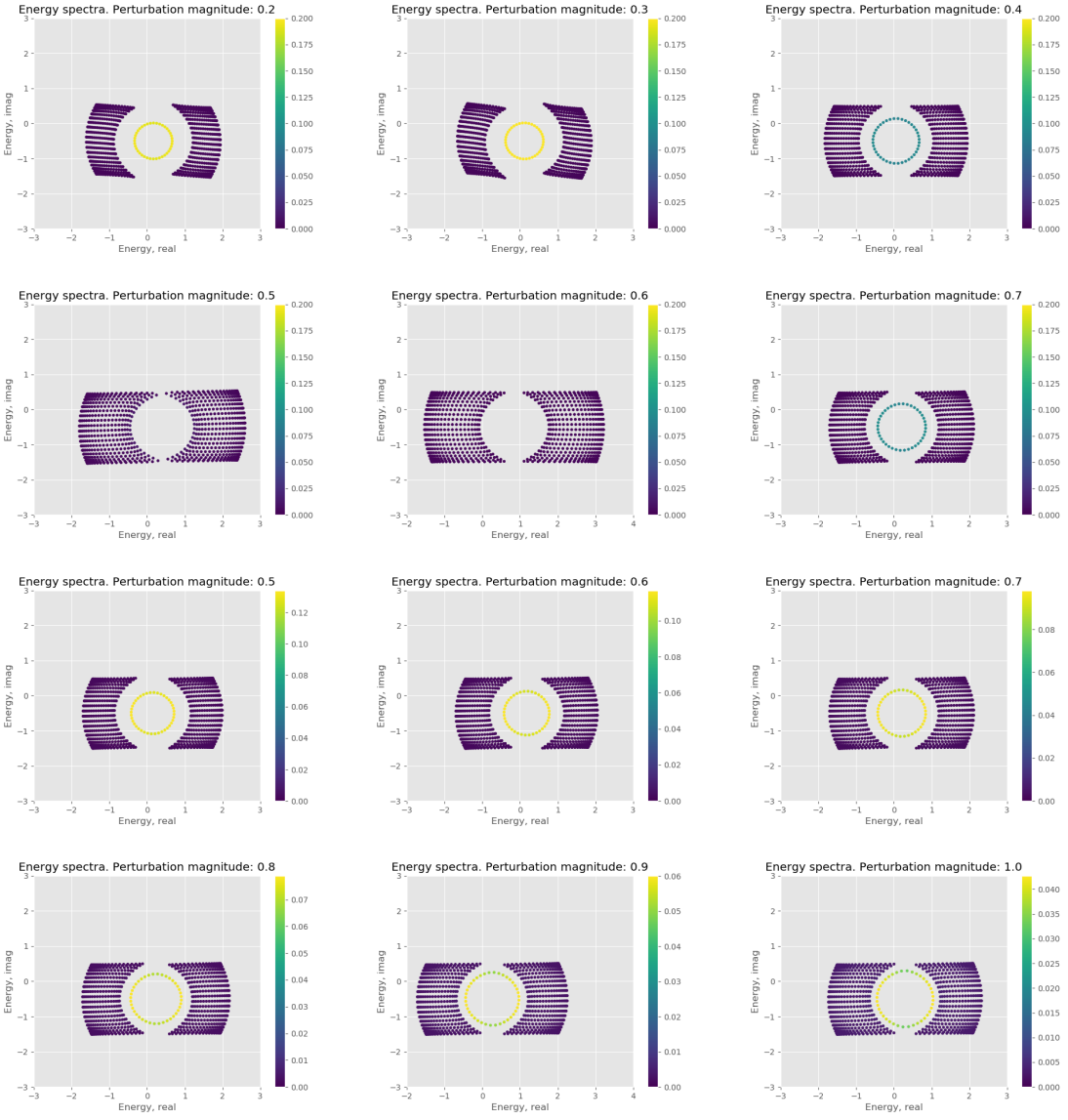

Figure E.20: *Reciprocal space. σ_x symmetric perturbation with different magnitudes. First six are with different random matrices, next six are with a same random matrix.*

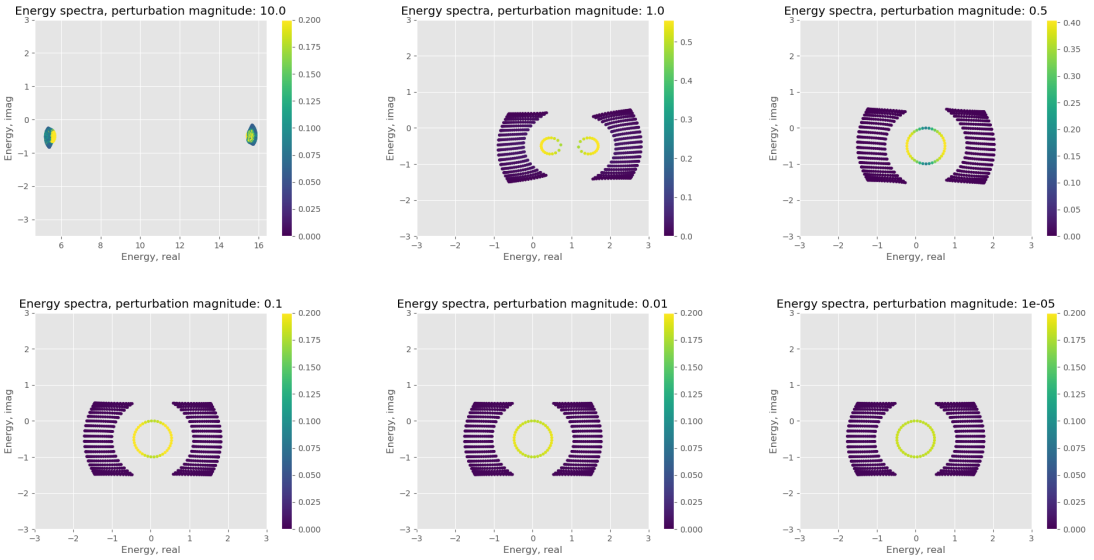

Figure E.21: *Reciprocal space. σ_z symmetric perturbation with different magnitudes, different random matrices.*

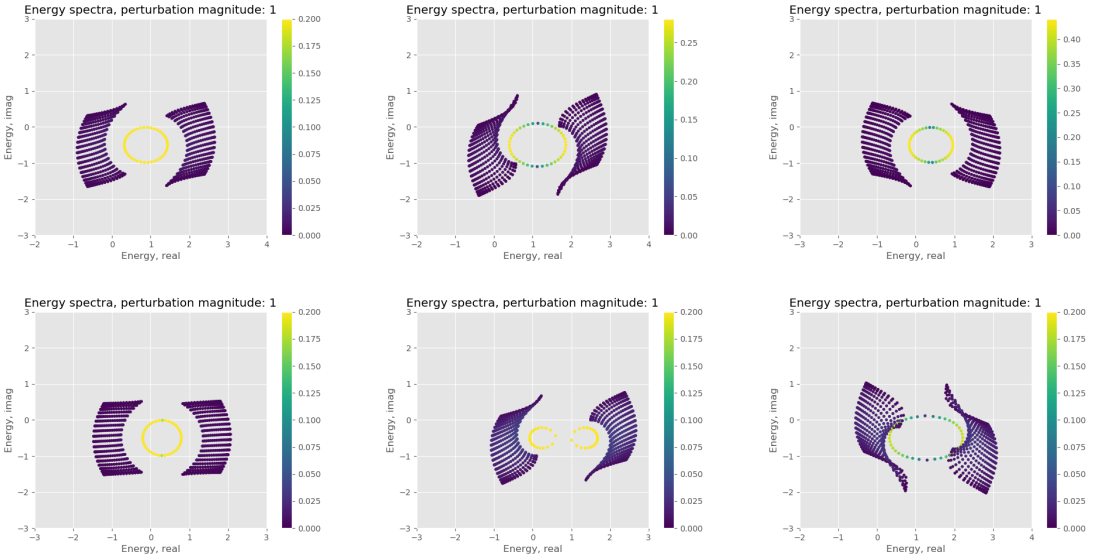

Figure E.22: *Reciprocal space. σ_z symmetric perturbation with magnitude=1, different random matrices*

Acknowledgements

I would like to thank Professor Dr. T. Neupert for giving me the chance to participate in a project from his condensed matter theory group at the University of Zurich, as well as for his valuable support and teachings. I want also to thank my supervisors for the guidance they gave me.

I want to thank my friends and my family for their unconditional support.

List of Figures

List of Tables

Bibliography

[1] Emil J. Bergholtz, Jan Carl Budich, and Flore K. Kunst. Exceptional topology of non-hermitian systems. *Rev. Mod. Phys.*, 93:015005, Feb 2021. doi: 10.1103/RevModPhys.93.015005. URL https://link.aps.org/doi/10.1103/RevModPhys.93.015005.

[2] Kohei Kawabata, Ken Shiozaki, Masahito Ueda, and Masatoshi Sato. Symmetry and topology in non-hermitian physics. *Phys. Rev. X*, 9:041015, Oct 2019. doi: 10.1103/PhysRevX.9.041015. URL https://link.aps.org/doi/10.1103/PhysRevX.9.041015.

[3] Kohei Kawabata, Masatoshi Sato, and Ken Shiozaki. Higher-order non-hermitian skin effect. *Phys. Rev. B*, 102:205118, Nov 2020. doi: 10.1103/PhysRevB.102.205118. URL https://link.aps.org/doi/10.1103/PhysRevB.102.205118.

[4] Tobias Hofmann, Tobias Helbig, Frank Schindler, Nora Salgo, Marta Brzezińska, Martin Greiter, Tobias Kiessling, David Wolf, Achim Vollhardt, Anton Kabaši, Ching Hua Lee, Ante Bilušić, Ronny Thomale, and Titus Neupert. Reciprocal skin effect and its realization in a topolectrical circuit. *Phys. Rev. Research*, 2:023265, Jun 2020. doi: 10.1103/PhysRevResearch.2.023265. URL https://link.aps.org/doi/10.1103/PhysRevResearch.2.023265.

[5] Tomoki Ozawa, Hannah M. Price, Alberto Amo, Nathan Goldman, Mohammad Hafezi, Ling Lu, Mikael C. Rechtsman, David Schuster, Jonathan Simon, Oded Zilberberg, and Iacopo Carusotto. Topological photonics. *Rev. Mod. Phys.*, 91:015006, Mar 2019. doi: 10.1103/RevModPhys.91.015006. URL https://link.aps.org/doi/10.1103/RevModPhys.91.015006.

[6] Ramy El-Ganainy, Mercedeh Khajavikhan, Ziad H. Musslimani, Stefan Rotter, and Demetrios N. Christodoulides. Non-hermitian physics and pt symmetry. *Nature physics*, 14:11, Jan 2018. doi: https://doi.org/10.1038/nphys4323. URL https://www.nature.com/articles/nphys4323.

[7] Emil J. Bergholtz, Jan Carl Budich, and Flore K. Kunst. Exceptional topology of non-hermitian systems. *Reviews of Modern Physics*, 93(1), Feb 2021. ISSN 1539-0756. doi: 10.1103/revmodphys.93.015005. URL http://dx.doi.org/10.1103/RevModPhys.93.015005.

[8] Kai Zhang, Zhesen Yang, and Chen Fang. Universal non-hermitian skin effect in two and higher dimensions, 2021.

[9] N. P. Armitage, E. J. Mele, and Ashvin Vishwanath. Weyl and dirac semimetals in three-dimensional solids. *Rev. Mod. Phys.*, 90:015001, Jan 2018. doi: 10.1103/RevModPhys.90.015001. URL https://link.aps.org/doi/10.1103/RevModPhys.90.015001.

[10] Elisabet Edvardsson, Flore K. Kunst, and Emil J. Bergholtz. Non-hermitian extensions of higher-order topological phases and their biorthogonal bulk-boundary correspondence. *Phys. Rev. B*, 99:081302, Feb 2019. doi: 10.1103/PhysRevB.99.081302. URL https://link.aps.org/doi/10.1103/PhysRevB.99.081302.

[11] Ryo Okugawa, Ryo Takahashi, and Kazuki Yokomizo. Non-hermitian band topology with generalized inversion symmetry. *Phys. Rev. B*, 103:205205, May 2021. doi: 10.1103/PhysRevB.103.205205. URL https://link.aps.org/doi/10.1103/PhysRevB.103.205205.

[12] Eunwoo Lee, Hyunjik Lee, and Bohm-Jung Yang. Many-body approach to non-hermitian physics in fermionic systems. *Phys. Rev. B*, 101:121109, Mar 2020. doi: 10.1103/PhysRevB.101.121109. URL https://link.aps.org/doi/10.1103/PhysRevB.101.121109.

[13] Hridesh Kedia, Anton Souslov, and D. Zeb Rocklin. Soft topological modes protected by symmetry in rigid mechanical metamaterials. *Phys. Rev. B*, 103:L060104, Feb 2021. doi: 10.1103/PhysRevB.103.L060104. URL https://link.aps.org/doi/10.1103/PhysRevB.103.L060104.

[14] Ryo Okugawa, Ryo Takahashi, and Kazuki Yokomizo. Second-order topological non-hermitian skin effects. *Phys. Rev. B*, 102:241202, Dec 2020. doi: 10.1103/PhysRevB.102.241202. URL https://link.aps.org/doi/10.1103/PhysRevB.102.241202.

[15] Hridesh Kedia, Anton Souslov, and D. Zeb Rocklin. Exceptional topological insulators. *Nature communications*, 12:5681, Sep 2021. doi: https://doi.org/10.1038/s41467-021-25947-z. URL https://www.nature.com/articles/s41467-021-25947-z.

[16] L. D. Landau. On the theory of phase transitions. *Zh. Eksp. Teor. Fiz.*, 7:19–32, 1937.

[17] Xiao-Gang Wen. Quantum orders and symmetric spin liquids. *Phys. Rev. B*, 65: 165113, Apr 2002. doi: 10.1103/PhysRevB.65.165113. URL https://link.aps.org/doi/10.1103/PhysRevB.65.165113.

[18] Hongming Weng, Rui Yu, Xiao Hu, Xi Dai, and Zhong Fang. Quantum anomalous hall effect and related topological electronic states. *Advances in Physics*, 64(3): 227–282, May 2015. ISSN 1460-6976. doi: 10.1080/00018732.2015.1068524. URL http://dx.doi.org/10.1080/00018732.2015.1068524.

[19] Xiao-Gang Wen. Quantum order: a quantum entanglement of many particles. *Physics Letters A*, 300(2-3):175–181, Jul 2002. ISSN 0375-9601. doi: 10.1016/s0375-9601(02)00808-3. URL http://dx.doi.org/10.1016/S0375-9601(02)00808-3.

[20] Alexei Kitaev and John Preskill. Topological entanglement entropy. *Phys. Rev. Lett.*, 96:110404, Mar 2006. doi: 10.1103/PhysRevLett.96.110404. URL https://link.aps.org/doi/10.1103/PhysRevLett.96.110404.

[21] Michael Levin and Xiao-Gang Wen. Detecting topological order in a ground state wave function. *Phys. Rev. Lett.*, 96:110405, Mar 2006. doi: 10.1103/PhysRevLett.96.110405. URL https://link.aps.org/doi/10.1103/PhysRevLett.96.110405.

[22] Zheng-Cheng Gu and Xiao-Gang Wen. Tensor-entanglement-filtering renormalization approach and symmetry-protected topological order. *Phys. Rev. B*, 80:

155131, Oct 2009. doi: 10.1103/PhysRevB.80.155131. URL https://link.aps.org/doi/10.1103/PhysRevB.80.155131.

[23] Hongming Weng, Rui Yu, Xiao Hu, Xi Dai, and Zhong Fang. Quantum anomalous hall effect and related topological electronic states. *Advances in Physics*, 64(3): 227–282, 2015. doi: 10.1080/00018732.2015.1068524. URL https://doi.org/10.1080/00018732.2015.1068524.

[24] M. Z. Hasan and C. L. Kane. Colloquium: Topological insulators. *Rev. Mod. Phys.*, 82:3045–3067, Nov 2010. doi: 10.1103/RevModPhys.82.3045. URL https://link.aps.org/doi/10.1103/RevModPhys.82.3045.

[25] D. J. Thouless, M. Kohmoto, M. P. Nightingale, and M. den Nijs. Quantized hall conductance in a two-dimensional periodic potential. *Phys. Rev. Lett.*, 49:405–408, Aug 1982. doi: 10.1103/PhysRevLett.49.405. URL https://link.aps.org/doi/10.1103/PhysRevLett.49.405.

[26] Xiao-Gang Wen. Topological orders and edge excitations in fractional quantum hall states. *Advances in Physics*, 44(5):405–473, 1995. doi: 10.1080/00018739500101566. URL https://doi.org/10.1080/00018739500101566.

[27] K. v. Klitzing, G. Dorda, and M. Pepper. New method for high-accuracy determination of the fine-structure constant based on quantized hall resistance. *Phys. Rev. Lett.*, 45:494–497, Aug 1980. doi: 10.1103/PhysRevLett.45.494. URL https://link.aps.org/doi/10.1103/PhysRevLett.45.494.

[28] Pascal Marc Vecsei. Two aspects of crystalline topological matter fractional corner charges with fourfold rotational symmetry and symmetry indicator invariants for non-hermitian topological materials. Master's thesis, University of Zurich, Feb 2021.

[29] Mikio Nakahara. *Geometry, Topology and Physics*. Location Boca Raton, 2 edition, 2003. URL https://doi.org/10.1201/9781315275826.

[30] Michael Victor Berry. Quantal phase factors accompanying adiabatic changes. *Proceedings of the Royal Society of London. A. Mathematical and Physical Sciences*, 392(1802):45–57, 1984. doi: 10.1098/rspa.1984.0023. URL https://royalsocietypublishing.org/doi/abs/10.1098/rspa.1984.0023.

[31] F. D. M. Haldane. Model for a quantum hall effect without landau levels: Condensed-matter realization of the "parity anomaly". *Phys. Rev. Lett.*, 61:2015–2018, Oct 1988. doi: 10.1103/PhysRevLett.61.2015. URL https://link.aps.org/doi/10.1103/PhysRevLett.61.2015.

[32] T. Jungwirth, Qian Niu, and A. H. MacDonald. Anomalous hall effect in ferromagnetic semiconductors. *Phys. Rev. Lett.*, 88:207208, May 2002. doi: 10.1103/PhysRevLett.88.207208. URL https://link.aps.org/doi/10.1103/PhysRevLett.88.207208.

[33] Masaru Onoda and Naoto Nagaosa. Topological nature of anomalous hall effect in ferromagnets. *Journal of the Physical Society of Japan*, 71(1):19–22, 2002. doi: 10.1143/JPSJ.71.19. URL https://doi.org/10.1143/JPSJ.71.19.

[34] Zhong Fang, Naoto Nagaosa, Kei S. Takahashi, Atsushi Asamitsu, Roland Mathieu, Takeshi Ogasawara, Hiroyuki Yamada, Masashi Kawasaki, Yoshinori Tokura, and Kiyoyuki Terakura. The anomalous hall effect and magnetic monopoles in momentum space. *Science*, 302(5642):92–95, 2003. doi: 10.1126/science.1089408. URL https://www.science.org/doi/abs/10.1126/science.1089408.

[35] Yugui Yao, Leonard Kleinman, A. H. MacDonald, Jairo Sinova, T. Jungwirth, Ding-sheng Wang, Enge Wang, and Qian Niu. First principles calculation of anomalous hall conductivity in ferromagnetic bcc fe. *Phys. Rev. Lett.*, 92:037204, Jan 2004. doi: 10.1103/PhysRevLett.92.037204. URL https://link.aps.org/doi/10.1103/PhysRevLett.92.037204.

[36] Masaru Onoda and Naoto Nagaosa. Quantized anomalous hall effect in two-dimensional ferromagnets: Quantum hall effect in metals. *Phys. Rev. Lett.*, 90:206601, May 2003. doi: 10.1103/PhysRevLett.90.206601. URL https://link.aps.org/doi/10.1103/PhysRevLett.90.206601.

[37] David Vanderbilt. *Berry Phases in Electronic Structure Theory: Electric Polarization, Orbital Magnetization and Topological Insulators*. Cambridge University Press, 2018. doi: 10.1017/9781316662205.

[38] Berry Michael Victor. Quantal phase factors accompanying adiabatic changes. *Proc. R. Soc. Lond.*., 392, 1984. doi: 10.1098/rspa.1984.0023. URL http://doi.org/10.1098/rspa.1984.0023.

[39] R. D. King-Smith and David Vanderbilt. Theory of polarization of crystalline solids. *Phys. Rev. B*, 47:1651–1654, Jan 1993. doi: 10.1103/PhysRevB.47.1651. URL https://link.aps.org/doi/10.1103/PhysRevB.47.1651.

[40] Nicola Marzari and David Vanderbilt. Maximally localized generalized wannier functions for composite energy bands. *Phys. Rev. B*, 56:12847–12865, Nov 1997. doi: 10.1103/PhysRevB.56.12847. URL https://link.aps.org/doi/10.1103/PhysRevB.56.12847.

[41] T. Thonhauser, Davide Ceresoli, David Vanderbilt, and R. Resta. Orbital magnetization in periodic insulators. *Phys. Rev. Lett.*, 95:137205, Sep 2005. doi: 10.1103/PhysRevLett.95.137205. URL https://link.aps.org/doi/10.1103/PhysRevLett.95.137205.

[42] Davide Ceresoli, T. Thonhauser, David Vanderbilt, and R. Resta. Orbital magnetization in crystalline solids: Multi-band insulators, chern insulators, and metals. *Phys. Rev. B*, 74:024408, Jul 2006. doi: 10.1103/PhysRevB.74.024408. URL https://link.aps.org/doi/10.1103/PhysRevB.74.024408.

[43] Lixin He and David Vanderbilt. Exponential decay properties of wannier functions and related quantities. *Phys. Rev. Lett.*, 86:5341–5344, Jun 2001. doi: 10.1103/PhysRevLett.86.5341. URL https://link.aps.org/doi/10.1103/PhysRevLett.86.5341.

[44] Raffaele Resta and Sandro Sorella. Electron localization in the insulating state. *Phys. Rev. Lett.*, 82:370–373, Jan 1999. doi: 10.1103/PhysRevLett.82.370. URL https://link.aps.org/doi/10.1103/PhysRevLett.82.370.

[45] Ivo Souza, Tim Wilkens, and Richard M. Martin. Polarization and localization in insulators: Generating function approach. *Phys. Rev. B*, 62:1666–1683, Jul 2000. doi: 10.1103/PhysRevB.62.1666. URL https://link.aps.org/doi/10.1103/PhysRevB.62.1666.

[46] Raffaele Resta. Why are insulators insulating and metals conducting? *Journal of Physics: Condensed Matter*, 14(20):R625–R656, may 2002. doi: 10.1088/0953-8984/14/20/201. URL https://doi.org/10.1088/0953-8984/14/20/201.

[47] T. Thonhauser and David Vanderbilt. Insulator/chern-insulator transition in the haldane model. *Phys. Rev. B*, 74:235111, Dec 2006. doi: 10.1103/PhysRevB.74.235111. URL https://link.aps.org/doi/10.1103/PhysRevB.74.235111.

[48] C. L. Kane and E. J. Mele. Quantum spin hall effect in graphene. *Phys. Rev. Lett.*, 95:226801, Nov 2005. doi: 10.1103/PhysRevLett.95.226801. URL https://link.aps.org/doi/10.1103/PhysRevLett.95.226801.

[49] H.A. Kramers. Hand und jahrbuch der chemischen physik. *Nature*, 136:125, July 1935. doi: https://doi.org/10.1038/136125a0. URL https://www.nature.com/articles/136125a0.

[50] Liang Fu and C. L. Kane. Time reversal polarization and a Z_2 adiabatic spin pump. *Phys. Rev. B*, 74:195312, Nov 2006. doi: 10.1103/PhysRevB.74.195312. URL https://link.aps.org/doi/10.1103/PhysRevB.74.195312.

[51] C. L. Kane and E. J. Mele. Z_2 topological order and the quantum spin hall effect. *Phys. Rev. Lett.*, 95:146802, Sep 2005. doi: 10.1103/PhysRevLett.95.146802. URL https://link.aps.org/doi/10.1103/PhysRevLett.95.146802.

[52] Alexander Altland and Martin R. Zirnbauer. Nonstandard symmetry classes in mesoscopic normal-superconducting hybrid structures. *Phys. Rev. B*, 55:1142–1161, Jan 1997. doi: 10.1103/PhysRevB.55.1142. URL https://link.aps.org/doi/10.1103/PhysRevB.55.1142.

[53] Alexander Altland and Martin R. Zirnbauer. Nonstandard symmetry classes in mesoscopic normal-superconducting hybrid structures. *Physical Review B*, 55(2): 1142–1161, Jan 1997. ISSN 1095-3795. doi: 10.1103/physrevb.55.1142. URL http://dx.doi.org/10.1103/PhysRevB.55.1142.

[54] H.B. Nielsen and Masao Ninomiya. The adler-bell-jackiw anomaly and weyl fermions in a crystal. *Physics Letters B*, 130(6):389–396, 1983. ISSN 0370-2693. doi: https://doi.org/10.1016/0370-2693(83)91529-0. URL https://www.sciencedirect.com/science/article/pii/0370269383915290.

[55] B. Andrei Bernevig and Shou-Cheng Zhang. Quantum spin hall effect. *Phys. Rev. Lett.*, 96:106802, Mar 2006. doi: 10.1103/PhysRevLett.96.106802. URL https://link.aps.org/doi/10.1103/PhysRevLett.96.106802.

[56] B. Andrei Bernevig, Taylor L. Hughes, and Shou-Cheng Zhang. Quantum spin hall effect and topological phase transition in hgte quantum wells. *Science*, 314(5806): 1757–1761, 2006. doi: 10.1126/science.1133734. URL https://www.science.org/doi/abs/10.1126/science.1133734.

[57] Markus König, Steffen Wiedmann, Christoph Brüne, Andreas Roth, Hartmut Buhmann, Laurens W. Molenkamp, Xiao-Liang Qi, and Shou-Cheng Zhang. Quantum spin hall insulator state in hgte quantum wells. *Science*, 318(5851):766–770, 2007. doi: 10.1126/science.1148047. URL https://www.science.org/doi/abs/10.1126/science.1148047.

[58] Markus König, Hartmut Buhmann, Laurens W. Molenkamp, Taylor Hughes, Chao-Xing Liu, Xiao-Liang Qi, and Shou-Cheng Zhang. The quantum spin hall effect: Theory and experiment. *Journal of the Physical Society of Japan*, 77(3): 031007, 2008. doi: 10.1143/JPSJ.77.031007. URL https://doi.org/10.1143/JPSJ.77.031007.

[59] Liang Fu and C. L. Kane. Probing neutral majorana fermion edge modes with charge transport. *Phys. Rev. Lett.*, 102:216403, May 2009. doi: 10.1103/PhysRevLett.102.216403. URL https://link.aps.org/doi/10.1103/PhysRevLett.102.216403.

[60] J. E. Moore and L. Balents. Topological invariants of time-reversal-invariant band structures. *Phys. Rev. B*, 75:121306, Mar 2007. doi: 10.1103/PhysRevB.75.121306. URL https://link.aps.org/doi/10.1103/PhysRevB.75.121306.

[61] Rahul Roy. Topological phases and the quantum spin hall effect in three dimensions. *Phys. Rev. B*, 79:195322, May 2009. doi: 10.1103/PhysRevB.79.195322. URL https://link.aps.org/doi/10.1103/PhysRevB.79.195322.

[62] Liang Fu, C. L. Kane, and E. J. Mele. Topological insulators in three dimensions. *Phys. Rev. Lett.*, 98:106803, Mar 2007. doi: 10.1103/PhysRevLett.98.106803. URL https://link.aps.org/doi/10.1103/PhysRevLett.98.106803.

[63] Hsieh et al. A topological dirac insulator in a quantum spin hall phase. *Nature*, Apr 2008. doi: https://doi.org/10.1038/nature06843. URL https://doi.org/10.1038/nature06843.

[64] Christian Brouder, Gianluca Panati, Matteo Calandra, Christophe Mourougane, and Nicola Marzari. Exponential localization of wannier functions in insulators. *Phys. Rev. Lett.*, 98:046402, Jan 2007. doi: 10.1103/PhysRevLett.98.046402. URL https://link.aps.org/doi/10.1103/PhysRevLett.98.046402.

[65] Ching-Kai Chiu, Jeffrey C. Y. Teo, Andreas P. Schnyder, and Shinsei Ryu. Classification of topological quantum matter with symmetries. *Rev. Mod. Phys.*, 88: 035005, Aug 2016. doi: 10.1103/RevModPhys.88.035005. URL https://link.aps.org/doi/10.1103/RevModPhys.88.035005.

[66] Frank Schindler, Ashley M. Cook, Maia G. Vergniory, Zhijun Wang, Stuart S. P. Parkin, B. Andrei Bernevig, and Titus Neupert. Higher-order topological insulators. *Science Advances*, 4(6):eaat0346, 2018. doi: 10.1126/sciadv.aat0346. URL https://www.science.org/doi/abs/10.1126/sciadv.aat0346.

[67] Wladimir A. Benalcazar, Jiho Noh, Mohan Wang, Sheng Huang, Kevin P. Chen, and Mikael C. Rechtsman. Higher-order topological pumping, 2020.

[68] G Lindblad. On the generators of quantum dynamical semigroups. *Commun.Math.Phys.*, 48:119–130, 1976. doi: https://doi.org/10.1007/BF01608499. URL https://link.springer.com/article/10.1007.

[69] R.P Feynman and F.L Vernon. The theory of a general quantum system interacting with a linear dissipative system. *Annals of Physics*, 24:118–173, 1963. ISSN 0003-4916. doi: https://doi.org/10.1016/0003-4916(63)90068-X. URL https://www.sciencedirect.com/science/article/pii/000349166390068X.

[70] Carl M Bender. Making sense of non-hermitian hamiltonians. *Reports on Progress in Physics*, 70(6):947–1018, may 2007. doi: 10.1088/0034-4885/70/6/r03. URL https://doi.org/10.1088/0034-4885/70/6/r03.

[71] Ingrid Rotter. A non-hermitian hamilton operator and the physics of open quantum systems. *Journal of Physics A: Mathematical and Theoretical*, 42(15):153001, mar 2009. doi: 10.1088/1751-8113/42/15/153001. URL https://doi.org/10.1088/1751-8113/42/15/153001.

[72] Mohammad-Ali Miri and Andrea Alù. Exceptional points in optics and photonics. *Science*, 363(6422):eaar7709, 2019. doi: 10.1126/science.aar7709. URL https://www.science.org/doi/abs/10.1126/science.aar7709.

[73] et al. Hodaei Hossein. Enhanced sensitivity at higher-order exceptional points. *Nature*, 548, June 2017. doi: https://doi.org/10.1038/nature23280. URL https://www.nature.com/articles/nature23280.

[74] W D Heiss. The physics of exceptional points. *Journal of Physics A: Mathematical and Theoretical*, 45(44):444016, oct 2012. doi: 10.1088/1751-8113/45/44/444016. URL https://doi.org/10.1088/1751-8113/45/44/444016.

[75] Zongping Gong, Yuto Ashida, Kohei Kawabata, Kazuaki Takasan, Sho Higashikawa, and Masahito Ueda. Topological phases of non-hermitian systems. *Phys. Rev. X*, 8:031079, Sep 2018. doi: 10.1103/PhysRevX.8.031079. URL https://link.aps.org/doi/10.1103/PhysRevX.8.031079.

[76] Huitao Shen, Bo Zhen, and Liang Fu. Topological band theory for non-hermitian hamiltonians. *Phys. Rev. Lett.*, 120:146402, Apr 2018. doi: 10.1103/PhysRevLett.120.146402. URL https://link.aps.org/doi/10.1103/PhysRevLett.120.146402.

[77] Naomichi Hatano and David R. Nelson. Localization transitions in non-hermitian quantum mechanics. *Phys. Rev. Lett.*, 77:570–573, Jul 1996. doi: 10.1103/PhysRevLett.77.570. URL https://link.aps.org/doi/10.1103/PhysRevLett.77.570.

[78] Flore K. Kunst, Elisabet Edvardsson, Jan Carl Budich, and Emil J. Bergholtz. Biorthogonal bulk-boundary correspondence in non-hermitian systems. *Phys. Rev. Lett.*, 121:026808, Jul 2018. doi: 10.1103/PhysRevLett.121.026808. URL https://link.aps.org/doi/10.1103/PhysRevLett.121.026808.

[79] V. M. Martinez Alvarez, J. E. Barrios Vargas, and L. E. F. Foa Torres. Non-hermitian robust edge states in one dimension: Anomalous localization and eigenspace condensation at exceptional points. *Phys. Rev. B*, 97:121401, Mar 2018. doi: 10.1103/PhysRevB.97.121401. URL https://link.aps.org/doi/10.1103/PhysRevB.97.121401.

[80] Ye Xiong. Why does bulk boundary correspondence fail in some non-hermitian topological models. *Journal of Physics Communications*, 2(3):035043, mar 2018. doi: 10.1088/2399-6528/aab64a. URL https://doi.org/10.1088/2399-6528/aab64a.

[81] Shunyu Yao and Zhong Wang. Edge states and topological invariants of non-hermitian systems. *Phys. Rev. Lett.*, 121:086803, Aug 2018. doi: 10.1103/PhysRevLett.121.086803. URL https://link.aps.org/doi/10.1103/PhysRevLett.121.086803.

[82] Flore K. Kunst and Vatsal Dwivedi. Non-hermitian systems and topology: A transfer-matrix perspective. *Phys. Rev. B*, 99:245116, Jun 2019. doi: 10.1103/PhysRevB.99.245116. URL https://link.aps.org/doi/10.1103/PhysRevB.99.245116.

[83] M.V. Berry. Physics of nonhermitian degeneracies. *Czechoslovak Journal of Physics*, 54, Oct 2004. doi: https://doi.org/10.1023/B:CJOP.0000044002.05657.04. URL https://link.springer.com/article/10.1023/B:CJOP.0000044002.05657.04.

[84] Vladyslav Kozii and Liang Fu. Non-hermitian topological theory of finite-lifetime quasiparticles: Prediction of bulk fermi arc due to exceptional point, 2017.

[85] Johan Carlström and Emil J. Bergholtz. Exceptional links and twisted fermi ribbons in non-hermitian systems. *Phys. Rev. A*, 98:042114, Oct 2018. doi: 10.1103/PhysRevA.98.042114. URL https://link.aps.org/doi/10.1103/PhysRevA.98.042114.

[86] Hengyun Zhou, Chao Peng, Yoseob Yoon, Chia Wei Hsu, Keith A. Nelson, Liang Fu, John D. Joannopoulos, Marin Soljačić, and Bo Zhen. Observation of bulk fermi arc and polarization half charge from paired exceptional points. *Science*, 359(6379):1009–1012, 2018. doi: 10.1126/science.aap9859. URL https://www.science.org/doi/abs/10.1126/science.aap9859.

[87] Zhiwang Zhang, María Rosendo López, Ying Cheng, Xiaojun Liu, and Johan Christensen. Non-hermitian sonic second-order topological insulator. *Phys. Rev. Lett.*, 122:195501, May 2019. doi: 10.1103/PhysRevLett.122.195501. URL https://link.aps.org/doi/10.1103/PhysRevLett.122.195501.

[88] D. Bernard and A. LeClair. *A Classification of Non-Hermitian Random Matrices. In: Cappelli A., Mussardo G. (eds).* Springer, Dordrecht, 2002. doi: https://doi.org/10.1007/978-94-010-0514-2_19. URL https://link.springer.com/chapter/10.1007/978-94-010-0514-2_19.

[89] Andreas P. Schnyder, Shinsei Ryu, Akira Furusaki, and Andreas W. W. Ludwig. Classification of topological insulators and superconductors in three spatial dimensions. *Phys. Rev. B*, 78:195125, Nov 2008. doi: 10.1103/PhysRevB.78.195125. URL https://link.aps.org/doi/10.1103/PhysRevB.78.195125.

[90] Ken Shiozaki and Masatoshi Sato. Topology of crystalline insulators and superconductors. *Phys. Rev. B*, 90:165114, Oct 2014. doi: 10.1103/PhysRevB.90.165114. URL https://link.aps.org/doi/10.1103/PhysRevB.90.165114.

[91] Kohei Kawabata, Sho Higashikawa, Yuto Ashida, and Masahito Ueda. Topological unification of time-reversal and particle-hole symmetries in non-hermitian physics. *Nature Communications*, 10:297, Jan 2019. doi: 10.1038/s41467-018-08254-y. URL https://doi.org/10.1038/s41467-018-08254-y.

[92] J Wess and B Zumino. Consequences of anomalous Ward identities. *Phys. Lett. B*, 37:95–97, 1971. doi: 10.1016/0370-2693(71)90582-X. URL http://cds.cern.ch/record/486885.

[93] Edward Witten. Global aspects of current algebra. *Nuclear Physics B*, 223(2):422–432, 1983. ISSN 0550-3213. doi: https://doi.org/10.1016/0550-3213(83)90063-9. URL https://www.sciencedirect.com/science/article/pii/0550321383900639.

[94] Kohei Kawabata, Masatoshi Sato, and Ken Shiozaki. Higher-order non-hermitian skin effect, 2020.

[95] Loïc Herviou, Jens H. Bardarson, and Nicolas Regnault. Defining a bulk-edge correspondence for non-hermitian hamiltonians via singular-value decomposition. *Phys. Rev. A*, 99:052118, May 2019. doi: 10.1103/PhysRevA.99.052118. URL https://link.aps.org/doi/10.1103/PhysRevA.99.052118.

[96] G. H. Golub, C. Reinsch, F. L. Bauer, A. S. Householder, F. W. J. Olver, H. Rutishauser, K. Samelson, and E. Stiefel. *Singular Value Decomposition and Least Squares Solutions*, pages 134–151. Springer Berlin Heidelberg, Berlin, Heidelberg, 1971. ISBN 978-3-642-86940-2. doi: 10.1007/978-3-642-86940-2_10. URL https://doi.org/10.1007/978-3-642-86940-2_10.

[97] Nema Salem and Sahar Hussein. Data dimensional reduction and principal components analysis. *Procedia Computer Science*, 163:292–299, 2019. ISSN 1877-0509. doi: https://doi.org/10.1016/j.procs.2019.12.111. URL https://www.sciencedirect.com/science/article/pii/S1877050919321507. 16th Learning and Technology Conference 2019Artificial Intelligence and Machine Learning: Embedding the Intelligence.

[98] Nicola Marzari, Arash A. Mostofi, Jonathan R. Yates, Ivo Souza, and David Vanderbilt. Maximally localized wannier functions: Theory and applications. *Rev. Mod. Phys.*, 84:1419–1475, Oct 2012. doi: 10.1103/RevModPhys.84.1419. URL https://link.aps.org/doi/10.1103/RevModPhys.84.1419.

[99] Wikipedia contributors. Tight binding — Wikipedia, the free encyclopedia, 2021. URL https://en.wikipedia.org/w/index.php?title=Tight_binding&oldid=1052750036. [Online; accessed 21-November-2021].

[100] J. C. Slater and G. F. Koster. Simplified lcao method for the periodic potential problem. *Phys. Rev.*, 94:1498–1524, Jun 1954. doi: 10.1103/PhysRev.94.1498. URL https://link.aps.org/doi/10.1103/PhysRev.94.1498.

[101] Peter Y. Yu and Manuel Cardona. *Fundamentals of Semiconductors: Physics and Materials Properties*. Springer-Verlag Berlin Heidelberg, 4 edition, 2010. URL https://1lib.ch/book/660055/567179?dsource=recommend.

[102] Barry Bradlyn, L. Elcoro, Jennifer Cano, M. G. Vergniory, Zhijun Wang, C. Felser, M. I. Aroyo, and B. Andrei Bernevig. Topological quantum chemistry. *Nature*, 547(7663):298–305, Jul 2017. ISSN 1476-4687. doi: 10.1038/nature23268. URL http://dx.doi.org/10.1038/nature23268.

[103] M Calixto and E Romera. Inverse participation ratio and localization in topological insulator phase transitions. *Journal of Statistical Mechanics: Theory and Experiment*, 2015(6):P06029, Jun 2015. ISSN 1742-5468. doi: 10.1088/1742-5468/2015/06/p06029. URL http://dx.doi.org/10.1088/1742-5468/2015/06/P06029.

[104] F. Wegner. Inverse participation ratio in $2+\epsilon$ dimensions. *Zeitschrift für Physik B Condensed Matter*, 36:209–214, Sep 1980. doi: https://doi.org/10.1007/BF01325284.

[105] Loïc Herviou, Nicolas Regnault, and Jens H Bardarson. Entanglement spectrum and symmetries in non-hermitian fermionic non-interacting models. *SciPost Physics*, 7(5), Nov 2019. ISSN 2542-4653. doi: 10.21468/scipostphys.7.5.069. URL http://dx.doi.org/10.21468/SciPostPhys.7.5.069.

[106] Dorje C Brody. Biorthogonal quantum mechanics. *Journal of Physics A: Mathematical and Theoretical*, 47(3):035305, dec 2013. doi: 10.1088/1751-8113/47/3/035305. URL https://doi.org/10.1088/1751-8113/47/3/035305.

[107] Zhesen Yang, A. P. Schnyder, Jiangping Hu, and Ching-Kai Chiu. Fermion doubling theorems in two-dimensional non-hermitian systems for fermi points and exceptional points. *Phys. Rev. Lett.*, 126:086401, Feb 2021. doi: 10.1103/PhysRevLett.126.086401. URL https://link.aps.org/doi/10.1103/PhysRevLett.126.086401.

[108] Wladimir A. Benalcazar, B. Andrei Bernevig, and Taylor L. Hughes. Quantized electric multipole insulators. *Science*, 357(6346):61–66, 2017. doi: 10.1126/science.aah6442. URL https://www.science.org/doi/abs/10.1126/science.aah6442.

[109] Sophie S. Shamailov, Dylan J. Brown, Thomas A. Haase, and Maarten D. Hoogerland. Anderson localisation in two dimensions: insights from localisation landscape theory, exact diagonalisation, and time-dependent simulations, 2021.

[110] latex4technics. Representing general transformations on a 3d grid using tikz, 2022. URL https://www.latex4technics.com/codesearch?q=3d.

[111] M.Michael Denner, Anastasiia Skurativska, Frank Schindler, Mark H. Fischer, Ronny Thomale, Tomáš Bzušek, and Titus Neupert. Exceptional topological insulators. *Nature Communications*, 12(5681):2041–1723, 2021. doi: https://doi.org/10.1038/s41467-021-25947-z. URL https://www.nature.com/articles/s41467-021-25947-z.

[112] Y. L. Chen, J. G. Analytis, J.-H. Chu, Z. K. Liu, S.-K. Mo, X. L. Qi, H. J. Zhang, D. H. Lu, X. Dai, Z. Fang, S. C. Zhang, I. R. Fisher, Z. Hussain, and Z.-X. Shen. Experimental realization of a three-dimensional topological insulator, bi¡sub¿2¡/sub¿te¡sub¿3¡/sub¿. *Science*, 325(5937):178–181, 2009. doi: 10.1126/

science.1173034. URL https://www.science.org/doi/abs/10.1126/science.1173034.